Dinámica de los Flujos Biogeoquímicos y sus Aplicaciones
Departamento de Ecología
Universidad de Granada

The Physical Control of Contaminant Distribution in Aquatic Ecosystems

El control físico de la distribución de contaminantes en ecosistemas acuáticos

Doctor of Philosophy

Andrea B. Hoyer
June 2014

Advisor: Francisco Rueda Valdivia

Editor: Editorial de la Universidad de Granada
Autor: Andrea B. Hoyer
D.L.: GR 1986-2014
ISBN: 978-84-9083-186-1

Preface

La doctoranda Andrea Hoyer y el director de la tesis Francisco Rueda Valdivia. Garantizamos, al firmar esta tesis doctoral, que el trabajo ha sido realizado por la doctoranda bajo la dirección del director de la tesis y hasta donde nuestro conocimiento alcanza, en la realización del trabajo, se han respetado los derechos de otros autores a ser citados, cuando se han utilizado sus resultados o publicaciones.

Granada,

El director de la tesis — La doctoranda

Fdo. Francisco Rueda Valdivia — Fdo. Andrea Hoyer

Live as if you were to die tomorrow.
Learn as if you were to live forever.

Mahatma Gandhi

To science

Abstract

Water contamination endangers aquatic ecosystems worldwide. The contamination of aquatic ecosystems impairs the system's functioning and its use as a water source. The spread of contaminants within a system is possible due to dispersal, i.e. the transport of a substance or organism by the movements of the ambient water. The knowledge and understanding of these movements is necessary to determine the contaminant's final distribution, its concentration, its fate, and, thus, the potential impacts on ecosystems and human health. Water currents and mixing can be determined mathematically by resolving the advection-diffusion equation. Hydrodynamic transport model have been applied for the study of contaminant transport in coastal systems, rivers, reservoirs and lakes. In lakes, currents are largely forced by winds, waves and convective processes, and are characterized by low magnitude as well as high temporal and spatial variability. However, little is known to date about the distribution of contaminants by wind-driven lake currents.

The objective of this thesis is to analyze the passive dispersal of living contaminants (organisms) by wind-driven lake currents. For this purpose, a mechanistic individual-based model grounded on the reaction-advection-diffusion equation has been developed. The model consists of three modules (**R**elease-**T**ransport-**S**urvival) that represent the basic processes of contaminant dispersal: (R) the incorporation of a given contaminant into the water column through entrainment or shedding, (T) passive transport and dispersal, and (S) contaminant survival (or inactivation) in function of environmental conditions endured during transport. The particular aim is to characterize the mechanisms of dispersal, the temporal and spatial variations of the pathways, and the contaminant's final distribution. The dispersal model has been applied to study the distribution of two contaminants, (i) an inva-

sive bivalve, Asian clam (*Corbicula fluminea*) and (ii) a human water-borne pathogen (*Cryptosporidium* ssp.), in a deep, alpine lake surrounded by a complex topography - Lake Tahoe, USA.

Asian clam is among the most aggressive freshwater invaders worldwide. Passive (natural) hydraulic transport by water currents is considered to be the main mechanism for the local dispersal of Asian clam. The local dispersal largely occurs during the larval and juvenile stages of their life when, as a result of their low density, larvae may remain suspended in the surface mixed layer even under minimal turbulence. Larvae are not motile, but can travel long distances drifting with water currents. The contribution of currents in the local dispersal of Asian clam larvae, however, is not known. Laboratory studies on the dispersal of Asian clam by water currents have focused on the transport of adults. The local dispersal of planktonic larvae of Asian clam by passive hydraulic transport has been evaluated in Lake Tahoe. The probability of dispersal of Asian clam larvae from the existing high density populations to novel habitats is determined by the wind regime, the magnitude of wind events and their timing. Larvae dispersal and migration occurs in form of pulses in response to episodic events of strong wind forcing. Dispersal of Asian clam occurs along a discrete number of preferential pathways. The impact of ultraviolet radiation during the pelagic stages on Asian clam mortality is low as a result of the short dispersal distances associated with relatively high larval settling velocity and the predominantly weak winds observed. The final distribution of dispersed larvae and the probability of their survival are sensitive to the larval settling velocity. Flow inside bays tends to exhibit recirculating currents, likely as the results of flow separation at the bay boundary. Bays that are characterized by low current velocities and re-circulation act as traps for suspended benthic larvae.

Pathogen contamination of aquatic ecosystems is a severe threats to human health worldwide. The protozoan parasite *Cryptosporidium* spp., or rather its oocysts, is widespread in lakes and reservoirs, even in developed countries. Only in the US, the presence of *Cryptosporidium parvum* is estimated to 55% of surface waters and 17% of drinking water supplies. *Cryptosporidium* poses a problem to water treatment as it is highly resistant to conventional methods of disinfection. The small size and omnipresence of its

oocysts has caused many health outbreaks in drinking as well as recreational waters. To the extent of the author's knowledge, no quantitative studies exist on the risk of pathogens entering drinking water intakes of lakes or reservoirs resolving the near-shore circulation and taking into account temperature as well as light inactivation. The specific aim is to assess the risk of infectious human water-borne pathogens, focusing on the example of *Cryptosporidium*, released at recreational beaches entering a sample water intake of Lake Tahoe. The risk of contamination by *Cryptosporidium* is analyzed using a modified version of the dispersal model, including a novel technique of back-tracking pathogens from the point of concern (water intake) toward the source regions (recreational beaches). This technique allows studying non-point contaminations at a modest computational cost and identifying time periods of potential drinking water contamination. For the case of *Cryptosporidium* dispersal in Lake Tahoe, the results reveal that for this particular lake (1) the risk of human water-borne pathogens entering drinking water intakes is low, but significant; (2) this risk is strongly related by the depth of the thermocline in relation to the depth of the intake; (3) the risk of increases with the seasonal deepening of the surface mixed layer; and (4) the risk increases at the night when the surface mixed layer deepens through convective mixing and inactivation by ultraviolet radiation is eliminated.

The work presented in the Chapter 2 has been accepted for publication in *Journal of Environmental Management* entitled "A 3D individual-based aquatic transport model for the assessment of the potential dispersal of planktonic larvae of an invasive bivalve" and authored by Hoyer, A.B., Wittmann, M.E., Chandra, S., Schladow, S.G. and F.J. Rueda. The work presented in Chapter 3 is currently in review by *Limnology and Oceanography: Fluids and Environment* entitled "Local Dispersion of Invasive Bivalve Species by Wind-driven Lake Currents" and authored by Hoyer, A.B., Schladow, S.G. and F.J. Rueda. Chapter 4 on the risk of human water-borne pathogens entering drinking water intakes is in preparation for submission to *Environmental Science and Technology* entitled "A hydrodynamics-based approach to evaluating the risk of waterborne pathogens entering drinking water intakes in a large lake" and authored by Hoyer, A.B., Schladow, S.G. and F.J. Rueda.

Resumen

La contaminación de las aguas supone una amenaza para los ecosistemas acuáticos a nivel global, ya que perjudica el funcionamiento de los mismos así como su uso como recurso acuícola. La distribución de los contaminantes en estos sistemas se hace posible debido a la dispersión de los mismos, es decir, debido al transporte de substancias u organismos por el hecho de encontrarse en un fluido en movimiento. Es necesario, por tanto, conocer los movimientos de las masas de aguas en estos sistemas para determinar la distribución final de los contaminantes, su concentración, su destino, y, en definitiva el impacto potencial que tienen sobre los ecosistemas y sobre la salud humana. Tanto los movimientos (corrientes) de las masas de agua como las tasas de mezcla de las mismas pueden determinarse matemáticamente resolviendo las ecuaciones de advección-difusión, por lo que la aplicación de modelos hidrodinámicos para el estudio del transporte de contaminantes en sistemas costeros, ríos, embalses y lagos es una práctica común. En el caso concreto de los lagos, estas corrientes están inducidas por el viento, el oleaje y por procesos de tipo convectivo, y se caracterizan por ser de pequeña magnitud así como por su alta variabilidad espacio-temporal; sin embargo, el conocimiento sobre la distribución de los contaminantes por dichas corrientes es, a día de hoy, escaso.

*El objetivo de esta tesis doctoral es analizar la dispersión mediante las corrientes inducidas por el viento en lagos, de contaminantes vivos (organismos). Con este fin, se ha desarrollado un modelo de tipo mecanístico y lagrangiano, basado en la ecuación de reacción-advección-difusión. Dicho modelo consta de tres módulos (**R**esuspensión-**T**ransporte-**S**upervivencia) que representan los procesos básicos en la dispersión de contaminantes: (R) La incorporación de un contaminante dado a la columna de agua por resuspensión*

o liberación, (T) el transporte pasivo y la dispersión de dicho contaminante, y (S) la supervivencia (o inactivación) del mismo en función de las condiciones ambientales experimentadas durante el transporte. El objetivo específico de esta tesis es caracterizar los mecanismos de dispersión de contaminantes, las variaciones temporales y espaciales de las rutas de dispersión y la distribución final del contaminante. Para ello, el modelo de dispersión propuesto (modelo RTS) se ha aplicado en un lago alpino profundo y rodeado por una topografía compleja (Lago Tahoe, EE.UU) para analizar la distribución de dos organismos: Corbicula fluminea *(almeja asiática), un bivalvo invasor, y* Cryptosporidium *ssp., un patógeno humano.*

El incremento en la distribución espacial de las especies acuáticas invasoras (como es el caso de la almeja asiática) es una de las mayores amenazas ecológicas y económicas para los ecosistemas acuáticos a nivel mundial. Tan solo en EE.UU el número de especies invasivas (terrestres y acuáticas) establecidas es de aproximadamente 50.000, que causan pérdidas económicas estimadas en más de 120 billones de dólares. Además, los efectos no deseados sobre los ecosistemas, asociados a la presencia de estas especies invasoras, son el factor más importante a nivel mundial, después de la pérdida de hábitat, en cuanto a lo que a la amenaza de la biodiversidad se refiere. La almeja asiática es un ejemplo de especie invasora de aguas dulces y es una de las más agresivas a nivel mundial. Se considera que su mecanismo principal de dispersión local en el agua es el transporte hidráulico pasivo (natural) por medio de las corrientes, el cual tiene lugar en mayor medida durante las fases larval y juvenil, ya que, como resultado de su baja densidad, las larvas son capaces de mantenerse en suspensión en la capa de mezcla incluso durante niveles bajos de turbulencia. De esta forma, aún no teniendo la capacidad de moverse, estas larvas podrían potencialmente viajar grandes distancias gracias a las corrientes de agua. Sin embargo, la contribución de las corrientes de agua en la dispersión local de las larvas de la almeja asiática es, hoy en día, un factor desconocido y los estudios de laboratorio existentes, se han basado únicamente en el transporte de individuos adultos.

En esta tesis, se ha evaluado la dispersión local de las larvas de la almeja asiática en su fase planctónica (mediante transporte hidráulico pasivo) en el Lago Tahoe. La probabilidad de dicha dispersión, desde las poblaciones

existentes (con alta densidad de individuos) hasta nuevos hábitats, viene determinada por el régimen de viento, la magnitud de eventos de viento y de su ocurrencia temporal. La dispersión y migración de las larvas ocurre en forma de pulsos, en respuesta a eventos episódicos de viento fuertes y tiene lugar a través de un número discreto de rutas preferenciales. El impacto sobre la mortalidad de la almeja asiática de la radiación ultravioleta durante el estado pelágico es bajo ya que las distancias que recorren tras cada evento (pulso) son cortas, debido a la relativamente alta velocidad de sedimentación de las larvas y a los vientos predominantemente suaves observados en el Lago Tahoe. La distribución final de estas larvas dispersadas y su probabilidad de supervivencia son, por tanto, sensibles a la magnitud de la velocidad de sedimentación de las mismas. Esta sensibilidad se ve aumentada en las regiones del lago donde existen bahías, donde la recirculación del flujo (separación del flujo de las paredes laterales del lago) unido con la baja magnitud de las velocidades de la corriente, actúan como trampas de sedimentación para las larvas de especies bentónicas en suspensión.

Por otro lado, la contaminación por patógenos de los ecosistemas acuáticos se considera una de las mayores amenazas para la salud humana. En concreto, la distribución del parásito protozoico Cryptosporidium *spp o, mejor dicho, de sus oocistos, está extendida en lagos y embalses, incluso en los países desarrollados. Tan solo en EE.UU, se estima que en el 55% de las aguas superficiales y en el 17% de las fuentes de agua potable está presente* Cryptosporidium parvum. *Esto supone un problema para el abastecimiento de agua ya que* Cryptosporidium *tiene una alta resistencia a los métodos convencionales de desinfección como es el caso de la cloración. Además, el pequeño tamaño de sus oocistos, unido a su abundancia, ha provocado brotes infecciosos tanto en aguas potables como en las de tipo recreativo. A pesar de estos hechos, según la literatura, no existe estudio alguno sobre el riesgo de contaminación por patógenos de las tomas de agua potable en lagos y embalses que resuelvan el transporte y la circulación costera en los mismos y que tengan en cuenta la inactivación de los patógenos por la temperatura y la luz.*

Otro objetivo de esta tesis es, por tanto, analizar y cuantificar el riesgo de patógenos humanos acuáticos infecciosos liberados en playas recreativas

llegasen a una toma de agua en el Lago Tahoe. Para ello, se ha analizado el riesgo de contaminación por Cryptosporidium *utilizando una versión modificada del modelo de dispersión RTS, en el que se incluye una técnica novedosa capaz de calcular, en el punto de interés (toma de agua), el movimiento seguido por los patógenos desde las fuentes (playas de uso recreativo) hasta llegar a ese punto. Esta técnica permite estudiar la contaminación difusa con un coste computacional moderado y permite identificar períodos de tiempo potenciales de contaminación del agua potable. El estudio de la dispersión de* Cryptosporidium *en el Lago Tahoe revela que el riesgo de que patógenos humanos acuáticos, provenientes de playas de uso recreativo, lleguen a la toma de agua potable viene determinado por la profundidad de la termoclina con respecto a la profundidad de la toma de agua: El riesgo de contaminación por patógenos aumenta a lo largo del verano con el aumento de la profundidad de la capa de mezcla y aumenta, a escala diaria, durante la noche, cuando la capa de mezcla aumenta en profundidad debido a la mezcla convectiva. Además, la radiación solar actúa como un desinfectante natural del agua, reduciendo el riesgo de contaminación.*

El trabajo presentado en el capítulo 2 ha sido aceptado para ser publicado en Journal of Environmental Management *con el título "A 3D individual-based aquatic transport model for the assessment of the potential dispersal of planktonic larvae of an invasive bivalve" con Hoyer, A.B., Wittmann, M.E., Chandra, S., Schladow, S.G. y F.J. Rueda de autores. El estudio de los mecanismos de dispersión presentado en el caítulo 3 está actualmente en revisión por* Limnology and Oceanography: Fluids and Environment *con el título de "Local Dispersion of Invasive Bivalve Species by Wind-driven Lake Currents" con Hoyer, A.B., Schladow, S.G. y F.J. Rueda de autores. Por último, el capítulo 4 sobre el riesgo de contaminación de las tomas de agua potable por patógenos humanos acuáticos está en preparación para ser enviado a* Environmental Science and Technology *con el título "A hydrodynamics-based approach to evaluating the risk of waterborne pathogens entering drinking water intakes in a large lake" y con Hoyer, A.B., Schladow, S.G. y F.J. Rueda de autores.*

Thanks to

Francisco Rueda for his critical comments, brilliant ideas, generous help and support. For introducing me to the world of Computational Fluid Dynamics. For his constant strive for perfection. For always keeping an open door.

Geoff Schladow for his encouragement, insightful comments and revisions. For generously funding me during the final phase of this thesis. For kindly hosting me at the Tahoe Environmental Research Center.

Everyone who has directly or indirectly contributed to making this thesis possible. In particular, to Marion Wittmann for her constructive comments, her help and positive feedback. To Sudeep Chandra for having me in the project. To Mario Acosta for the parallelization and optimization of the hydrodynamic model. To Kristin Eastman Reardon, Marion Wittmann, Bill Fleenor, Simon Hook and Todd Steissberg for providing the field data. To Patricio Moreno and Fabian Bombardelli for providing the wave model. To Oliver Ross for his help during the development of the particle tracking model. To Luis Cruz for signing the original project proposal of the PhD fellowship. To Michael Anderson and Ben Hodges for evaluating the thesis. To Julia Leschinski, Cintia Ramón, Antonio Ureña and Emilio Moreno for kindly proof reading.

My Colleagues Anna, Kristin, Emilio, Cintia, Alicia, Mario and Alex (just to name of few) for their help, discussion and feedback. For being there during long office hours and short coffee breaks. To Alicia for guiding me through the jungle of university administration.

My Friends, Julia, Isabel, Julius, Martin, Marc, Antonio, Laura, María José, Charo, Yolanda, Cristina, Nona, María José, Javier, Paloma, Axel, Martín, Ángel, Josu, Steffi, Rüdiger, Martina and many others for the great company along the path, trail and run.

My Family (last but not least), Annemarie, Frank and Silke, for their unconditional love and support. For encouraging me in all my plans.

Contents

List of Figures

List of Tables

Chapter 1

Introduction and objectives

Water contamination endangers aquatic ecosystems worldwide. The contamination of aquatic ecosystems impairs the system's functioning and its use as water source for a particular purpose. Water sources are used, for example, for drinking water, industry, or recreation. A contaminant is any substance or organism released accidentally or deliberately into a system, where it is not naturally present or in concentrations above the natural concentration. Common contaminants of aquatic ecosystems are temperature increase (Teixeira *et al.*, 2009), organic (Koelmans *et al.*, 2001) and inorganic chemicals (Gillis, 2012), radioactive substances (Kryshev, 1995), pharmaceuticals (Heberer, 2002), invasive species (Wilcove *et al.*, 1998), and water-borne pathogens (Signor *et al.*, 2005). The source of contaminants can be local (point-source) or wide spread (non-point source). Typical point-sources are river inflows (Hipsey *et al.*, 2004; MacIntyre *et al.*, 2006), water discharge (MacIsaac *et al.*, 2002), or isolated populations of invasive species (Griffiths *et al.*, 1991), where as non-point sources are, for example, surface run-off (Walker & Stedinger, 1999), sediment resuspension (Zeng & Venkatesan, 1999) or recreational activities (Abdelzaher *et al.*, n.d.). The near-shore of aquatic ecosystems is prone to perturbations, typically induced by anthropogenic activities (e.g. Carpenter *et al.*, 1998; Liu *et al.*, 2006; Wang *et al.*, 2011).

The distribution of contaminants within a given ecosystem is possible due to dispersal, i.e. the transport of a substance or organism by the movements of the ambient water. Water movements are able to transport contaminants large distances through currents and maintain it in suspension through turbulent diffusion, while dispersing it at the same time. The knowledge and

understanding of these movements is necessary to determine the contaminant's final distribution, its concentration or dilution, its fate, and, thus, the potential impacts on ecosystems and human health. Water currents and mixing can be measured in the field or be determined mathematically by resolving the advection-diffusion equation (ADE), also known as transport equation. The solution of the ADE is approximated numerically by dividing the water column at given location with the system into a number of vertical layers (computational grid). For this location, one can determine and predict the spatio-temporal variations over a given period of interest. Where the lake bottom morphology (bathymetry) is known, the lake can be represented by a high number of vertical columns to resolve the system in the three-dimensional (3D) space. This way, numerical models are used to determine and predict water movements over large temporal scale and at high spatial resolutions, which are difficult or even impossible to measure in the field. Hydrodynamic transport model have been successfully applied for the study and analysis of contaminant transport in rivers (Wu *et al.*, 2009), coastal systems (Grifoll *et al.*, 2013), reservoirs (Hipsey *et al.*, 2004) and lakes (Rueda *et al.*, 2008).

The fate of a contaminant in a given system is determined by the environmental conditions, such as temperature and solar radiation, which may influence the contaminant's survival or inactivation (e.g. Brookes *et al.*, 2004b). In stratified lakes or reservoirs, these environmental stressors are seldomly constant in space or time, but exhibit spatio-temporal variability. Further a contaminant suspended in surface layers may change its vertical position continuously between the surface and the depth of the surface mixed layer driven by turbulent mixing. Due to these variations in environmental conditions encountered by a contaminant during the dispersion process, the survival of a given individual depends to a large extent on the particular conditions endured during its trajectory. Within a known flow field, individual particle trajectories can be determined and tracked using Lagrangian, individual-based models. Individual-based models have been applied for the study of larval dispersal of marine species (Guizien *et al.*, 2006; Tang *et al.*, 2006; Nickols *et al.*, 2012). Tang *et al.* (2006), for example, studied the hydrodynamic connectivity and its effect on the dispersal of the pelagic fish

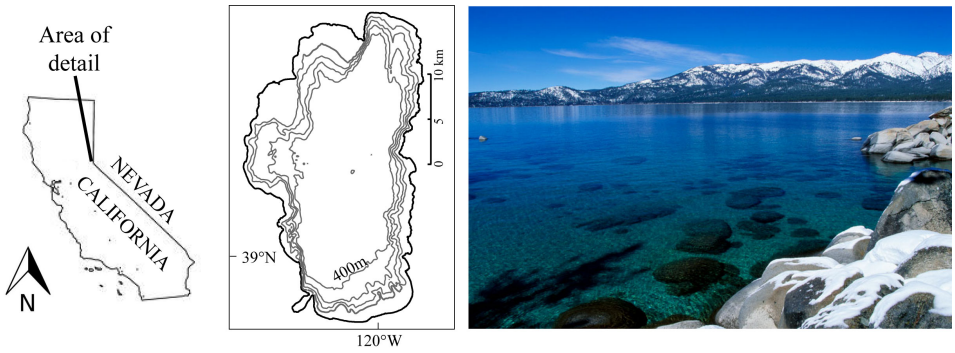

Figure 1.1: Lake Tahoe location, shoreline, bathymetry (at 100m intervals) and impression.

larvae between coral reefs. Guizien *et al.* (2006) used an individual-based model based on a 3D coastal circulation model to analyze the dispersal of the motile larvae of a benthic species by wind driven currents. A 2D individual-based model was applied by Nickols *et al.* (2012) of the planktonic marine larvae in the coastal boundary layer along the Californian coast. In contrast to coastal system, currents in lakes can have additional complexities, driven as they are by episodic, variable wind, subject to waves and convective processes, and with the interaction of boundaries. However, little is known to date about the dispersion of contaminants by wind-driven lake currents (Rueda *et al.*, 2008).

The objective of this thesis is to analyze and understand the passive dispersal of contaminants by wind-driven lake currents. For this purpose, a mechanistic individual-based model grounded on the reaction-advection-diffusion equation has been developed (dispersal model hereafter). The particular aim is to characterize the mechanisms of dispersal and the temporal and spatial variations of the pathways, for the study case of Lake Tahoe, USA (Fig.1.1). The dispersal model has been applied to study the distribution of two living contaminants: (i) one of the most aggressive freshwater invaders worldwide (McMahon, 1999), the invasive bivalve *Corbicula fluminea* (Asian clam) (Fig.1.2a,b), and (ii) a human water-borne pathogen, *Cryptosporidium* ssp. (Fig.1.2c,d), that has caused many public health outbreaks (cryptosporidiosis) in drinking as well as recreational waters (MacKenzie *et al.*, 1994; Yoder *et al.*, 2004). This thesis is organized as follows. First the

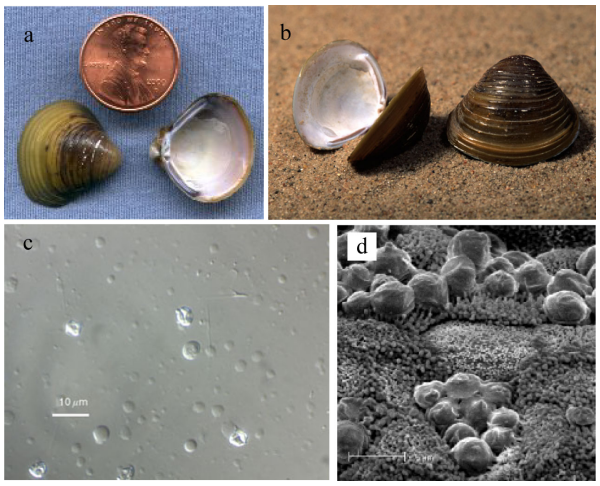

Figure 1.2: Contaminants: (a) Asian clam *Corbicula fluminea* and (b) shells on the beach (photographer: J. Van Arkerl), and (c) *Cryptosporidium parvum*, differential interference contrast (DIC) image of oocysts (photographer: H.D.A Lindquist, U.S. EPA) and (d) oocysts on an intestinal cell surface (photographer: Dr. U. Hertzel).

dispersal model is presented and applied to the potential dispersal of Asian clam. Next, the mechanisms of species dispersal, their dependence on the local wind forcing and the consequences for the existing population are determined. Finally, the risk of drinking water contamination by *Cryptosporidium* was analyzed using a modified version of the dispersal model, including a novel technique of back-tracking pathogens from the point of concern (water intake) toward the source regions (recreational beaches). This technique allows studying non-point contaminations at a feasible computational cost, and identifying time periods of potential drinking water contamination.

A detailed and specific introduction is given in each of the Chapters 2-4, which are written as stand alone chapters. Some of the information presented in the first figure of each chapter (Lake Tahoe location) and the methods section is partially repetitive. The intention of this repetition is to provide the reader with all necessary information within the specific chapter and, thus, avoid the necessity of going back to previous chapters in search of missing information.

Chapter 2

A 3D individual-based aquatic transport model for the assessment of the potential dispersal of planktonic larvae of an invasive bivalve

Abstract

The unwanted impacts of nonindigenous species have become one of the major ecological and economic threats to aquatic ecosystems worldwide. Assessing the potential dispersal and colonization of nonindigenous species is necessary to prevent or reduce deleterious effects that may lead to ecosystem degradation and a range of economic impacts. A three dimensional (3D) numerical model has been developed to evaluate the local dispersal of the planktonic larvae of an invasive bivalve, Asian clam (*Corbicula fluminea*), by passive hydraulic transport in Lake Tahoe, USA. The probability of dispersal of Asian clam larvae from the existing high density populations to novel habitats is determined by the magnitude and timing of strong wind events. The probability of colonization of new near-shore areas outside the existing beds is low, but sensitive to the larvae settling velocity w_s. High larvae mortality was observed due to settling in unsuitable deep habitats. The impact of ultraviolet radiation on Asian clam mortality during the pelagic stages was low. This work provides a quantification of the number of propagules that may be successfully transported as a result of natural processes and in function of population size. The knowledge and understanding of the relative contribution of different dispersal pathways may directly inform decision-making and resource allocation associated with invasive species management.

2.1 Introduction

The spread of aquatic nonindigenous species (NIS) is one of the major ecological and economic threats to lakes and waterways worldwide (Wilcove *et al.*, 1998; Pimentel *et al.*, 2005). In the US alone, there are about 50,000 invasive species (terrestrial and aquatic) established that cause economic losses estimated at more than $120 billion per year (Pimentel *et al.*, 2005). The introduction and establishment of NIS may cause dramatic changes to ecosystems through perturbations to inter-specific competition, predator-prey interactions, food web structure, nutrient dynamics, hydrologic cycle, and sedimentation rates (Cox, 1999; Simberloff, 2005; Tatem *et al.*, 2006). Unwanted effects associated with invasive species have been ranked second only to habitat loss in the factors that threaten native biodiversity at the global scale (Wilcove *et al.*, 1998).

Species invasions are a multiple stage process comprised of transport and introduction of organisms to a novel habitat from the native range, establishment of self-sustaining populations within the new habitat, and secondary spread of the organism to nearby habitats (Kolar & Lodge, 2001). Preventing NIS introductions is likely the most efficient strategy to reduce damages associated with invasions, and is a key component of invasive species management programs (Leung *et al.*, 2002; Ricciardi & MacIsaac, 2008). However, even the most effective prevention efforts do not eliminate all introductions, and some species will establish and have undesired ecological and economic impacts. Thus, the development of management guidelines for early detection (e.g. through surveillance and monitoring), control and/or eradication (e.g. through biocontrol, physical removal, pesticide treatment, etc.) is also a critical tool necessary to maintain the ecological integrity of un-invaded habitats (Vander Zanden *et al.*, 2010). Given the limited resources available to natural resource managers, investment in the detection or control of NIS depends upon the severity of the potential negative effect, as well as the probability (or likelihood) of the invasion to occur (Andersen *et al.*, 2004; Keller *et al.*, 2009). Thus, the ability to predict spatially explicit probabilities of where NIS may establish is a valuable component to the development of both preventative and invasive species management.

A number of mathematical models have been used to predict the likelihood of invasion. For example, species distribution models are generally applicable over large spatial extents, and estimate species establishment as a function of climate or environmental variables in the native range and the availability of suitable habitat in a novel range (Hortal *et al.*, 2010; Poulos *et al.*, 2012; Schleier III *et al.*, 2008). Reaction-diffusion-equation (RDE) models have been used to describe species dispersal as a function of local population growth and radial population spread (see for example Shigesada & Kawasaki, 1997). RDE models have also been modified to include long-distance dispersal events, which have formed the basis for a federal program to control gypsy moth invasion in the U.S. (Liebhold *et al.*, 2007). Where dispersal is mediated by animal or human movement and the movement pathways (vectors or invasion corridors) are known, gravity models have been used to estimate the overland dispersal of NIS to unconnected waterways (MacIsaac *et al.*, 2001; Leung *et al.*, 2004). A particle transport coupled with a growth model was used by Beletsky *et al.* (2007) to analyze the dispersal and recruitment of yellow perch larvae in Lake Michigan.

This work focuses on the passive dispersal of planktonic larvae entrained by wind-driven currents in lakes. We assess the likelihood of local dispersal of one of the most aggressive freshwater invaders worldwide (McMahon, 1999), the invasive bivalve Asian clam (*Corbicula fluminea*), in Lake Tahoe (USA, Fig.2.1). Asian clam was first observed in Lake Tahoe in 2002 in low abundances, but its population has since increased to nuisance level densities ($> 10^3 ind.m^{-2}$) with unwanted impacts to shoreline aesthetics (Hackley *et al.*, 2008; Wittmann *et al.*, 2012) (Fig.2.1d). No work to date has been conducted to evaluate the dispersal of NIS in this lake and little is known about NIS dispersal in other large lake ecosystems (Griffiths *et al.*, 1991). We utilize a mechanistic individual-based model grounded on the reaction-advection-diffusion equation to quantify the dispersal of Asian clam larvae from existing colonies to different locations in the lake. This work is organized as follows. First the conceptual model designed and used to represent the behavior of larvae (dispersal model here after) is described. Next, the modeling tools (i.e. wave, hydrodynamic, and particle tracking model) the dispersal model is based on are outlined. Finally, the results of the model

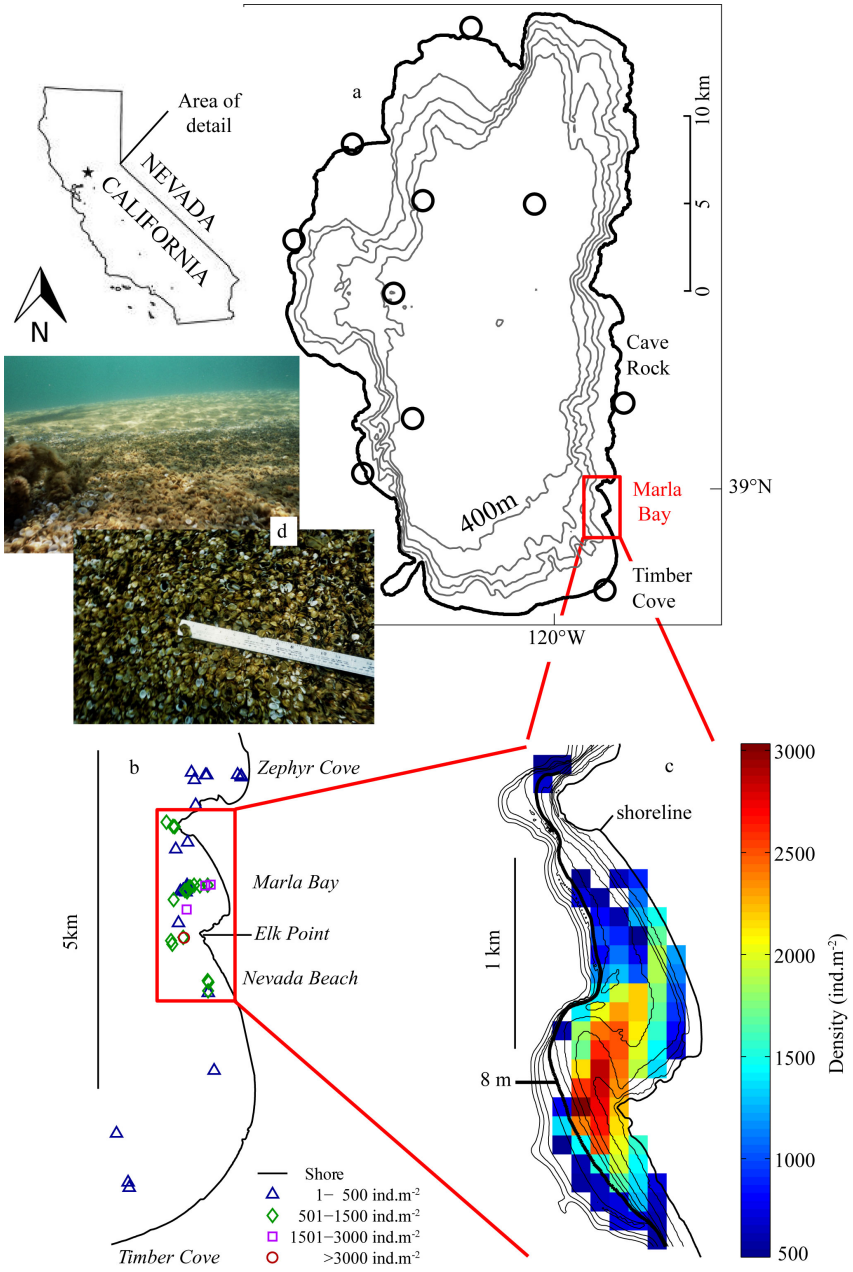

Figure 2.1: Lake Tahoe (a) location and bathymetry (at 100m intervals), location of meteorological stations (circles), and area of interest. Density distribution of Asian clam adult population in 2005, (b) discrete sampling locations (Wittmann *et al.*, 2009), (c) interpolated clam densities ($> 500 ind.m^{-2}$), black lines mark depth contours (1,2,3,4,5,8,10,20,30 and 40m) for orientation, 8m contour marked for reference, and (d) high density clam beds (taken from Wittmann *et al.* (2009).

application to Lake Tahoe are presented focusing on the final dispersion map. This map represents the probability of transport of viable larval individuals based on the transport pathways and environmental stressors (temperature and light) experienced by the particles during their journey.

2.2 Methods

2.2.1 Approach

A Lagrangian, individual-based model has been developed to predict the local dispersal of particles representing any tracer (i.e. passive substance or organism), such as Asian clam larvae, by lake currents. The final particle distribution is then used to assess the probability of dispersal and settling in new suitable areas from localized areas where Asian clams are known to exist. The individual-based model consists of three modules, run sequentially but independently of one another. The first module (release module) represents the growth of larvae in existing beds and their incorporation into the water column through entrainment. The second module simulates the passive dispersal and settling of larvae during a period of time T. This module, referred to as the transport module, tracks the position and the environmental conditions (water temperature and radiation levels) experienced by each individual. The third module estimates the probability of larvae survival as they are transported and settle to the sediment (survival module). Individuals are considered to have colonized new near-shore areas if (i) they settle in favorable habitats and (ii) the environmental conditions endured in the pelagic do not affect their viability. This model is termed RTS model (for **R**elease-**T**ransport-**S**urvival). The different modules are designed so that they can have different time resolutions, Δt, and therefore different numbers of time steps n. R, T and S are used as subscripts to specify the module to which variables (time steps and number of steps) refer to. A Cartesian grid discretizes the physical domain and the larvae locations in the computational grid will be indicated by the indexes (i, j, k) for the E-W, N-S and vertical direction, respectively. The sequence of calculations done in the RTS model to estimate dispersion maps is presented in Fig.2.2.

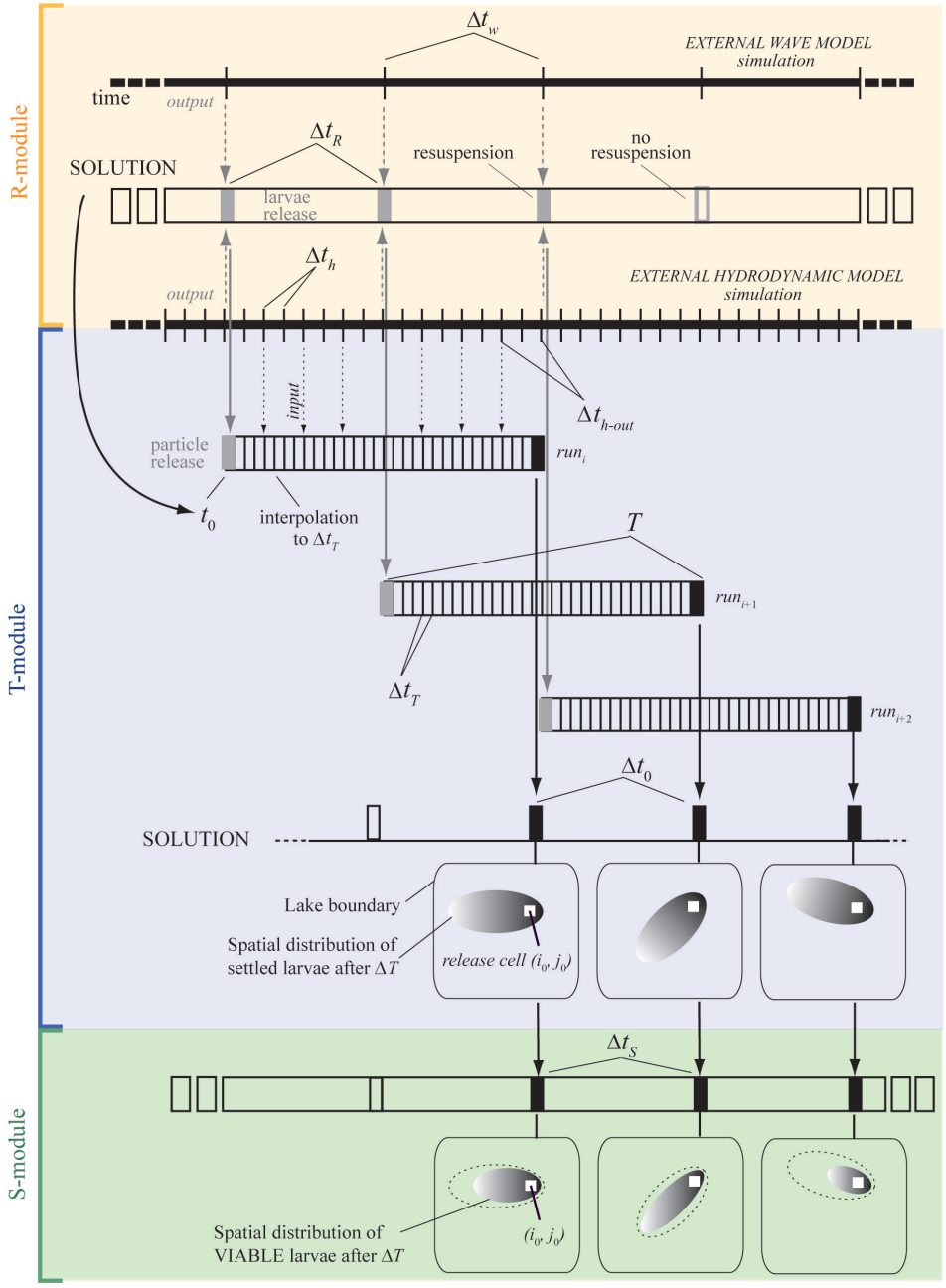

Figure 2.2: Flow diagram of larvae dispersal model. Horizontal lines represent time lines (simulations and runs). Thin vertical bars mark time steps. Thick vertical bars mark module solutions and beginning/end of transport simulations. Solid vertical arrows show dependencies between modules. Dashed vertical arrows show output/input dependencies. Shaded ellipses represent model output of final larvae distribution and the indices i_0, j_0 indicate the point of larvae release into the pelagic (*see* Methods for details).

2.2.2 Release module

The larvae population existing at the lake bottom at any given location (i, j) of the computational domain and available for entrainment at time t will be referred to as $L_{ij}(t)$. The number of larvae existing at time $t + \Delta t_R$, $L_{ij}(t + \Delta t_R)$ is calculated as a function of the population at the previous time $L_{ij}(t)$ as follows

$$L_{ij}(t + \Delta t_R) = L_{ij}(t) + \underbrace{\mu_g A_{ij} \Delta t_R}_{1} - \underbrace{\mu_d L_{ij}(t) \Delta t_R}_{2} - \underbrace{\delta_{ij}(t + \Delta t_R)}_{3} \quad (2.1)$$

The terms (1)-(3) represent the three processes contributing to the change in the number of larvae. The production of new larvae (term 1) is modeled as a zero-order process, with a reproduction rate μ_g proportional to the number of adults, A, existing at site (i, j), A_{ij}. The population A_{ij} is considered constant in time, as Asian clam larvae reach maturity 3-9 months after their release (Sousa *et al.*, 2008). The decay processes (term 2) are assumed to follow a first-order model. The decay rate, μ_d, represents the rate at which larvae die and become unavailable for dispersal. The third term represents the effects of entrainment processes on the larvae population. Here larvae are assumed to behave like passive and negatively-buoyant particles, similar to non-cohesive sediment particles. Accordingly, larval entrainment can be parameterized in terms of the ratio of the bottom shear (or friction) velocity u_* to the particle settling velocity w_s, u_*/w_s (Bagnold, 1966), widely used for sediment resuspension. The shear velocity at the bottom u_* is largely determined by the hydrodynamic conditions (wave-induced orbital motions and current-induced motions) at the sediment-water interface, and will vary in space and time. The wave-induced shear velocity is calculated using a wave model, current-induced shear stress, in turn, is calculated with a three dimensional (3D) hydrodynamic model. All individuals existing at time t on cell (i, j) will be entrained and incorporated in the water column if the ratio $u_*/w_s > 1$ (Bagnold, 1966). In that case, the larvae population at that cell is 'reset' to zero, i.e. $L_{ij}(t+\Delta t_R) = 0$. Otherwise, the population will continue growing and decaying as dictated by terms (1) and (2). Consequently, the

last term δ_{ij} accounting for the effect of entrainment processes on larval growth takes the following non-linear form

$$\delta_{ij}(t+\Delta t_R) = \begin{cases} L_{ij}(t) + \mu_g A_{ij} \Delta t_R + \mu_d L_{ij}(t) \Delta t_R & \text{if} \quad \dfrac{u_*(t+\Delta t_R)}{w_s} > 1 \\ 0 & \text{otherwise} \end{cases} \tag{2.2}$$

This entrainment term links the release module to the transport module. All larvae existing on cell (i, j) and entrained at time t become available in the water column for transport by lake currents (simulated in the transport module) at time $t + \Delta t_R$. The entrained larvae are presumed uniformly distributed either over the water column of depth $H(i, j)$ or over a fraction f of H. To parameterize the height above the sediments up to which the particles are entrained, the non-dimensional suspension number Z proposed by Rouse (1937) (also known as Rouse number) is used,

$$Z = \frac{w_s}{\kappa u_*} \tag{2.3}$$

where κ is the von Kármán constant ($= 0.4$). For $1.2 < Z < 2.5$, particles are entrained up to mid-water depth ($f = 0.5$); and for $Z < 1.2$, entrained particles are distributed over the entire water column ($f = 1$). Temporal variation of the larvae population temporal is independent of larval settling, which implies that larvae that settle after being in suspension burrow into the sediment substrate and do not contribute to the larvae population available for entrainment. This is equivalent to assuming that the time during which larvae are incapable of settling (pre-competency period, e.g. Gaylord & Gaines, 2000) is zero, and was taken to make the different modules independent.

2.2.3 Transport module

The transport module simulates the horizontal and vertical displacement and the environmental conditions experienced by individual larvae that have been entrained at any given time from a grid cell in the existing clam beds. The 2D time varying particle tracking model used by Rueda *et al.* (2008) was

Table 2.1: Model parameters.

Symbol	Parameter	Value/ Range	Units	Comments/Reference
tl	Length of study period	2	month	Reproduction period (Denton *et al.*, 2012)
θ_{min}	Minimal temperature for reproduction	15	°C	McMahon (1999)
θ_{max}	Lethal temperature	30	°C	McMahon (1999)
Δt_R	Time step of release module	6	h	-
Δt_T	Time step of transport module	10	s	Ross & Sharples (2004)
Δt_0	Time between consecutive particle	6	h	-
T	Length of particle tracking simulation	2	d	Kraemer & Galloway (1986)
Δt_s	Time step of survival module	6	h	-
μ_g	Larvae growth rate	10	d^{-1}	Denton *et al.* (2012)
μ_d	Larvae decay rate	0.1	d^{-1}	Jørgensen (1981)
ρ_w	Water density	10^3	kgm^{-3}	-
N_0	Number of released particles	10^4	ind.	-
k_{UV}	Attenuation coefficient of UV radiation	0.15	m^{-1}	Rose *et al.* (2009)
LD_{50}	Median lethal light dose	5×10^4	Jm^{-2}	Lewis & Whitby (1997), McMahon (pers. comm.)
m	Exponent of light probability function	1.45	-	Lewis & Whitby (1997)
H_{min}	Minimal water column depth	2	m	Wittmann *et al.* (2009)
H_{max}	Maximal water column depth	39	m	Wittmann *et al.* (2009)

adapted to simulate larval trajectories in three dimensions (*see* Appendix A-1). At the start of the simulation t_0, an elevated number of particles N_0 (to guarantee statistically significant results in each experiment), representing N_0 larvae, is uniformly distributed over a given fraction f of the water column (see Eq.2.3) at the horizontal cell (i_0, j_0). Each of those particles tracked in any given simulation is represented by the index l ($l = 1, N_0$). We will identify each simulation by the location and time of the release, and the fraction of the water column seeded, i.e. (i_0, j_0, t_0, f). The position of particle l at time t will, then, be referred to as $\boldsymbol{R}(l, t|i_0, j_0, t_0, f)$. Once settled to the sediments, the particle position will remain constant during the simulation time and will be given by $\boldsymbol{R} = (x_l, y_l, z_l)$, with $z_l = -H(x_l, y_l)$, where H is the water column depth at the horizontal position (x_l, y_l).

The transport module also tracks and outputs the temperature and solar radiation levels experienced by each individual particle, referred to as transport histories, during the simulations period T, $\theta(l, t|i_0, j_0, t_0, f)$ and $I(l, t|i_0, j_0, t_0, f)$ respectively. Of particular interest for the survival of clam larvae is the solar radiation in the ultraviolet (UV) wavelengths, which negatively affects many aquatic organisms (UV-B, 280-315nm) (Häder, 2003). The fraction of UV radiation (UVR) is estimated as 1% of the global radiation (Grant *et al.*, 1997). The UVR reaching a given individual l at time t is calculated from its vertical position $z(l, t)$, being positive from the surface downward, and the incident UVR reaching the free surface $I_0(t)$ (Wm^{-2}), as follows,

$$I(l, t) = I_0(t) \cdot exp\big[- k_{UV}(t) \cdot z(l, t)\big] \tag{2.4}$$

where $k_{UV}(t)$ is the UVR specific attenuation coefficient set to 0.15 m^{-1} in agreement with observations of Rose *et al.* (2009). The time-dependent UV intensity reaching a given particle is then used to calculate the UV dose over a given period of time. The light dose experienced by the individual l, as it travels in the pelagic, $Id(l, t)$ (Jm^{-2}), is calculated as the amount of

UV energy received, as follows

$$Id(l,t) = \sum_{t_0}^{t} I(l.t) \cdot \Delta t_T \tag{2.5}$$

Here Δt_T is the time step of the transport module. Note that the dose is a cumulative variable, and provides a measure of the energy above harmful levels that a given individual may have received, from time t_0 when it was entrained to the time it settles and burrows in the sediments at any given site, t_s $(t = t_s)$.

2.2.4 Survival module

The survival module uses the final particle position and particle transport histories simulated in the transport module to evaluate the probability of dispersal and settling of viable larvae in suitable habitats P_C. The probability P that larvae, released from site (i_0, j_0) at time t_0, will spread to new near-shore areas outside existing beds after the transport period T is evaluated for each cell (i, j). P depends on the probability of the larvae reaching a given horizontal cell (i, j) P_T, and the viability of those larvae P_V, i.e.

$$\begin{aligned} &P(i, j, t_0 + T | i_0, j_0, t_0, f) \\ &\qquad = P_T(i, j, t_0 + T | i_0, j_0, t_0, f) \times P_V(i, j, t_0 + T | i_0, j_0, t_0, f) \end{aligned} \tag{2.6}$$

The probability P_T, (first term on the right hand side) depends on the interaction between the physical processes of transport by currents and turbulence, and particle settling. The second term, P_V, represents the probability that larvae reaching a horizontal location (i, j) are viable to grow and, thus, colonize the lake sediments. For simplicity, it is assumed that all suitable habitats are equally favorable and that there is no demographic stochasticity. The number of particles that were released at cell (i_0, j_0) and time t_0, and are settled at a given location (i, j) of the lake bottom at time $t = t_0 + T$ is referred to as $N(i, j, t_0 + T | i_0, j_0, t_0, f)$ and was calculated as follows,

$$N(i,j,t_0+T|i_0,j_0,t_0,f) = \sum_{l=1}^{N_0} \delta[\boldsymbol{R}(l,t_0+T|i_0,j_0,t_0,f), \boldsymbol{S}(i,j,k_m(i,j))] \quad (2.7)$$

Here $k_m(i,j)$ is the index used in the model to point to the cell closest to the bottom in any given water column (i,j), and $\boldsymbol{S}(i,j,k_m)$ is the spatial domain of that bottom cell. The function δ is defined as follows,

$$\delta(R,S) = \begin{cases} 1 & \text{if} \quad \mathbf{R}(l,t_0+T|i_0,j_0,t_0,f) \in \mathbf{S}(i,j,k_m) \\ 0 & \text{otherwise} \end{cases} \quad (2.8)$$

The probability of one larva reaching the lake sediment substrate after a period of time T, is then calculated as the ratio of the number of particles settled at that cell by the total number of particles initially released

$$P_T(i,j,t_0+T|i_0,j_0,t_0,f) = \frac{N(i,j,t_0+T|i_0,j_0,t_0,f)}{N_0(i_0,j_0,t_0,f)} \quad (2.9)$$

The viability of the larvae reaching any given site is a function of the local habitat conditions and the ambient (temperature and light) conditions along the migration paths. Hence, the probability of a given individual, that has reached site (i,j) within time T after release, to grow and establish is represented as follows,

$$P_V(i,j,t_0+T|i_0,j_0,t_0,f) = P_H(i,j) \times P_S(i,j,t_0+T|i_0,j_0,t_0,f) \quad (2.10)$$

The first term refers to the probability that the larva encounters suitable conditions at the local habitat and is measured in terms of the type of sediment substrate and the water column depth at the point settled. The critical upper (H_{max}) and lower (H_{min}) water column depth for larvae sur-

vival define the limits for colonization. Hence,

$$P_H(i,j) = \begin{cases} 1 & \text{if} \quad H_{min} < H(i,j) \leq H_{max} \\ 0 & \text{otherwise} \end{cases} \tag{2.11}$$

The second term on the right hand side of Eq.2.10 represents the probability of survival and colonization due to the life histories. The probability of survival $P_S(l,t_0)$ of a given individual was evaluated based on the temperature and light history, and a generated random number from a uniform distribution in the range [0 1]. The individual will survive for $a \leq P_S$; but will be marked dead for $a > P_S$. The probability of survival is calculated as the product of the probabilities of survival due to temperature conditions P_θ and due to UV radiation P_I (i.e. $P_S = P_\theta \times P_I$). The model is developed under the assumption that water temperatures during the study period are favorable, and hence, $P_\theta = 1$. If LD_{50} refers to the median lethal dose of light for the larvae, the probability of survival P_I due to the effect of light, i.e. UVR, is evaluated as (Shen *et al.*, 2008)

$$P_I(l,t) = 1 - \frac{1}{1 + \left(\frac{LD_{50}}{Id(l,t)}\right)^m} \tag{2.12}$$

Here m determines the slope of the probability function.

2.2.5 Dispersion maps

Dispersion maps were constructed based on the series of simulations conducted with the T-module. For each simulation, the probability of any given cell (i,j) being colonized is calculated as in Eqs.(2.6)-(2.12). The probability of colonization of cell (i,j) during the study period is then estimated as the sum of the probabilities of being colonized by larvae entrained from any of the cells in the source area, as follows

$$P_C(i,j) = \frac{1}{L_T} \sum_{j_0=1}^{j_m} \sum_{i_0=1}^{i_m} \sum_{t_0=1}^{n_S} P(i,j,t_0+T|i_0,j_0,t_0,f) \times \delta_{i_0,j_0}(t_0) \tag{2.13}$$

Here, L_T represents the total number of larvae available for entrainment

during the study period. The constants i_m, j_m, and n_S represent the total number of grid cells in the i- and j- direction, and the number of time steps in the study period, respectively. All other functions and variables have been defined above. The ratio of $\delta_{ij}(t)/L_T$ is the fraction of larvae generated during the reproduction period entrained on any given cell and on any given time, and can be used to identify the conditions under which the risk of seeding and colonization increases.

2.2.6 Asian-clam dispersal in Lake Tahoe

The RTS model was applied to Lake Tahoe to simulate the dispersion of Asian clam larvae during their release period. Asian clams are highly fecund simultaneous hermaphrodites and brood their larvae in the inner demibranchs (gills). Asian clams are able to reproduce by self-fertilization and have a life span ranging from one to seven years (McMahon & Bogan, 2001). Water temperatures of Lake Tahoe are above the minimum value for clam reproduction (i.e. θ>15℃) between the beginning of July and end of September. Denton *et al.* (2012) observed a lag of 4 weeks between the time when water temperatures start to be suitable for Asian clam gamete production and the time when clams actively reproduce. Therefore, the study period starts at August 1 (day 214), after a month of suitable water temperatures, and lasts for two months, until day 274. The species' current known distribution (area $\simeq 10^6 m^2$, Forrest *et al.*, 2012) is patchy along the southeast and south shore of the lake, with the highest density populations established in Marla Bay (Fig.1). The density distribution of adults in the largest area of Asian clams identified to date (with clam densities in excess of $500\, ind.m^{-2}$) is shown in Fig.2.1c. This area is taken as the only source of larvae in the simulations and is referred to as the existing clam beds. All other locations in the lake were assumed to be non-colonized.

At the start of the study period, the larval population L was assumed to be zero, i.e. $L(0) = 0$. The R-module was run with a time step of $6h$, $\Delta t_R = 6h$, based on the output of the external wave and hydrodynamic models (see Fig.2.2). The T-module, in turn, was run with a time step $\Delta t_T = 10s$, to satisfy the convergence criterion for particle tracking simulations

proposed by Ross & Sharples (2004). The input predictions of current speed, current directions, vertical turbulence, and temperature in the 3D domain had previously been output (by the underlying 3D hydrodynamic code) at a time step of $1h$ and was then interpolated to the transport time step (see Fig.2.2). Clam reproduction was continuous and not bound to a specific time of the day, so that larvae were free to be entrained into the water column at every time step n_R, whenever shear conditions were favorable ($u_*/w_s > 1$). The settling velocity w_s was equal to $10^{-3}ms^{-1}$, based on laboratory experiments conducted with non-living juveniles in which the average w_s was $1.4 \times 10^{-3}ms^{-1}$ (Chandra, unpubl. data). The number N_0 of particles released at the start of each simulation was set to 10^4, above which the probability of settling was found invariant, based on a series of preliminary experiments. The simulation period of this module, T, is 2 days, equal to the maximum length of time that Asian clam larvae have been observed to persist in the pelagic (Kraemer & Galloway, 1986). The observed solar radiation was provided at $10min$ intervals. The solution of the T-module was output at the end of each 2-day simulation period (i.e. every $6h$), and it was with this time interval that the survival module was run ($\Delta t_S = 6h$), see Fig.2.2 for a schematic overview of the different time steps and periods. The probability of survival and colonization was evaluated based on parameter values found in the literature. Asian clams are found preferentially on coarse sand beds, which is the most common type of near-shore substrate along the shore line in Lake Tahoe (Herold *et al.*, 2007). Hence, the type of sediment substrate does not pose any limitation on the likelihood of colonization. The preferred depths of establishment of Asian clam range 2m to 39m Wittmann *et al.* (2009). The probability of survival was established based on UVR exposure only, given that temperature in Lake Tahoe is always within the acceptable range of temperature for Asian clam (3℃$<\theta<$30℃ McMahon, 1999). The particular values for the kinetic parameters used in the model runs are given in Tab.2.1. Note that some of the parameter values are specific for Asian clam. Other parameter values are taken from studies conducted on other bivalves, given that specific values for Asian clam have not been found in the literature. Hence, our results should be taken as a first estimate to characterize the probability of colonization of

Asian clam.

2.2.7 Wave and hydrodynamic variables

The wave-induced bottom shear stresses, used in the release module, were simulated using the phase-averaged spectral wave model STWAVE, a two-dimensional (2D) finite difference model developed by the U.S. Army Corps of Engineers Research and Development Center (ERDC Smith *et al.*, 2001). The model is based on the wave action balance equation (Smith, 2007) and has been previously used to model near-shore waves in lake environments (Chader *et al.*, 2006; Smith & Sherlock, 2007) with successful results in all cases. The model can use spatially variable winds, encountered in large systems surrounded by complex topography. Wind records collected at ten meteorological stations around the lake (Fig.2.1a) were corrected for height and roughness (*see* Appendix A-2), filtered and sampled at $6h$-intervals. Note that this time step was a compromise between the time of wave generation, estimated to be of the order of magnitude of 1h ($\mathcal{O}(1)h$) (Hamilton & Mitchell, 1996), and the computational cost. The interpolation method proposed by Barnes (1964) (*see* Appendix A-2) was applied to construct the spatially variable wind fields used to force the model. The same interpolation method was used to create the 10min wind field necessary to force the hydrodynamic simulations, used for the R-module (currents-induced shear) and the T-module (velocity field, vertical diffusivity and water temperature). The hydrodynamic simulations of lake currents and mixing variables were carried out using a parallel version of the 3D hydrodynamic model of Smith (2006) (Acosta *et al.*, 2010), and based on the numerical solution of the 3D form of the shallow water equation. The model has been extensively validated against analytical solutions (Rueda & Schladow, 2002) and field data sets (Rueda & Schladow, 2003; Rueda & Cowen, 2005) in particular for Lake Tahoe (*see* Appendix A-3). The model grid was constructed with a spatial resolution of $100m$ in both EW and NS directions. The vertical resolution was variable, ranging from $\Delta z = 0.5m$ at the surface to $\Delta z = 10m$ near the bottom (i.e. at a depth of $500m$). The bathymetry was from Gardner *et al.* (1998) and corrected in the southern near-shore region (T. Steissberg,

pers. comm.). The time step of the hydrodynamic model was $50s$, primarily based on stability considerations. The horizontal eddy diffusivity K_h was estimated based on the horizontal grid resolution and the time step, following Castanedo & Medina (2002), and set to $1m^2s^{-1}$.

2.2.8 Sensitivity analysis

A sensitivity analysis was conducted to evaluate the effects of selected model parameters on the probability of colonization predicted by the RTS model, and to quantify the possible changes in the dispersion maps if more accurate values are introduced in the model. This analysis is based on simulations conducted during a period of one week within the study period. A first-order variance analysis (FOVA), as outlined by Blumberg & Georgas (2008) and the associated dimensionless sensitivity coefficients to quantify model sensitivity were used. The dimensionless sensitivity coefficient S_p of any model output variable F (in our case, the probability of colonization after a given simulation period) to perturbations in any given parameter or forcing variable p was determined numerically as

$$S_p(p_0) = \frac{\Delta F/F(p = p_0)}{\Delta p/p_0} \tag{2.14}$$

where ΔF is the change in the output variable from a sufficiently small (typically $< 10\%$) change or perturbation in the parameter Δp from a reference value p_0. S_p can be interpreted as the percentage change in the output variable F resulting from a 1% uncertainty in the model parameter p. The fraction $\Delta F/F$ was evaluated as the L_1 norm (Trefethen & Bau III, 1997) of the difference between the output variable for the perturbed $F(p_0 + \Delta p)$ and non-perturbed $F(p_0)$ values of the parameter p. The L_1 norm was also used to evaluate the magnitude of $\Delta p/p_0$ in cases where the input variable was spatially variable. Once S_p is calculated for a range of parameters, a normalized measure of the output uncertainty $|S|$ can be estimated as

$$|S| = \sqrt{\sum_{i=1}^{n} S_{p(i)}^2} \tag{2.15}$$

where n is the number of parameters being considered in the sensitivity

analysis, and $S_p(i)$ is the dimensionless sensitivity coefficients to the parameter $p(i)$. One can also calculate the relative contribution R_i of each of the assessed input parameters to the total measure of output uncertainty as

$$R_i = \frac{S^2_{p(i)}}{|S|^2} \tag{2.16}$$

Equation 2.16 can then be used to rank the contribution of each input parameter, assuming that each is known within the same uncertainty range, to the total resulting uncertainty in F.

2.3 Results and discussion

2.3.1 Entrainment and dispersal in response to wind forcing

The probability of larvae being entrained in the water column and subsequently dispersed in the pelagic is tightly linked to wind forcing over the lake. A given wind event can be classified as strong or weak, depending on whether the condition expressed in Eq.2.2 ($u_* > w_s$) holds or not. Wind magnitude and direction, the depth of the water column or its geographical position control the magnitude of u_* and, thus, the timing and intensity of larvae entrainment.

If we consider a patch of cells, each developing a different value of u_* induced by wave and currents in response to a given wind forcing, the strength of the wind event is measured based on the fraction of the patch being entrained. Stronger winds, in general, will cause entrainment over larger areas. Figure 2.3, for example, shows the time series of wind speed and magnitude in Marla Bay during the study period, together with the time series of the fraction of the existing beds where entrainment conditions occur (Fig.2.3c).

Larval entrainment into the water column is controlled by wind-driven turbulence levels over the existing beds, but depends also linearly on (1) the time lag between consecutive strong events (*see* Eq.2.1), and (2) the density of the adult population in the area where entrainment occurs. The numbers of larvae entrained from the existing patches in Marla Bay (term δ_{ij} in Eq.2.1) are shown in Fig.2.4d. Note that the peaks in larval loads tend to occur during strong events, with few notable exceptions.

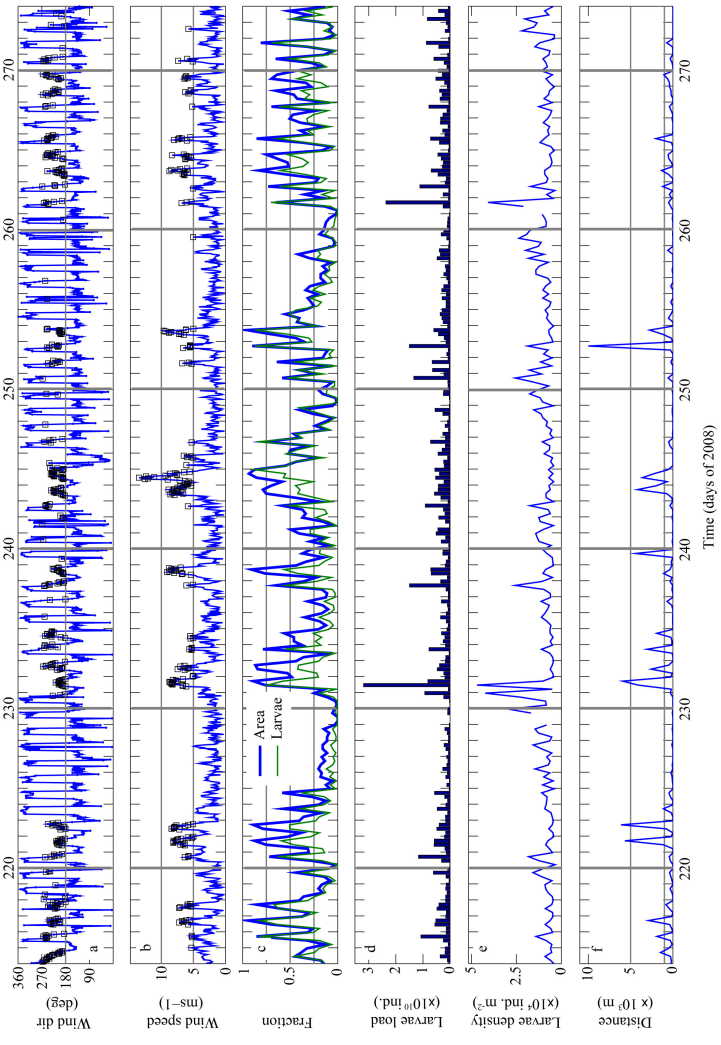

Figure 2.3: Dispersal response to wind forcing: (a) Wind direction (deg) (black squares mark SW events), (b) wind speed (black squares mark events $> 5ms^{-1}$), (c) area of infested clam beds subject to entrainment (thick line) as fraction of infested clam beds and number of entrained larvae (thin line) as fraction of larvae available at sediments, (d) larvae load per entrainment even, (e) entrained larvae density ($\times 10^4 ind.m^{-2}$), and (f) maximal dispersal distance ($\times 10^3 m$), black lines mark $10^3 m$ and $5 \times 10^3 m$ for reference.

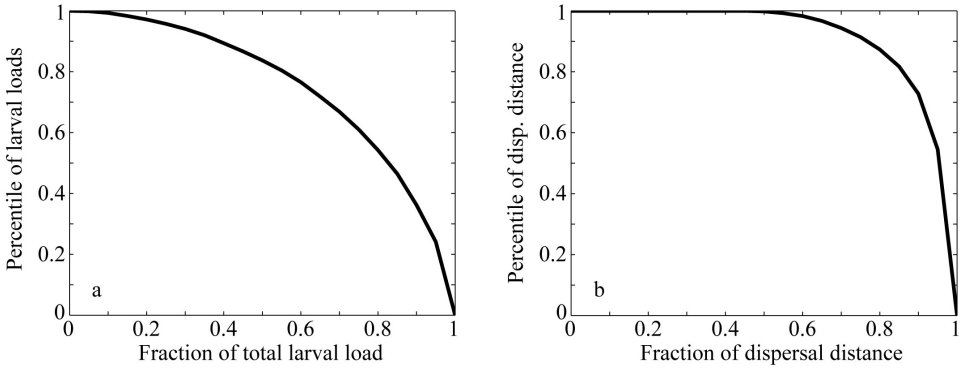

Figure 2.4: Probability distributions: (a) fraction of the load of larvae injected during an entrainment event (the summation of the term $\delta_{ij}(t)/L_T$ in Eq.2.2, for all cells in the existing beds) vs. percentiles of larval loads, and (b) fraction of total maximal dispersal distance $dmax_T$ vs. percentiles of maximal dispersal distance $dmax$.

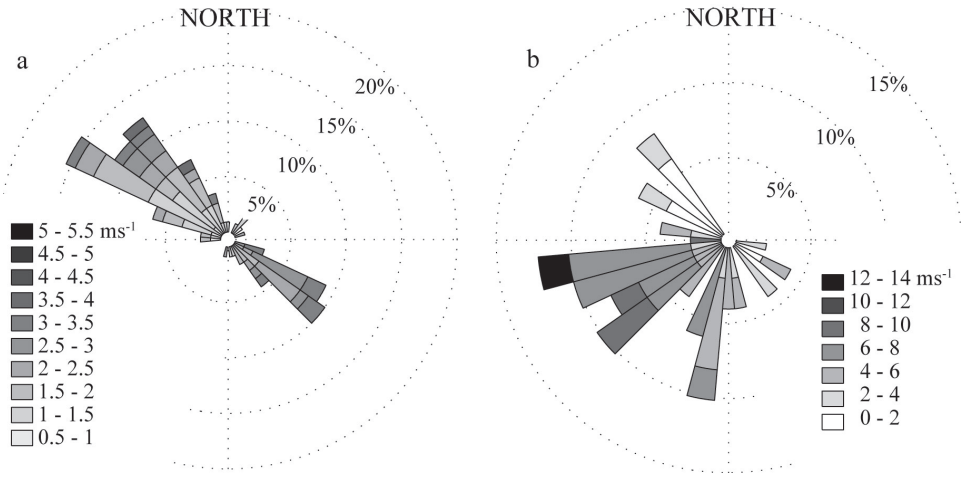

Figure 2.5: Predominant wind direction at Marla Bay for percentile of larvae loads (a) ≥ 0.4 and (b) < 0.4

For example, on day 221 and 222 two strong wind events induced entrainment conditions over a large fraction of the existing beds. Nevertheless, the number of larvae released in the water column (Fig.2.3c) was low, compared to the loads on day 220. The difference between loads is linked to the period of calm prior to the wind events. Prior to day 220, no significant entrainment occurred for a period of 2-3 days, which allowed the larval population to grow in abundance. The larval population at the sediment diminished in abundance by the entrainment event on day 220 and had only one day to increase before it was affected again by entrainment on day 221. As shown in Fig.2.3d, the largest peaks of larval loads occur after extended periods of calm wind conditions over the lake (see for example, the peak in larval load occurring on day 231, after 7 days of low winds). These events of entrainment account for a significant fraction of the number larvae seeded into the water column during the active period of reproduction. The fraction of the total load of larvae injected during an event is presented in Figure 2.4a against the percentiles of the larval loads. Winds over Marla Bay are predominantly weak and along the SE-NW axis (Fig.2.5a). Hence, the likelihood of entrainment conditions over the existing beds is only 10% during the study period. Note that 55% of the larvae are injected in the water column in the course of the 20% strongest events. The largest seeding events are driven by strong SW winds (Fig.2.5b) with maximum speeds exceeding $5ms^{-1}$ and it is during these events that the likelihood of entrainment from the existing patches increases consiberably. These conditions recur at a time interval of ca.7-10 days in Lake Tahoe (see Fig.2.3a-b).

Wind magnitude controls the rate at which larvae travel in suspension prior to settling. Figure 2.3e represents the distance the larvae are transported away from the existing beds (or dispersal distance) as a function of time. The maximal dispersal distance $dmax$ per entrainment event was calculated as the maximal distance from the point of larvae release to the point of final particle location ($dmax = max((x_0 - x_{end})2 + (y_0 - y_{end})^2)^{1/2}$). Larvae that settled at the cell of release (i_0, j_0) were assigned a dispersal distance of zero. In general, maximal dispersal distances are low ($< 10^3 m$, Fig. 2.3e) during periods of calm winds from N or SE. However, during continuous wind forcing from the SW with wind speed $> 5ms^{-1}$, larvae disperse

more than $5 \times 10^3 m$ away from the existing beds. Such long distance dispersal occurred, for example, on day 221, 231 and 252. Note that the time of maximal dispersal distance corresponds to the time of release t_0 and that subsequent wind conditions (Fig.2.4a,b) drive larvae dispersal. Considering that the area of infested clam beds is approximately 1km, larvae would have to disperse 1km to reach new habitats outside the existing beds. Larvae disperse $> 1km$ during 46 of the 61 days of study, hence, the probability of dispersal is approximately 0.75. Events of no dispersal, when larvae settle in proximity of the point of entrainment and replenish the existing clam population, occur generally at night or in the morning, with a probability of 0.35 (Fig.2.4,2.5b).

The timing of larval pulses into the water column and its subsequent dispersal have implications for risk management. The likelihood of larvae seeding and, in turn, the likelihood of colonization increase with increasing larval loads (see Eq.2.2). Consequently, cost-efficient monitoring programs should concentrate sampling efforts after strong SW events, after extended periods of calm. It is in response to those events, when larvae loads are highest and dispersal distance reach $\sim 5km$. Hence, monitoring programs should focus on bays within a 5-km distance from the existing patches.

2.3.2 Probability of dispersal and survival

The probability of viable Asian clam larvae reaching new areas away from the existing beds was 7%, taken as the sum of local probabilities outside the beds (see Fig.2.6). Close to the existing beds, the likelihood of transport and settling of viable larvae was highest but still did not exceed 0.1%. The probability of dispersal and settling in suitable habitats (i.e. the propagule pressure) decreased rapidly with distance away from the clam beds, and is largest north of Marla Bay along the eastern shoreline (Fig.2.6a). Almost 83% of the released larvae settled within the existing clam beds. Large spatial gradients in the probability of colonization and predominant probabilities of clam larvae settling in the areas of the existing population (self-seeding) is a common feature observed for benthic larvae. Siegel *et al.* (2003), for example, showed that short-lived pelagic larvae stages (<5d) are most likely

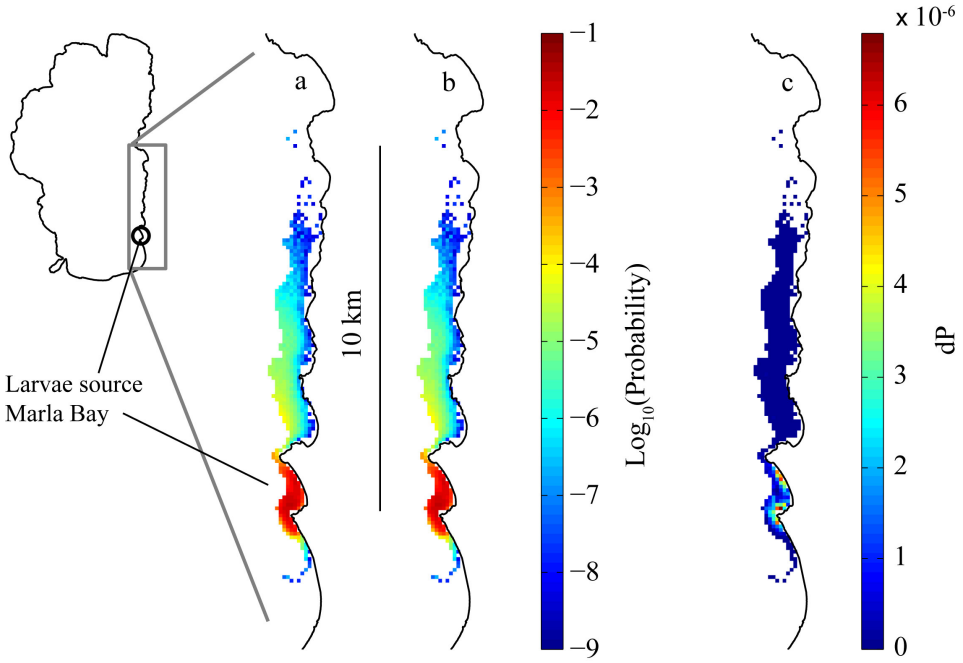

Figure 2.6: Dispersion map: Probability of survival (a) due to habitat P_H and (b) due to habitat and light P_C, and (c) and difference of probability $dP = P_C - P_H$

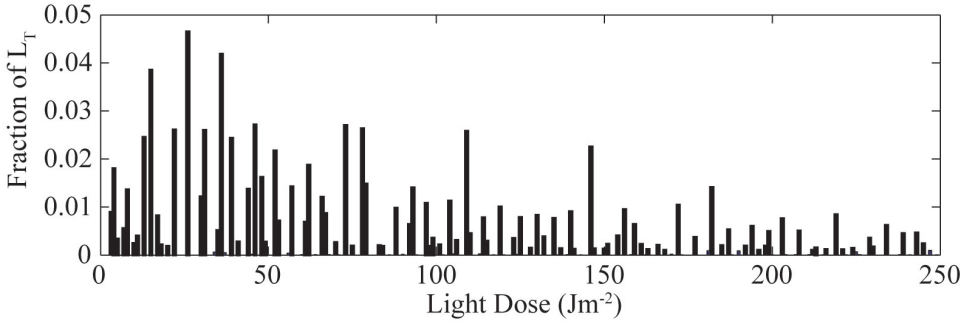

Figure 2.7: Histogram of light doses received by larvae on their migration paths. Number of larvae expressed as fraction of total number of particles (i.e. larvae) released L_T.

to replenish the existing population. Short dispersal distances, in general, will reduce the chances of the population to expand and colonize. On the other hand, it secures the persistence of the existing population. Settling in the existing beds guarantees a high probability of survival, as habitat conditions are favorable. Migration away from the existing beds contains a potential risk of mortality. Larvae migrating off-shore are more likely to die before they find shallow habitat. Approximately 10% of the larvae die due to unsuitable habitat conditions (depth$>H_{max}$). During events of alongshore dispersal, however, larvae are able to colonize. Long distance dispersal, like the dispersal 10 km northward along the eastern coast, has been reported previously in the literature. Coe (1953), for example, found that rare long-distance pulses of larvae dispersal were able to resurge the clam (*Donax gouldi*) population along the Californian coast. In Lake Tahoe, single clam adults have been observed 5-8 km from the core population in the Southeast as well as >10km away in the Southwest of the lake, but the larvae for these subpopulations may also be transported by human activity such as boat movement.

The main cause for larvae loss was depth limitation of suitable habitat and the impact of UV radiation was low. The vertical larvae position and the time a larva remains in suspension, or, equivalently, the exposure time, determined the light dose received by an individual. A 2d-exposure at the lake surface results in a light dose of $5 \times 10^5 Jm^{-2}$, considering average light intensities during the course of a day. The dose would be $2 \times 10^5 Jm^{-2}$ at

a depth of 8m, and only $2.4 \times 10^4 Jm^{-2}$ ($= 0.24 LD_{50}$), at a depth of 20m. With a settling velocity $w_s = 10^{-3} ms^{-1}$, a particle falls 20m in less than 6h, assuming that the vertical upward velocity associated to turbulent eddies is low compared to w_s, and the average light dose during that period would is $2.3 \times 10^4 Jm^{-2}$. In the existing beds, with a water column depth of 8m, the average suspension times for this settling velocity is 2 hours at most. The light dose experienced by those larvae settling near the colonized areas would only be 0.24 times the LD_{50}. Light doses experienced by the simulated particles during the study period varied between 0 and $2.5 \times 10^2 Jm^{-2}$ below the 99th percentile (Fig.2.7), with extreme values up to $1.3 \times 10^4 Jm^{-2}$. The maximal doses were, in any case, smaller than the critical value $LD_{50} = 5 \times 10^4$. The individual probabilities of mortality due to UV radiation ranged from 0 to 0.01, and, in consequence, the probability of settling and survival are nearly identical (Figs.2.6).

The spatial distribution of colonizing Asian clam larvae predicted by the model (Fig.2.6a) is consistent with observations of clam individuals north of Marla Bay along the eastern coast up to the latitude of Cave Rock (unpublished data). In general, proximity to a source of dispersing individuals increases propagule pressure (e.g., the number of individuals that are transported), and therefore the likelihood that an invasive species will establish (Lockwood *et al.*, 2005). Propagule pressure or the probability of dispersal, however, is to be discerned from the probability of establishment due to demographic or environmental conditions such as high juvenile mortality in bivalves, characteristics of the receiving microhabitat, or density dependence (Gosselin & Qian, 1997; Jerde & Lewis, 2007). Although Cataldo *et al.* (2001) found relatively low mortality rate of Asian clam larvae, the species (adults and larvae) is sensitive to low water temperatures during the winter period (Werner & Rothhaupt, 2008). In Lake Tahoe, surface water temperatures remain between 5 and 6 ℃ during a 3 month period between approximately day 15 and day 100; an exposure which may cause extensive mortalities. Consequently, only a low number of larvae released during the reproduction period, is expected to survive the winter conditions and contribute the maintenance of the established clam population.

2.3.3 Sensitivity analysis

The model sensitivity was analyzed based on four physiological traits characterizing the behavior of Asian clam larvae in the aquatic environment: (i) the settling velocity w_s, (ii) the larvae production rate and (iii) mortality rate in the source areas, and (iv) the median lethal light dose LD_{50}, determined with non-living juveniles. The settling velocity of living organisms, however, could be 60% lower than the velocities exhibited by their non-living counterparts with equivalent diameters (Reynolds, 1984). For $w_s = 0.6 \times 10^{-3} ms^{-1}$ (40% lower than the values shown in Table 1), the larvae could remain suspended in the 15-20m surface mixed layer for at almost 1 days, even if turbulence levels were low. The median lethal dose LD_{50} for UVR was taken from the existing literature for *Dreissena polymorpha* (zebra mussel) (Lewis & Whitby, 1997). Lewis & Whitby (1997) found that 50% of the population of zebra mussels died after an exposure of $\tilde{4}5$min to a constant UVR (365nm) of $2.85 Wm^{-2}$ ($LD_{50} = 7000 Jm^{-2}$). This light intensity was of the same order of magnitude as the incident UV-B intensity at Lake Tahoe, calculated from the meteorological observations. However, Asian clam larvae are exspected to exhibit a higher LD_{50}, because they are larger on release than zebra mussel larvae and have a better developed and thicker shell which makes them more resistant to harmful UV radiation (McMahon, pers. comm.). The growth rate was taken from observations of Asian clam reproduction in Lake Tahoe (Denton *et al.*, 2012). The decay rate was taken from the literature and was considered equal to those reported for blue mussel (*Mytilus edulis*) larvae in the pelagic phase (Jørgensen, 1981).

The settling velocity influences the results of all modules and is the parameter to which the model exhibits the highest sensitivity ($S_p = 1.37$, $R = 0.43$, *see* Tab.2.2). In the R-module it controls the magnitude and frequency of the pulses of larvae injected in the water column in response to wave or current-induced shear stress, and, therefore, the size of the larval population at the existing beds. In the T-module, it controls the length of time they remain in suspension, the horizontal extension of the sites that can be reached within the 2-days they are viable in the pelagic, and the light dose to which they are subject in the water column. In general, the

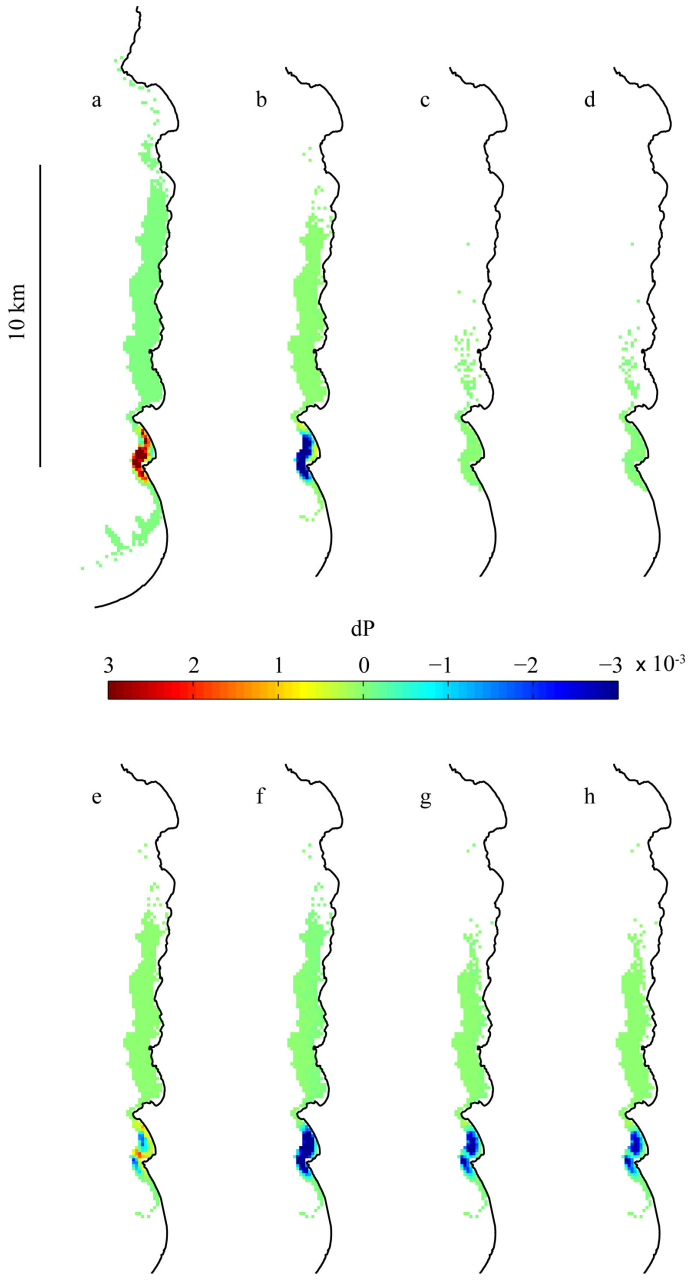

Figure 2.8: Difference in probability of colonization P_c obtained with reference values (see Fig.2.6b) and (a) P_c for settling velocity $w_s = 0.6 \times 10^{-3} ms^{-1}$, (b) $w_s = 1.4 \times 10^{-3} ms^{-1}$, (c) growth rate $\mu_g = 9d^{-1}$, (d) $\mu_g = 11d^{-1}$, (e) decay rate $\mu_d = 0.09d^{-1}$, (f) $\mu_d = 0.11d^{-1}$, (g) lethal dose $LD_{50} = 4.5 \times 10^4 Jm^{-2}$, (h) and $LD_{50} = 5.5 \times 10^4 Jm^{-2}$.

Table 2.2: Sensitivity coefficients S and R for dispersal model.

Model parameter	Baseline value	Perturbation			
	p_0	$p_0 \pm \Delta p$	$100(\%)$	$\frac{\Delta p}{p_0} \times S_p$	R
w_s (ms^{-1})	10^{-3}	0.6×10^{-3}	-40	0.9118	0.1899
	10^{-3}	1.4×10^{-3}	40	1.3739	0.4311
μ_g (d^{-1})	10	9	-10	0.6439	0.0947
		11	10	0.6439	0.0947
μ_d (d^{-1})	0.1	0.09	-10	0.6532	0.0975
		0.11	10	0.6351	0.0921
LD_{50} (Jm^{-2})	5×10^4	4.5×10^4	-10	0	0
		5.5×10^4	10	0	0

lower the settling velocity the weaker the bottom shear needed for larvae entrainment, the higher the frequency of entrainment events simulated in the R-module, the larger the area subject to entrainment and, consequently, the larger the number of larvae injected in the water column. On average, 2.85×10^5 larvae were entrained from a mean area of $3 \times 10^5 m^2$ during 98% of the study period for $w_s = 10^{-3} ms^{-1}$. For a 40% reduction in ws, an average of 3.5×10^5 larvae entrained from a mean area of $4.5 \times 10^5 m^2$ during 100% of the study period. As a result, the larval population tended to be more stable in simulations with lower ws. The maximal light doses received by individuals decreased with increasing ws. For example, light doses $61591 Jm^{-2}$ and $9743 Jm^{-2}$ for -40% and +40% of w_s, respectively, compared to $12987 Jm^{-2}$ for w_s $(= 10^{-3} ms^{-1})$ during the same period of time. However, less than 1% of larvae died in response to UVR, independently of the settling velocity w_s. The changes in the dispersion maps between the reference simulation and the simulations conducted with perturbed parameter values, were 43% ($S_p = 1.37$, $R = 0.43$). This difference in colonization probability was obtained for a 40% increase in w_s, mainly due to the higher accumulation of particles in the existing beds. For a 40% ws reduction, the sensitivity coefficient S_p was 0.91, with $R = 0.19$. The probability of colonization calculated by the model with a simulation period of one week, after a 40% reduction in ws (to a value of $0.6 \times 10^{-3} ms^{-1}$), are shown in Figs.2.8a. Note that the area with significant probability (taken as sites with $P_C > 0.0001$) is $19 \times 10^4 m$ (171% larger) for $w_s = 0.6 \times 10^{-3} ms^{-1}$, compared to $7 \times 10^4 m$

with the reference value ($w_s = 10^{-3} ms^{-1}$). The sites with significant risks in the simulations conducted with the lower settling rate extend further north, >10km north of Marla Bay, and south, down to Timber Cove, along the eastern coast. For a 40% increase in w_s ($= 1.4 \times 10^{-3} ms^{-1}$), dispersal is restrained (Fig.2.8b) compared to the reference simulations (Fig.2.6b). Due to the elevated settling rate, larvae sediment earlier and therefore, they do not reach as far north and south along the eastern coast, as well as close to the shoreline of the bays north of Marla Bay (e.g. Zephyr Cove).

The model is weakly sensitive to changes in growth or mortality rates. For example, a 10% change in the growth rate results in a 10% change in the larvae population, consistent with the zero-order nature of the growth model (Eq.2.1). Likewise the probability of colonization (Fig.2.8c,d) is equal for a higher/lower growth rate ($S_p = 0.64$). The effect of 10% change in the mortality rate on the larvae population is weaker (6%), given the first order kinetics used to simulate the decay of larvae in the bed. The colonization probability is more sensitive to a decrease in mortality rate ($S_p = 0.65$) compared to an increase ($S_p = 0.64$) (Fig.2.8e,f). In general, changes in growth or mortality rate have little effect on the probability of colonization compared to chance in settling velocity w_s. The critical light value LD_{50} is the parameter to which the model exhibits the lowest sensitivity ($S_p = 0$) (Fig.2.8g,h). Indeed, the number of particles affected by UVR during the study period is <1%, independently of whether the values of LD_{50} are subject to 10% changes. For a 10% reduction/increase in LD_{50} ($4.5 \times 10^4 Jm^{-2}$ and $5.5 \times 10^4 Jm^{-2}$, respectively), the sensitivity S_p is zero, that is the dispersion map remains unaffected by chances in the value of LD_{50}.

2.4 Summary and conclusions

A three-dimensional model of wind-driven dispersion patterns of juveniles of the non-indigenous Asian clam from existing beds areas has been developed. The model simulates the processes of entrainment, transport and survival of pelagic bivalve larvae in independent modules. The modules are used sequentially, hence, allowing one to separate the analysis of the different processes and factors influencing the spread of invasive species. The model

was applied to simulate the likelihood of Asian clam larval dispersal (e.g., propagule pressure) to near-shore areas around Lake Tahoe as a result of physical transport from existing Asian clam populations. The model predicts a small, but finite, likelihood of the dispersal and settling of viable larvae outside the existing population, rapidly declining with distance from these areas where settling is more likely to occur.

The results presented here suggest that the probability of dispersal is largely controlled by the wind regime, the magnitude of wind events and their timing. A large fraction of the larvae (almost 40%) were dispersed during these episodic wind events, increasing the likelihood of larvae entrainment, dispersal distance from the existing beds, and the likelihood of viable transport to un-invaded habitats. The impact of UV radiation during the pelagic stages on Asian clam mortality was low; less than 1% of the released larvae exceeded the lethal exposure to UVR during their trajectories. This low UVR impact resulted from the short dispersal distances (and thus, low UVR exposure times) associated with relatively high larval settling velocity and predominantly weak winds observed during the study period. A sensitivity analysis revealed that the final model results are most sensitive to the settling velocity ws, which directly influences the frequency and intensity of larvae entrainment into the pelagic, dispersal distance, and UVR exposure times.

The presented results provide an important understanding of the movement of aquatic species, particularly those with a pelagic larval stage, in relation to physical limnological processes (e.g., wind, sediment resuspension, surface currents, UVR) and as a function of population size. A number of studies have focused on identifying or quantifying the human-mediated, overland dispersal of aquatic invasive species (Bossenbroek *et al.*, 2001; Rothlisberger *et al.*, 2010), however, fewer have quantified this unwanted dispersal within lakes. While the prevention of invasive species introduction from external sources is a key component to efficient ecosystem management (Leung *et al.*, 2006), understanding the localized expansion of invasive populations is necessary for the management of invaded and connected aquatic systems. The knowledge about the relative contribution of different dispersal pathways may directly inform decision-making and resource allocation associated with

invasive species management. Understanding dispersal trajectories will not only provide information about where to focus mitigation or control efforts, but these actions to reduce the population size within one ecosystem can also reduce the likelihood of spread to other ecosystems (Lockwood *et al.*, 2005). Although the present study does not address active migration of adult individuals or human mediated vectors, such as recreational boating, future research may link human-mediated transport vector models with physical transport models such as the dispersal model developed here.

Chapter 3

Local Dispersal of Invasive Bivalve Species by Wind-driven Lake Currents

Abstract

Asian clam (*Corbicula fluminea*) is among the most aggressive freshwater invaders worldwide causing major ecological and economic damage. However, the mechanisms leading to the dispersion of the species within aquatic ecosystems, particularly lakes, is an area where research is at a relatively early stage. A numerical model has been developed to analyze and describe the dispersion that is produced by the actions of waves and currents. The model represents the basic particle processes of release (R), water-borne transport (T) and survival (S). The model has been applied to a large, deep lake - Lake Tahoe. The dispersion model results reveal that (1) under episodic, extreme wind forcing, larvae are carried away from the original areas, along a discrete number of preferred pathways, (2) bays can act as retention zones, with low current velocities and re-circulating eddies, and (3) the majority of the larvae released in the infested areas stay within these areas or disperse on a small spatial scale.

3.1 Introduction

The spread of aquatic invasive species is one of the major ecological and economic threats to lakes and waterways worldwide (Wilcove *et al.*, 1998; Pimentel *et al.*, 2005). In the US alone, there are about 50,000 invasive species established that cause economic losses estimated at more than $120 billion per year (Pimentel *et al.*, 2005). Invasive species may cause dramatic

changes in the ecosystems through perturbations to the inter-specific competition, predator-prey interactions, food web structure, nutrient dynamics, hydrologic cycle, and sedimentation rates. Those changes typically lead to the displacement of native species from their natural habitats. The pressure posed by invasive species on native organisms is of such magnitude that their introduction has been ranked second only to habitat loss in the factors that threaten native biodiversity at the global scale (Wilcove *et al.*, 1998). The development of management guidelines for early detection and eradication appears as the primary tool to maintain the ecological integrity of un-invaded habitats (Vander Zanden & Olden, 2008). But these guidelines need to be grounded on the sound understanding of the mechanisms by which invasive species spread and colonize new habitats. Such understanding, however, still remains incomplete due to the complex interactions among non-indigenous and indigenous species, humans, and local environmental conditions (Moles *et al.*, 2008).

Several modeling approaches have been proposed in the literature to represent the dispersion of aquatic invasive species. Most approaches, though, have focused on the analysis of dispersion between aquatic ecosystems conceptualized as 'islands' isolated by extended areas of non-suitable terrestrial habitats (Figuerola & Green, 2002). Dispersion in this case is largely mediated by human activities (Green & Figuerola, 2005). For example, the pattern of recreational boating traffic between inland water bodies has been shown to be a good proxy for the spatial distribution patterns of the aquatic invasive bivalve *Dreissena polymorpha* (zebra mussel) (Buchan & Padilla, 1999). Adult mussels and their larvae tend to attach primarily to macrophytes that entangle on boat trailers (Johnson *et al.*, 2001).

Once in a given water body, the local dispersion of the invasive species from colonized to uncolonized areas can be facilitated by natural processes, such as water currents (Prezant & Chalermwat, 1984; Forrest *et al.*, 2012). Mixing and dispersion of invasive species in a river and a semi-enclosed harbor have been investigated through recent tracer studies (Carr *et al.*, 2004; Wells *et al.*, 2011; Sun *et al.*, 2013). Similarly, Hrycik *et al.* (2013) have taken a modeling and measurement approach to this problem in a strongly, tidally forced coastal system. In all these cases, there is either unidirectional

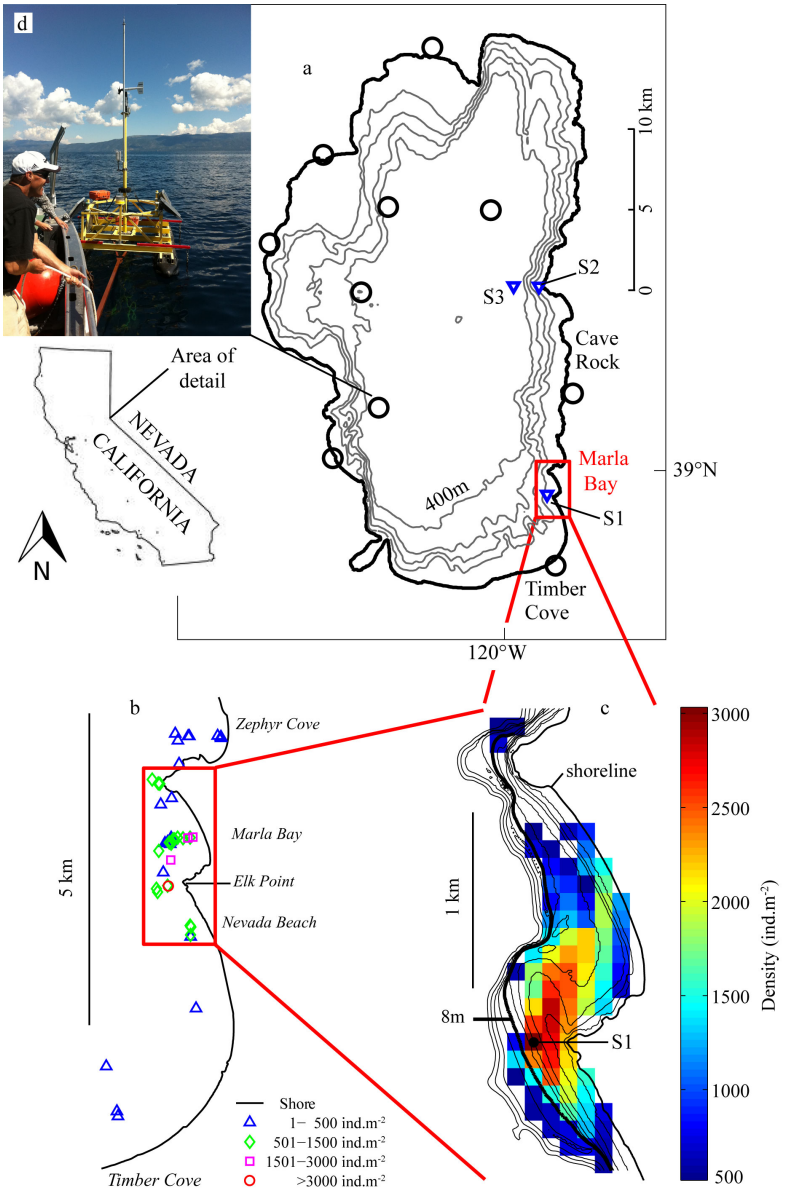

Figure 3.1: Lake Tahoe (a) location, bathymetry (at 100 m intervals) and location of meteorological stations (circles), initial temperature profile (S3), stations of model output (triangles) and area of interest. Density distribution of Asian clam adult population in 2005: (b) discrete sampling locations (Wittmann *et al.*, 2009), and (c) interpolated clam densities ($> 500\,ind.m^{-2}$). (d) Impression of off-shore meteorological station. Gray lines mark depth contours (1,2,3,4,5,8,10,20,30 and 40m) for orientation, 8m contour marked for reference. S1-3 mark sampling station for model output.

flow (albeit reversing for a tidal system) or an enclosed environment. In lakes, however, the flows can have additional complexities, driven as they are by episodic, variable wind, subject to waves, and with the interactions of boundaries. For these reasons, less is known about the role of currents in the local dispersion of invasive species (Prezant & Chalermwat, 1984; Tapia *et al.*, 2004) or other planktonic organisms. This work focuses on the local dispersion of the larval form of an invasive species by wind-driven and wave-driven currents in lakes. Specifically, the local transport and dispersion patterns and spatial evolution of the invasive bivalve *Corbicula fluminea* (Asian clam) is predicted in Lake Tahoe, a large sub-alpine lake on the crest of the Sierra Nevada mountain range (CA-NV) (Fig.3.1a). *C. fluminea* was first observed in Lake Tahoe in 2002 in very low numbers (Hackley *et al.*, 2008; Herold *et al.*, 2007). Its population has increased now to a level where it is having apparent environmental impacts. Its current known distribution (area $\simeq 10^6 m^2$) is patchy along the southeast and south shore of the lake, with the densest population established in Marla Bay (Fig.3.1). This distribution is believed to be changing, though, due to *C. fluminea*'s rapid growth rate and the presence of abundant suitable habitat existing along the shoreline in Lake Tahoe (Wittmann *et al.*, 2009).

C. fluminea is among the most aggressive freshwater invaders worldwide (McMahon, 1999). Its invasion success is based on its rapid population growth, early sexual maturity and short turn over time rather than on its tolerance to environmental fluctuations (McMahon, 2002). The species is sensitive to low oxygen conditions and requires sustained water temperatures of 15-16°C or above for reproduction (McMahon, 1999; Sousa *et al.*, 2008; Wittmann *et al.*, 2012). *C. fluminea* generally forms colonies or beds with densities that may exceed 6000 clams m^{-2} (Aldridge & McMahon, 1978; Wittmann *et al.*, 2012), preferably in areas of coarse and sandy sediments (Karatayev *et al.*, 2003). *C. fluminea* filters out phytoplankton and other suspended particles in the water column which are also food sources for native filter-feeding organisms. It can use its pedal foot to feed on organic matter in the sediment and competes for food resources with native benthic organisms (Hakenkamp *et al.*, 2001). *C. fluminea* can also affect aquatic ecosystem processes in other ways. Excretion of inorganic nutrients, partic-

ularly nitrogen can stimulate the growth of algae and macrophytes (Sousa *et al.*, 2008). The species is believed to facilitate the introduction of parasites, diseases and other invasive species (Vaughn & Hakenkamp, 2001; Sousa *et al.*, 2008). They have also been shown to facilitate the invasion of zebra or quagga mussel by creating localized high calcium environments, as shells from dead clams leach this potentially limiting element (see Hessen *et al.*, 2000, and references therein).

Passive (natural) hydraulic transport by water currents is considered to be the main mechanism for the local dispersal of *C. fluminea* (McMahon, 1999). The local dispersion largely occurs during the larval and juvenile stages of their life when, as a result of their low density (total dry weight of 0.1mg at $\sim 200\mu m$ shell length, Aldridge & McMahon, 1978), larvae may remain suspended in the surface mixed layer even under minimal turbulence (McMahon, 1999). Larvae are not motile, but can travel long distances drifting with water currents. The contribution of currents in the local dispersion of Asian clam, however, is not known. Laboratory studies on the dispersion of *C. fluminea* by water currents have focused on the transport of adults (Prezant & Chalermwat, 1984; Williams & McMahon, 1989). These studies have been conducted with strong, unidirectional and steady currents, more characteristic of rivers than lakes. In lakes, currents are largely forced by winds, waves and convective processes, and are characterized by lower magnitude as well as a higher temporal and spatial variability.

Our goal is to characterize the transport pathways of young life stages of *C. fluminea* and analyze the development of the clam population in a lake environment. Lake Tahoe (CA-NV) is used as a test case, although the modeling approach may be applied in any aquatic system. The approach embodies a number of consecutive steps. These are the determination of the mechanism of larval entrainment (suspension) into the ambient flow; the transport and dispersion characteristics due to the spatially and temporally varying meteorological conditions, lake stratification and larval density; the resulting preferred migration pathways; and the exposure to environmental stressors (temperature and light) experienced during their journey.

3.2 Methods

3.2.1 Approach

A three-dimensional (3D) Lagrangian, individual-based dispersal model (the larval dispersal model) has been developed (*see* Chapter 2, Methods) to simulate the dispersion of Asian clams larvae. This model is driven by estimates of the advection and turbulence provided by two external computational models: a wave model STWAVE and a 3D hydrodynamic model Si3D. Both these latter models have been widely used and validated in other locations (*see* Wave and hydrodynamic simulations). The wave model was validated against field observations from Lake Tahoe by Reardon *et al.* (2014). The results of a validation of the hydrodynamic model are presented in the Appendix A-3. The simulations were conducted for a two month period in 2008 (the study period), when temperature conditions in the lake are known to favor the release of Asian clam larvae.

3.2.2 Wave and hydrodynamic simulations

Wave conditions and wave-induced bottom shear stresses in Lake Tahoe were simulated using the phase-averaged spectral wave model (STWAVE). STWAVE is a two-dimensional (2D) finite difference model developed by the U.S. Army Corps of Engineers Research and Development Center (ERDC, Smith *et al.*, 2001). As STWAVE is a steady-state model, the changing state of the wave field in the lake is calculated as a sequence of quasi-steady states, calculated every Δt_w seconds (wave time step). Wind conditions are averaged over Δt_w, the magnitude of which should be longer than the time it takes for the wave field to be generated. The time varying lake currents and vertical diffusivity were computed using a parallel version of the 3D Cartesian hydrodynamic model of Smith (2006) (Acosta *et al.*, 2010). This model is based on the numerical solution of the 3D form of the shallow water-wave equation, and has been extensively validated both against analytical solutions (Rueda & Schladow, 2002; Rueda *et al.*, 2003) and field data sets (Rueda & Schladow, 2003; Rueda & Cowen, 2005). In contrast to the wave model, the transport and mixing model is a truly dynamic model

that predicts the changes in the hydrodynamic conditions of the lake every Δt_h seconds (hydrodynamic time step).

To simulate the wave and hydrodynamic conditions in Lake Tahoe, both models were forced using sequences of spatially variable wind fields, constructed through spatial interpolation of 10-minute wind records collected at 10 stations around the lake (Fig.2.1a,d). Wind records were corrected for height and roughness (*see* Appendix A-2). The method proposed by Barnes (1964) (*see* Appendix A-2) was used for spatial interpolation. The grids were constructed with a spatial resolution of 100m in both EW and NS directions. This grid resolution was considered as a compromise between the need to resolve the circulation within Marla Bay and the increasing cost associated with larger model resolutions. The bathymetry data was from Gardner *et al.* (1998) and corrected in the southern near-shore region (Steissberg, pers. comm.). The vertical resolution in the hydrodynamic model was variable, ranging from $\Delta z = 0.5m$ at the surface to $\Delta z = 10m$ near the bottom (at a depth of 500m). The initial temperature profile was obtained from thermistor-chain records (thermistors located at 5,10,15,20,25,30,40,60,80,100,120,140,180,200,240,280,320,360,400, and 440m depth) at S3 (Fig.3.1a) interpolated to the vertical grid spacing. The time step of the hydrodynamic model was $\Delta t_h = 50s$, primarily based on stability considerations. The horizontal eddy diffusivity K_h was estimated based on the horizontal grid resolution and the time step, following Castanedo & Medina (2002), and set to $1m^2s^{-1}$. The wave-model was run at $\Delta t_w = 6h$ intervals. As discussed in Chapter 2, this time step was a compromise between the time of wave generation, estimated to be $\mathcal{O}(1)$h (Hamilton and Mitchell 1996), and the computational cost.

3.2.3 Larval dispersal model

The three different modules are designed to run sequentially and independently of each other. The model is driven by the output of the wave and hydrodynamic models and run on the same Cartesian grid. The **R**elease module (R-module) represents the growth of larvae in the existing beds, and their release into the water column. Release is parameterized using the ratio

of shear u^* to settling w_s velocities (Bagnold, 1966). The settling velocity is a fixed model parameter, representing the larval size and density. Bottom shear velocities are variable both in space and time, and are calculated from the wave model and the hydrodynamic model. The output of this module consists of a time series of number of larvae individuals released into the pelagic for every grid cell (i_0, j_0), with a time step of Δt_0 seconds.

The **T**ransport module (T-module) tracks the position and the environmental conditions experienced by larvae in the pelagic after resuspension. The transport simulations are conducted using the time-varying particle tracking model proposed by (Rueda *et al.*, 2008) adapted to simulate larval trajectories in three dimensions (*see* Appendix A-1). These simulations, in turn, are driven by the three-dimensional time varying velocity and diffusivity fields produced by the hydrodynamic model. One transport simulation is conducted for every cell (i_0, j_0) of the gridded bottom, where the invasive species is known to exist (and reproduce), at every Δt_0 seconds. In each of these simulations a total of N_0 particles are released from a source cell (i_0, j_0) at time t_0, and tracked during a period ΔT, the time the particles stay in suspension. Once settled, the particles stay at a fixed location and are not able to resuspend again, representing larvae burrowing in the sediments (McMahon & Bogan, 2001; Vaughn & Hakenkamp, 2001). The solution of this module consists of a spatially varying field of the fraction of the N_0 particles released that have settled after ΔT on any given grid cell (i, j) and the history of environmental conditions experienced by each individual prior to settling. This solution should be thought of as the response, in terms of the spatial distribution of settled larvae on the lake bottom, to a unit pulse of larvae injected in the water column from cell (i_0, j_0) at time t_0. Note that the solution is calculated every Δt_0.

The **S**urvival module (S-module) accounts for the death/survival of settled larvae subject to the habitat conditions encountered at the site of sedimentation and the transport conditions calculated in the T-module. Individuals reaching a site (i, j) are considered viable if (i) they settle in favorable habitats and (ii) if the environmental conditions endured in transit do not negate their survival. The output of the S-module is a modified version of the spatially variable fields calculated in the T-module, and is also cal-

culated every Δt_0 seconds. Here, the fields represent the fraction of viable larvae reaching each site in the lake after a pulse of larvae from a given source cell (i_0, j_0) and at time t_0. From the set of response functions calculated in the T and S modules, together with the results of the R-module through a convolution exercise, one can reconstruct the changes in the spatial distribution of the larval population during the study period. The final larvae distribution is the result of the S-module where the fractions of simulated particles (larvae) that remain viable upon settlement in favorable habitats are weighted. The respective weights $\delta_{i_0 j_0}(t_0)$ are obtained from the number of larvae resuspended at cell (i_0, j_0) and at time t_0 divided by the total number of resuspended larvae at the existing clam beds during the study period L_T. A more detailed description of this model can be found in Chapter 2, Methods.

3.2.4 Application to Lake Tahoe

The larval dispersion model was applied to Lake Tahoe to simulate the dispersion of Asian clam larvae during their release period. Water temperatures of Lake Tahoe are above the minimum value for clam reproduction (i.e. θ>15℃) between the beginning of July and end of September. However, Denton *et al.* (2012) observed a lag of minimal 4 weeks between the time when water temperatures are first suitable for Asian clam reproduction and the time when clams actively reproduce. Therefore, the simulation starts August 1 (day 214), after a month of suitable water temperatures, and lasts for two months, until day 274. Water temperatures above 30℃, lethal for Asian clam and its larvae, were not recorded at Lake Tahoe during the study period. The density distribution of adults in the largest contiguous area of Asian clam identified to date (with clam densities in excess of $500 ind.m^{-2}$, Wittmann *et al.*, 2009) is shown in Fig.3.1c. For the purpose of this study, this area is taken as the only source of larvae in the simulations and is referred to as the existing clam beds.

At the start of the study period, the larvae population was assumed to be zero (i.e. $L(0) = 0$). Clam reproduction was assumed continuous and not bound to a specific time of the day, so that larvae were free to be released

whenever shear conditions were favorable for resuspension of larvae from the adult population at the sediment. The R- and the S-modules were run with a time step equal to Δt_w (i.e $\Delta t_0 = \Delta t_w = 6h$). The T- module, in turn, was run with a time step $\Delta t_T = 10s$, to satisfy the convergence criterion for particle tracking simulations proposed by Ross & Sharples (2004). The transport simulations were driven using velocity and diffusivity fields output every $3600s$ ($\Delta t_{h-output} = 1h$) from the hydrodynamic model and interpolated to Δt_T. The solar radiation data was also passed to the T-module, every 10 min, to estimate the ultraviolet radiation (UVR) affecting the viability of larvae along their trajectories. The number N_0 of particles released in the T-module was set to 10^4. In a series of preliminary experiments, the spatial distribution of larvae after ΔT, expressed as a fraction of released individuals, was invariant for $N_0 > 10^4$. The simulation period of this module, T, is 2 days, equal to the maximum length of time that Asian clam larvae have been observed to persist in the pelagic (Kraemer & Galloway, 1986). The probability of survival and colonization was evaluated based on parameter values reported in the literature. Asian clams are found preferentially on coarse sand beds, which is the most common type of near-shore substrate in Lake Tahoe (Wittmann *et al.*, 2009). Hence, the lake substratum does not pose any limitation on the potential of colonization. The preferred depths of establishment are set at between 2m (H_{min}) and 39m (H_{max}) (Wittmann *et al.*, 2009). The probability of survival was established based on UVR exposure only, given that temperature in Lake Tahoe is always within the acceptable range for Asian clam (3℃$<\theta<$30℃) (McMahon, 1999). The particular values for the model parameters used in the model runs are given in Chapter 1 (Tab.2.1). Note that some of the kinetic parameter values are specific for Asian clam. Other parameter values were taken from studies conducted on other bivalves, where specific values for Asian clam were not available.

3.3 Results

3.3.1 Currents

The depth of the seasonal mixed layer (SML) of Lake Tahoe during the study period was $\sim 20m$. The stability of the water column was high based on the calculated values of the Wedderburn number, W, and the Lake number, L_N, which were both well above unity (Stevens & Imberger, 1996). Assuming a two-layer stratification with an upper mixed layer of thickness H, the displacement of the interface, Δh, in response to by wind forcing can be estimated as $\Delta h = 0.5H/W$ (Shintani *et al.*, 2010). Interface displacement was therefore a maximum of 8m at most, suggesting that the water column above the 12m isobath in the existing clam beds at Marla Bay (Fig.3.1) was within in the SML and, hence, subject primarily to mixing conditions and currents driven directly by winds and wind-waves. The basin-scale wind-driven circulation in the SML was generally stable throughout the study period, and consisted of three large counter-rotating gyres (Fig.3.2a). At the latitude of Marla Bay the large-scale circulation was convergent producing currents away from the coast.

Currents off Elk Point at the southern end of Marla Bay (Fig.3.1b), in the vicinity of the largest clam densities, exhibited changes at both diurnal and synoptic scales in direct response to local winds (Fig.3.3a-c). Winds at Marla Bay during the study period were mostly aligned along the NW-SE axis (Fig.3.4), and subject to diurnal changes (Fig.3.3a,b). They were typically moderate ($< 5ms^{-1}$) from the NW during the afternoon and weak ($< 2ms^{-1}$) from the SE at night and early morning. Long-shore currents varied in magnitude and direction in response to these diel changes in wind forcing. Currents were southwards during the day, and northwards in the evening. The largest currents were to the north and reached values of $\mathcal{O}(10^{-1})ms^{-1}$ and up to $0.45ms^{-1}$ in the evening, shortly after peak NW winds (e.g. day 244, Fig.3.3c). These peak northward currents likely occurred as a result of the relaxation of baroclinic pressure gradients set up by the NW winds. These relaxation motions in the evening were in the same direction as the currents associated with the large-scale circulation (Fig.3.2a).

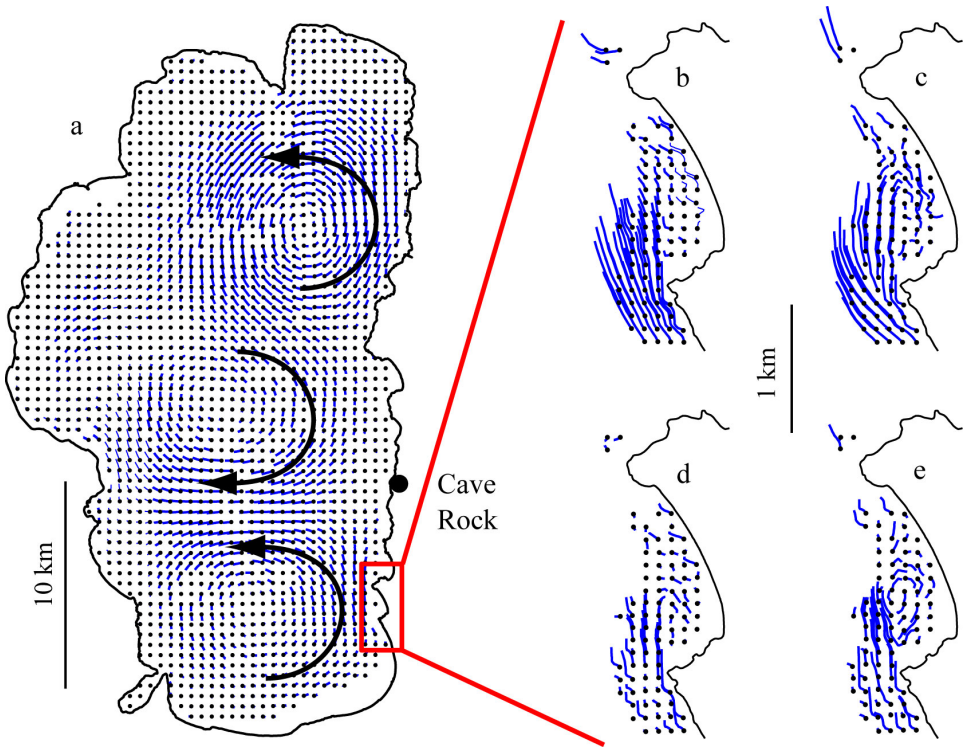

Figure 3.2: Circulation patterns at the surface at basin-scale (a), at surface (b,c) and bottom (d,e) at the existing clam beds for SE wind (left) and SW wind (right). Streamlines were generated from hourly velocity fields averaged over the study period used as steady state condition during 1h.

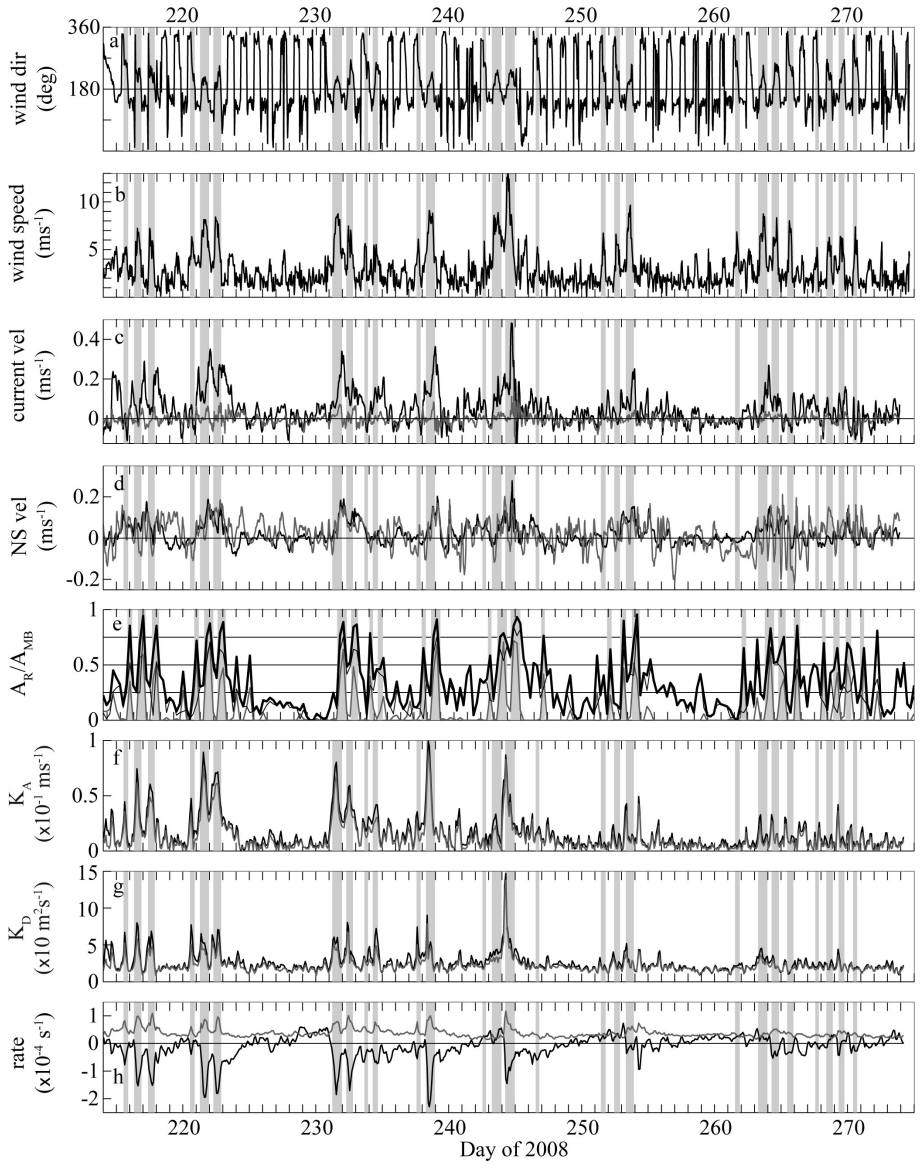

Figure 3.3: Temporal variation of wind direction (a); wind speed (b); along-shore (black) and cross-shore (gray) currents at S1 (c); NS current velocities in the coastal boundary layer at S2 (black) and S3 (gray) (d) (for Stations see Fig.3.1); area where the condition $u^*/w_s > 1$ holds (A_R) as fraction of Marla Bay (A_{MB}) for the wave-induced shear (gray), current-induced shear (thin black) and both wave- and current-driven shear velocities (thick black) (e); advection rate (f) and dispersion rate (g) for neutrally (black) and negatively buoyant (gray) particles; and shear (black) and strain rate (gray) (h). Gray vertical bars mark events were wind direction is 180°-270° and wind speed is $> 5ms^{-1}$.

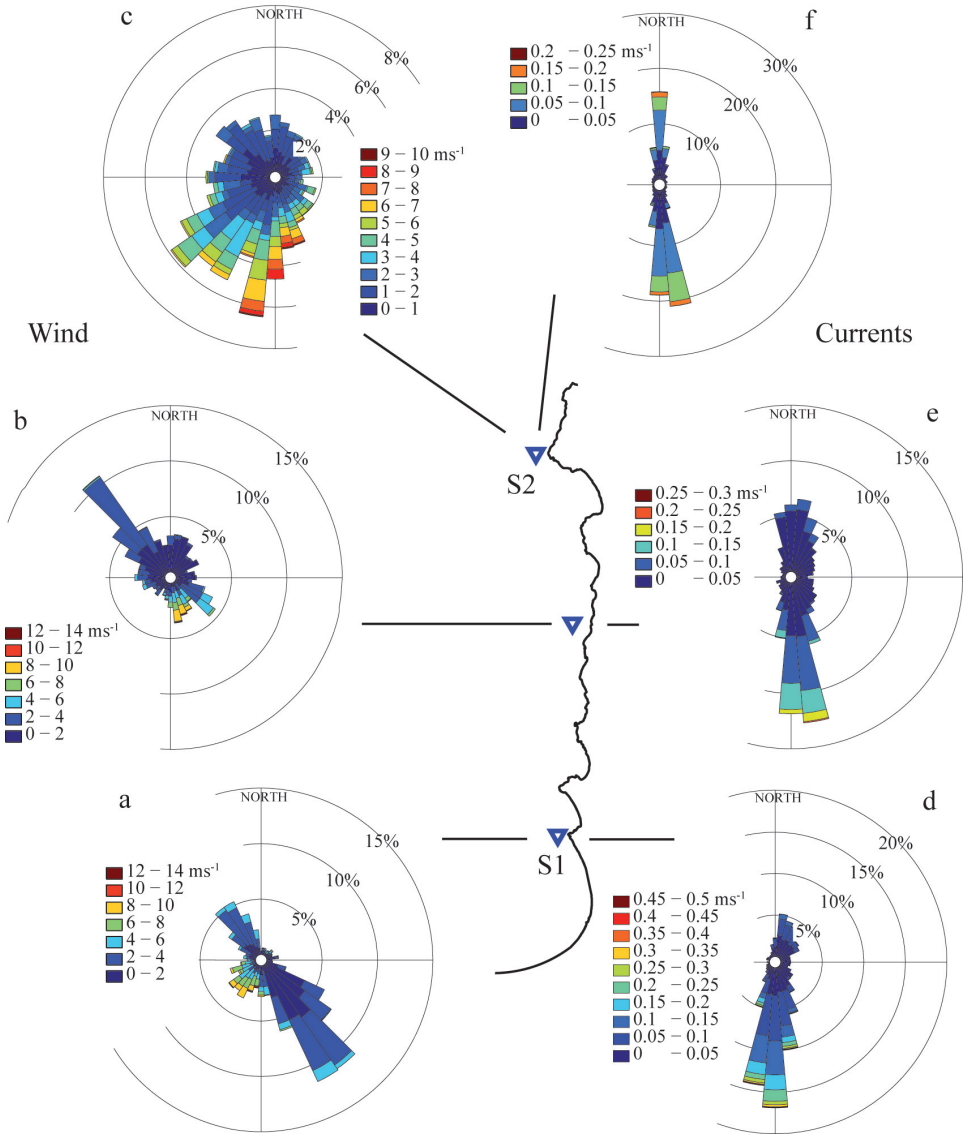

Figure 3.4: Dominant wind (left) and current (right) directions and speed in Marla Bay (S1), near Cave Rock and at S2.

Cross-shore currents (not shown) were an order of magnitude lower, alternatively on- and off-shore having a zero net displacement (Fig.3.3c). The strongest long-shore currents occurred on the shallowest near-shore regions, off Elk Point (Fig.3.2b-e). By contrast, currents inside Marla Bay were weaker and tended to re-circulate flowing southward inside the bay (Fig.3.2b-e). Recirculation within the bay tended to occur at the times of peak northerly currents off Elk-Point during the evening, due to flow separation at Elk Point.

The weak-to-moderate wind regime was disrupted on synoptic scales by strong, episodic forcing events, with SW winds of $\sim 10ms^{-1}$ occurring with a return period of 7-10 days (Fig.3.4a,3.3a,b). During these SW wind events, currents all along the eastern coast of Lake Tahoe were to the north (Fig.3.4d-f, Fig.3.3c,d), particularly evident during the event of day 243-244 (Fig.3.3a-d). This northward coastal flow was in the same direction as the currents associated with the southern cyclonic gyre, but opposite to the southward basin-scale currents north of Marla Bay (Fig.3.2a). Currents off Elk-Point reached velocities of up to $0.45ms^{-1}$ shortly after peak SW winds (e.g. day 244, Fig.3.3c). Within the bay, near-surface water was also forced to flow to the north, but more slowly. Once the SW winds ceased, currents inside Marla Bay, with less inertia, decreased more rapidly than those off Elk Point, leading to the formation of a steep velocity gradient and flow separation in the bay (Fig3.2c,e).

3.3.2 Larval suspension

Suspension of simulated larvae occurred episodically, in response to strong wind forcing events, when the combination of wave orbital velocities and near-shore currents was large enough to entrain and maintain them in the water column. Those events were mainly from the SW and occurred with a return period of ca. 7 days during the study period (Fig.3.3a,b). Such strong wind forcing occurred for ca. 17% of the entrainment events but was responsible for 43% of the suspended larvae. The relative contribution of currents and wind-waves to bottom shear in Marla Bay, and the fraction of the existing patch contributing larvae into the water column varied in

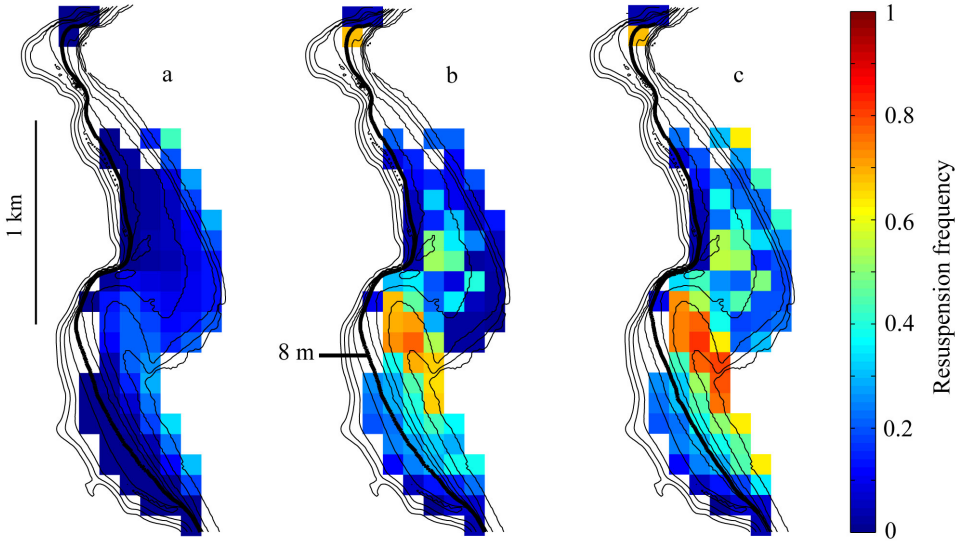

Figure 3.5: Horizontal distribution of resuspension frequency in Marla Bay induced by waves (a), currents (b), and combined wave and currents (c). Black lines mark depth contours (1,2,3,4,5,8,10,20,30 and 40m) for orientation, 8m contour marked for reference. The frequency of resuspension is estimated at each site as the fraction of time during the study period when the condition $u_*/w_s > 1$ holds.

the simulations depending on the exact time and location considered. In general, the really broadest resuspension events were episodic, coinciding with the strong SW wind events. During these events turbulence levels were sufficiently energetic ($u^*/w_s > 1$) to induce larval resuspension in over 75 percent of the existing clam area (Fig.3.3e), and the contributions of wave- and current-induced shear stress on the lake bottom tended to be similar. By contrast, under weak-to-moderate wind forcing, bottom shear was dominated by currents (Fig.3.3e), and only a small fraction of the patch could be contributing larvae to the water column. As a result of the turbulence at the lake bottom (Fig.3.5c), some parts of the existing clam beds could be injecting larvae into the water column almost continuously. The number of larvae released fluctuates as a result of changes in the area with sufficient levels of turbulence to induce resuspension and the number of larvae available for resuspension.

3.3.3 Transport and dispersion

Larvae transport and dispersion was also controlled by the nature of the wind events. The greatest transport occurred during the strong SW wind events and after long calm periods. Under weak-to-moderate conditions larvae were resuspended but settled within the existing beds, thereby not contributing to the colonization of new areas. A series of simulations was conducted to evaluate advection and dispersion rates of neutrally- and negatively buoyant particles from the existing clam beds. A total of 10,000 particles were uniformly seeded in the entire water column above the existing colonies every $T_K = 2h$ over the study period. The horizontal displacement of the center of mass of the particle cloud D_M provided information about the average cloud velocity V $(= D_M(T_K)^{-1})$. The size and the shape of the cloud calculated at any given time t after the release provided information about the dispersion rates (Peeters *et al.*, 1996). The difference between initial area, A_0 $(= 8.9 \times 10^5 m^2$, see Fig.3.1c), and final area of the cloud after 2h of simulation, A_e, was used to estimate an overall dispersion rate K_D as $(A_e - A_0)/T_K$.

For neutrally-buoyant particles K_D was $\mathcal{O}(10)m^2s^{-1}$ during most of the

study period (Fig.3.3g). Dispersion rates were variable during the study period, largely driven by variations in wind forcing. The largest values of K_D, of $\mathcal{O}(10^2)m^2s^{-1}$, occurred during the strong SW-wind events, when lake currents (Fig.3.3c-d), shear and strain rates (Fig.3.3h) were maximal. The largest migration rates, quantified in terms of the initial velocity of the cloud (Fig.3.3f), also exhibited changes with the largest values of $\mathcal{O}(1)ms^{-1}$ occurring during the episodic SW wind events. At those rates, the cloud could travel up to $\mathcal{O}(10)$km during a period of 2 hours. These estimates of K_D and V should be considered as upper bounds to the dispersion rates and migration velocities of larvae. First, settling of larvae was not considered. The estimates were on average 20% and 28% smaller in the simulations conducted with negatively buoyant particles (with a settling velocity $w_s = 10^{-3}ms^{-1}$), with differences most pronounced during periods of stronger winds (Fig.3.3a,f,g). Second, the area of the initial cloud was always assumed to be that of the existing clam beds and that the larvae occupied the whole water column. This is only true during the events of strong SW winds, but not during the periods of weak-to-moderate winds. The dispersion coefficient estimated from experiments conducted with the initial clouds occupying only half the area of the clam beds was approximately 60% of the values shown in Fig.3.3g. For the initial cloud of particles occupying only the lower half of the water column above the beds, the overall dispersion coefficient reduced by 17%. The dispersion rates of larvae released within Marla Bay was low and larvae re-settled at or in the vicinity of their point of suspension. Indeed, 100% of the larvae that were resuspended within Marla Bay (near its SE shore) remained within the existing beds. At Elk Point, 20% of the resuspended larvae, in turn, were able to leave the existing clam patches.

3.3.4 Pathways of migration

Approximately 13% of the larvae released during the 2 month study period were able to leave the existing beds, 77% of which (10% of total) left during periods of strong wind forcing. Nearly 10% of these remained viable and reached favorable habitats. End points, reached by migrating larvae (both

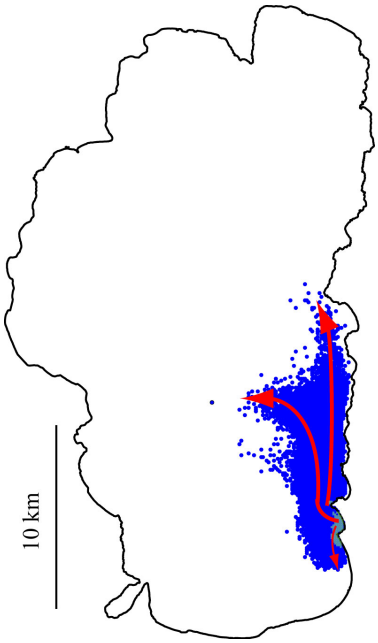

Figure 3.6: Final distribution of simulated particles representing Asian clam larvae (see text for details). Arrows mark pathways of migration and shaded area marks existing clam beds.

successful and unsuccessful) within 48h after being suspended, are shown in Fig.3.6. The distribution of these sites suggests the existence of three migration pathways: (1) to the north, along the eastern shoreline of the lake; (2) to the south, along the shoreline; and (3) westward and offshore, following the large scale circulation. About 50% of the larvae migrating and reaching favorable sites travelled to the North largely during the strong SW events. The remaining travelled to the South. All larvae migrating off-shore, 90% of those that dispersed, died due to sedimentation in habitats of depth above the critical value (>39m) for Asian clam growth and survival.

The distance traveled along the northward path could be up to 10km during the strongest SW wind events. Winds during those events are largely uniform over the lake and lead to the development of transport corridors along the coastal-boundary layer where strong along-shore currents (see Fig.3.3c,d) during periods of up to 5h are capable of advecting larvae large distances, while keeping them in suspension. The directionality of the winds during these events largely determine preferential pathway of migration. Veloci-

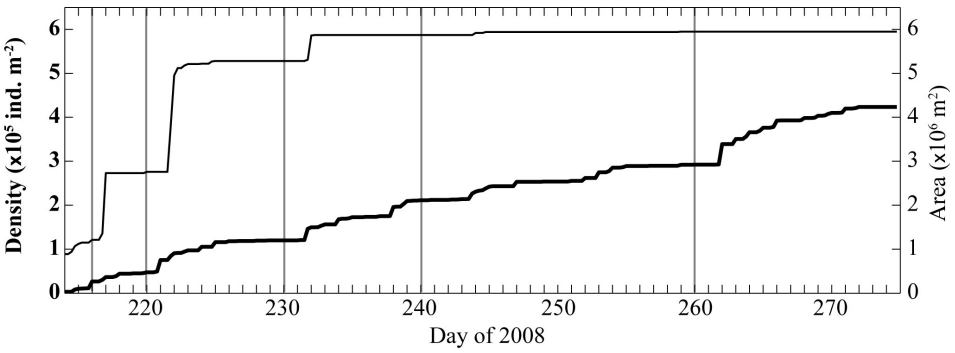

Figure 3.7: Temporal development of simulated Asian clam population (adult and larvae) density at S1 (see Fig.3.1c) (thick line) and spatial extension (thin line). Note that at the beginning of the study period, the density is equal to the adult density (dens $= 3 \times 10^3 ind.m^{-2}$) and the area is equal to the area covered by the existing clam population ($A = 8.9 \times 10^5 m^2$). Vertical bars mark instants of time shown in detail in Figure 3.8.

ties were up to $0.5ms^{-1}$, and turbulence levels in the SML were sufficient to keep the larvae in suspension ($K_z = \mathcal{O}(10^{-2}) - \mathcal{O}(10^{-3}) m^2 s^{-1}$). Larvae were transported to the south, during periods of weak-to-moderate winds, largely during the afternoon, in response to NW winds. However, the distances traveled along this path were at most 1-2km. Large migration distances, in general, increased the chances of the population to expand and reach new habitats, but also contained a potential risk of mortality. Short migration distances or sedimentation in the existing beds, in turn, enhanced the chances of larval survival. Out of the larvae that settled in vicinity of the existing beds (distance $<$ 1km) $\sim$50% remained viable, compared to $<$5% of viable larvae from those that migrated $>$1km.

3.3.5 Evolution of clam population

Almost 84% of the larvae produced in Marla Bay settled over the existing patch, even under extreme wind forcing. Hence, littoral embayments could be potential hot-spots in the process of development and colonization of lakes. Released larvae primarily added to the existing clam population in Marla Bay (Fig.3.1c), with large spatial gradients away from the actual beds. The area of the clam population could increase up to 600% (from $8.9 \times 10^5 m^2$ to $\sim 6 \times 10^6 m^2$) during the two month period (one reproduction period,

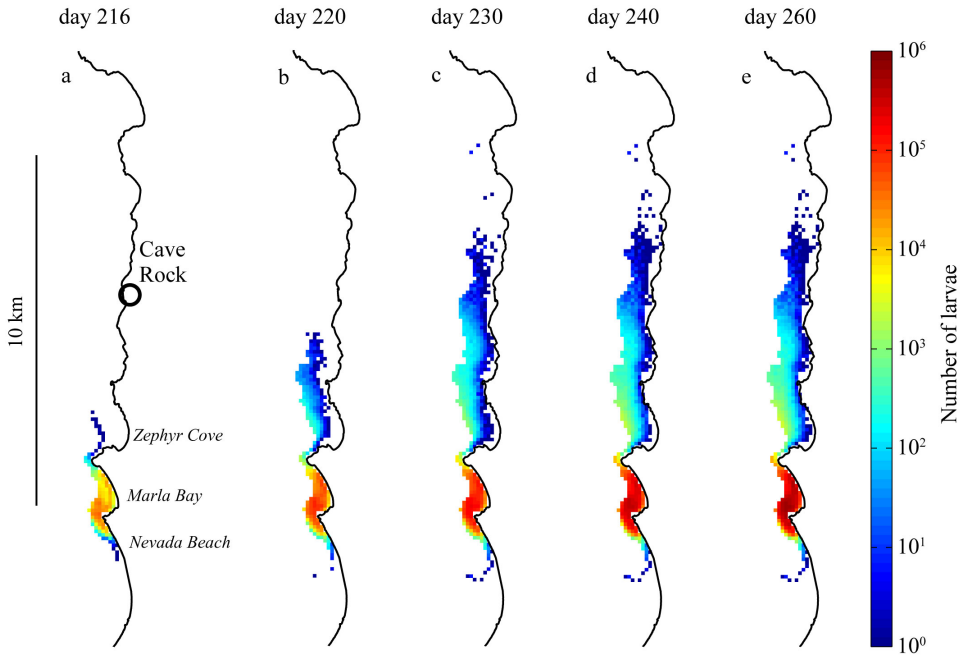

Figure 3.8: Simulated larvae distribution on day 216 (c), 220 (b), 230 (c), 240 (d), and 260 (e).

Fig.3.7, 3.8e). However, these newly colonized sites would have much lower clam densities than what is currently seen in Marla Bay. An increase in spatial extent is consistent with observations of clam individuals north of Marla Bay along the eastern coast up to the latitude of Cave Rock, although there are no quantitive estimates of the exact extent or of the densities (M.E. Wittmann pers. comm.).

3.4 Discussion

In the vicinity of the eastern near-shore, flows are mainly directed along-shore driven by strong and episodic SW winds. Along-shore currents within the coastal boundary layer have also been reported in other lakes and near-shore coastal regions (Largier, 2003; Rao & Schwab, 2007; Nickols *et al.*, 2012). By contrast, flow inside Marla Bay, where Asian clam has established, exhibits re-circulating currents. Such eddies are likely the results of flow separation at the bay boundary. Similar observations of separation eddies have been reported in other wind-driven systems (see Rueda & Vidal, 2009).

The lake bottom in near-shore areas is frequently perturbed by wind-waves and wind-driven lake currents, that induce shear above the sediment (Jin & Sun, 2007; Chung *et al.*, 2009; Hofmann *et al.*, 2011), and lead to resuspension of sediments and non-attached living organisms (such as larvae). The large contribution of currents to resuspension within the clam beds in Marla Bay (in the range of 2m - 8m depth), compared to waves, contrasts with previous publications in which wave-induced shear stress was reported to be the dominant driver of bottom shear in shallow waters (Luettich *et al.*, 1990; Jin & Sun, 2007), and even in other near-shore areas of Lake Tahoe (Reardon *et al.*, 2014). Large fluctuations in the number of resuspended larvae are driven by the episodic nature of the wind regime. The strength and direction of the wind forcing determines in the area with sufficient levels of turbulence to induce resuspension and, thus, the number of larvae available for resuspension. The amount of available larvae at the sediments, in turn, depends on the length of time between wind events inducing resuspension and the number of adults present (*see* Chapter 2).

Larvae dispersion and migration occurs in form of pulses in response to the episodic nature of the strong wind forcing. The episodic nature of larval migration away from the existing clam beds at Marla Bay is consistent with earlier reports. Coe (1953), for example, found that rare long-distance pulses of larvae dispersal were able to resurge the clam (*Donax gouldi*) population along the Californian coast. MacIsaac *et al.* (2001) refer to those episodic events of strong impulsive long-distance dispersal as jump dispersal. The dispersion of suspended larvae over the existing population patch is driven predominantly by wind-driven shear and strain deformation rates in the flow field. The initial dispersion rates largely control whether the suspended larvae settle in the area of the existing population patch, travel within the coastal boundary layer and follow along-shore transport paths, or, if they in turn, move off-shore drifting with basin-scale currents. The simulated dispersion rates are one order of magnitude larger than the turbulent diffusion coefficient used in the hydrodynamic simulations, but comparable to those reported by others in field-scale numerical experiments (Okely *et al.*, 2010, in Valle Bravo Reservoir, Mexico). Predicted overall dispersion rates K_D are also large compared to those expected in surface layers of lakes calculated as

$K = 3.2 \times 10^{-4} \ell^{1.1}$ (Lawrence *et al.*, 1995) based on a characteristic length scale ℓ $(= (A_0)^{1/2})$, here taken to represent the initial size of the cloud. This difference can be explained by the high vertical and horizontal shear (Fig.3.3h) above the existing clam beds, due to the proximity of boundaries, compared to the offshore regions of the lake.

Bays that are characterized by low current velocities and recirculation act as traps for suspended benthic larvae. During periods of low physical forcing, the suspended larvae tend to remain within the area of the existing beds, partly as a result of the low displacement rate of the negatively buoyant larvae, but also as a result of the re-circulation in Marla Bay (*see above*), which will tend to trap the suspended larvae inside the bay. The trapping effect of bay-scale eddies has been reported in previous studies conducted in large coastal systems. Brooks *et al.* (1999), for example, showed that eddies forming in Cobscook Bay, Maine, could trap particulates in the side-arms of the estuary. Similar conclusions were obtained by Nishimoto & Washburn (2002), who observed high concentrations of juvenile fish in the center of a large eddy in the Santa Barbara Channel. The trapping effect of shoreline irregularities could favor the preservation of existing population patches at those sites, given that newly produced and trapped larvae can contribute to replenish of the existing population, balancing mortality rates.

In lake systems, the size of the population patch increases in the form of pulses induced by the physical (wind) forcing that drives the dispersal mechanisms of suspension and transport. The spatial expansion of the patch of newly settled viable larvae A_L (= total extension of larvae patch − extension of existing adult population) is used to estimate the effective diffusion coefficient K_e as $(A_L)^2(T_e)^{-1}$. Here T_e is the time from the beginning of the reproduction/migration period until the larvae patch has reached its maximal size. The larvae simulations predict an effective diffusivity K_e of $\mathcal{O}(1)m^2s^{-1}$. This value is within the range of dispersion estimates from diffusion-models found in the literature (Andow *et al.*, 1990). Therefore, the area to be colonized by larvae is limited by the distance larvae can migrate within the time they stay in suspension. High sedimentation rates, thus, decrease the chance of dispersion, but increase the chance of survival. Further, the expansion of a population restricted to shallow near-shore areas is

bounded by the shore-line on one side and deeper waters on the other side. Off-shore transport routes are unfavorable for larval survival, given that they end up on long-transport paths and sedimentation in deep and unsuitable habitats. In this sense, local dispersion of invasive species within a bounded aquatic system differs from unbounded overland dispersion between systems or terrestrial dispersion, where the square root of the population area may increase linearly in time (Skellam, 1951). Once the maximal spatial extension is reached, all newly released larvae sediment at previously occupied site and, thus, add to the pressure exerted on new habitats which will be colonized and will host a new population patch (Lockwood *et al.*, 2005). The final establishment, however, may be jeopardized by demographic or environmental conditions such as high juvenile mortality in bivalves, characteristics of the receiving microhabitat, or density dependence (Gosselin & Qian, 1997; Jerde & Lewis, 2007).

Chapter 4

A hydrodynamics-based approach to evaluating the risk of waterborne pathogens entering drinking water intakes in a large lake

Abstract

Pathogen contamination of drinking water lakes and reservoirs is a severe threat to human health worldwide. A major source of pathogens in surface sources of drinking waters is from body contact recreation in the water body. There is a demonstrated positive relationship between bather density and ambient concentration of pathogens. However, dispersion pathways of human waterborne pathogens from recreational beaches where body contact recreation is known to occur to drinking water intakes and the associated risk of pathogens entering the drinking water supply remain largely undocumented. A high spatial resolution, three-dimensional hydrodynamic and particle tracking model has been developed to analyze the risk and mechanisms presented by pathogen dispersion. The model represents the processes of particle release, transport and survival. Here survival is a function of both water temperature and cumulative exposure to UV radiation. Pathogen transport is simulated using a novel and computationally efficient technique of tracking particle trajectories backwards, from a drinking water intake toward their source areas. The model has been applied to a large, alpine lake - Lake Tahoe. The dispersion model results reveal that for this particular lake (1) the risk of human water-borne pathogens entering drinking water intakes is low, but significant; (2) this risk is strongly related to the depth of the thermocline in relation to the depth of the intake; (3) the risk of increases

with the seasonal deepening of the surface mixed layer; and (4) the risk increases at the night when the surface mixed layer deepens through convective mixing and inactivation by ultraviolet radiation is eliminated. While these risk factors will quantitatively vary in different lakes, these same mechanisms will govern the process of pathogen transport.

4.1 Introduction

Pathogen contamination of aquatic ecosystems is a severe threats to human health worldwide (Sherchand, 2012). Even in developed countries, the risk of pathogen contamination is significant. The protozoan parasites *Cryptosporidium* spp. and *Giardia* spp., or rather their (oo)cysts, are widespread in lakes and reservoirs (Jellison *et al.*, 2002; Brookes *et al.*, 2004b). In the US, the presence of *Cryptosporidium parvum* is estimated to occur in 55% of surface waters and 17% of drinking water supplies (LeChevallier *et al.*, 1991; Rose *et al.*, 1991). The Center of Disease Control (CDC), the U.S. Environmental Protection Agency (USEPA), and the Council of State and Territorial Epidemiologists maintain a collaborative surveillance system for collecting and reporting data about the occurrences and causes of waterborne-disease outbreaks related to drinking water and recreational waters (USEPA, 2002). The Beaches Environmental Assessment of Coastal Health (BEACH) Act (USEPA, 2002; Wade *et al.*, 2006) requires testing recreational beach waters for fecal coliforms (enterococci or Escherichia coli) on a weekly basis. In Europe, the Directive 76/160/EEC governs the quality of bathing waters specifying threshold values for microbiological and physicochemical parameters (CEC, 1976). Parasites, however, are not monitored on a regular basis. Although indicator organisms, such as enterococci and *E. coli* are used to monitor pathogens, they are not necessarily indicative on the presence of parasites such as Cryptosporidium or Giardia (Harwood *et al.*, 2005; Abdelzaher *et al.*, n.d., and references therein).

The Safe Drinking Water Act currently requires drinking water treatment plants of surface water sources to have the technical capacity to remove 99.9% of *Giardia* cysts (USEPA, 1989). *Cryptosporidium* poses a problem to water treatment as it is highly resistant to conventional methods of disinfection,

such as chlorination (Betancourt & Rose, 2004; Standish-Lee & Loboschefsky, 2006; WHO, 2008). The small size and omnipresence of its oocysts has caused many health outbreaks in drinking as well as recreational waters (Craun *et al.*, 2005; Coupe *et al.*, 2006). The most severe outbreak due to the transmission of *Cryptosporidium* through drinking water in Wisconsin in 1993 resulted in 403,000 infected persons (MacKenzie *et al.*, 1994), including lethal cases (Hoxie *et al.*, 1997). The first recreational outbreak of cryptosporidiosis was reported in 1988 in Los Angeles (CDC, 2000, 2001). Yoder *et al.* (2004) reported 15 water-borne outbreaks in recreational waters associated with *Cryptosporidium* between 2001 and 2002, in spite of prior water treatment. Gastrointestinal illness associated with these pathogens inflict morbidity in healthy people and mortality in children, immune-suppressed individuals and the elderly (Masur *et al.*, 2002; Farthing, 2006; WHO, 2008). Fortunately, a treatment for cryptosporidiosis has been found (Smith & Corcoran, 2004; Farthing, 2006; Rossignol *et al.*, 2006, reported in King & Monis 2007).

The major source of pathogens in surface sources of drinking waters is human wastes (Gallaher *et al.*, 1989; Rose *et al.*, 2002; Fayer, 2004). A fecal accident by an infected person is the most common cause of recreational water outbreaks (Rose *et al.*, 2002). Recreational activities increase pathogen contamination of surface waters (Carswell *et al.*, 1969; Stuart *et al.*, 1971; Sherry, 1986, reported in Gerba 2000). Empirical studies have demonstrated a positive relationship between bather density and the level of *Cryptosporidium* and *Giardia* (Graczyk *et al.*, 2007; Sunderland *et al.*, 2007). Swimming and other body-contact recreational activities have been identified by the USEPA, California Department of Public Health (DPH) and other public health professionals as a potential source of microbiological contamination of recreational waters. The concentration of shed pathogens in recreational water bodies is of high spatial and temporal variability being greatest in zones associated with body-contact recreation, such as water skiing, jet skiing and swimming, and times of maximal recreational use (Anderson *et al.*, 1998). Anderson *et al.* (1998) showed that high loads of pathogens due to body-contact recreation may reach drinking water intakes on a regular basis and, thus, constitute a potential risk for disease outbreaks through drinking

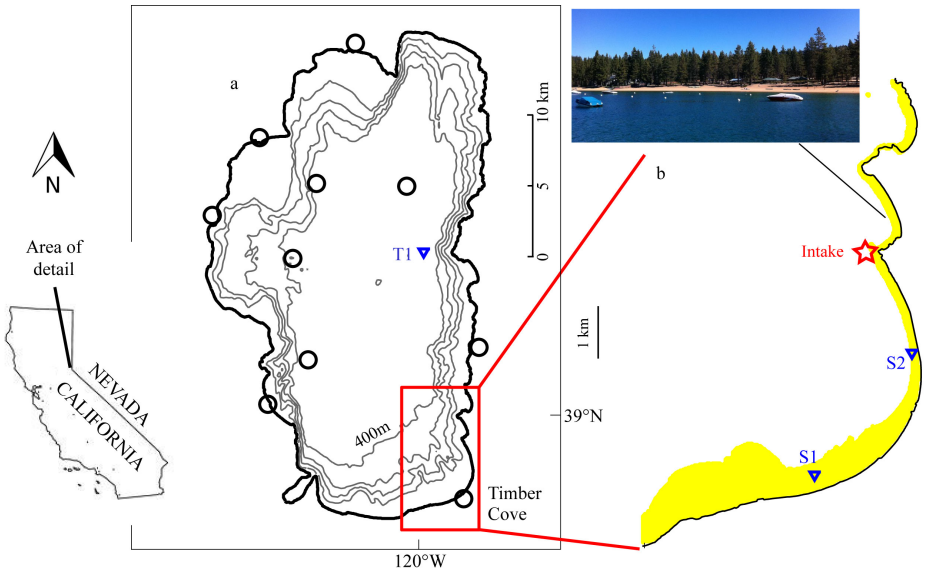

Figure 4.1: Lake Tahoe: (a) location, bathymetry (at 100m intervals) and location of meteorological stations (circles), initial temperature profile (triangle), and (b) area of interest: location of water intake (star), beach areas and locations of simulated velocity output (triangles).

water supplies. The approach used by Anderson *et al.* (1998) and Stewart *et al.* (2002) was based on relatively simple finite segment model with a coarse horizontal resolution (500m × 500m segments) and a two-layer vertical grid. For the analysis of pathogens released in near-shore areas, such as recreational beaches, however, a finer spatial resolution is necessary to adequately resolve the complex coastal bathymetry and circulation patterns. While sufficiently high model resolutions were out of reach in the past due to hardware limitations, today they are feasible. Further, Anderson *et al.* (1998) considered pathogens inactivation due to temperature only. Laboratory and field studies have shown that *Cryptosporidium* is highly sensitive to ambient UV radiation (Rochelle *et al.*, 2005; Connelly *et al.*, 2007; King *et al.*, 2008).

The goal is to assess the risk of viable/infectious human intestinal pathogens, focusing on *Cryptosporidium* as an example, released at beach areas to enter water intakes. In contrast to previous studies on the risk assessment, the present work is based on a time-varying, high spatial resolution three-dimensional (3D) hydrodynamic model. Model resolution in the horizontal

plane was 20m × 20m, and as small as 0.5m in the vertical. As well as predicting the transport and dispersion of particles (viz., pathogens) the model integrates the exposure to temperature and solar radiation experienced by all the particles. Lake Tahoe is used as a test case. It is a large, ultra-oligotrophic, sub-alpine lake on the border between CA-NV (Fig.4.1), is well known for its clear, blue water. In addition to its use for recreation, Lake Tahoe serves as a source of unfiltered drinking water.

The results presented here are based on the particle transport and dispersal model proposed in Chapter 2, but extended for the case of pathogen transport. A novel technique of back-tracking pathogens trajectories is used which allows studying non-point contaminations at a modest computational cost. This technique provides a very direct way to represent the likely transport of pathogens to the water intakes from near-shore areas where recreation is taking place. Several key issues are addressed in this work. First, the pathogen dispersal model is presented. Next, the sources of pathogens entering drinking a drinking water intake and the pathogens pathways of migration are determined. Based on these pathways, the environmental stressors (i.e. temperature and light) are quantified those pathogens that originated from beach areas are exposed to during their journey. Finally, the likelihood of survival of pathogens is evaluated and potential periods of drinking water contamination are determined.

4.2 Methods

4.2.1 Approach

A 3D Lagrangian, individual-based particle model (*see* Chapter 2) was modified to assess the risk of pathogens entering the drinking water supply from intakes in a lake, hereafter referred to as the pathogen model. These simulations are driven by lake current and turbulence simulations conducted with a 3D hydrodynamic model. The same Cartesian grid is used for both the hydrodynamic model and the pathogen model. Unlike the conventional approach where pathogens are tracked from the beach area(s) to a water intake, the velocity fields are inverted and the points of origin of individual pathogens are calculated by back-tracking their individual trajectories from

the points of withdrawal.

This technique is computationally efficient. The non-point source nature of pathogens released by body-contact recreation would require a large number of simulations from different beach areas, containing many potential points of origin. In contrast, the knowledge of the point of concern (water intake) makes it possible to consider only those (simulated) particles originating from sources areas (recreational beaches) that reach the water intake. In the following, the term 'particles' refers to all individual particles simulated by the model, while 'pathogens' are those particles that were predicted to origin from recreational beaches. The validation of the hydrodynamic model is given in the Appendix A-3. The simulation results permitted the establishment of the risk patterns, their temporal variations and the link existing between risk and local lake circulation and stratification dynamics. Although this study focuses on *Cryptosporidium*, the pathogen dispersal model is a generic model and may be applied to any other pathogen, such as for example *Giardia* spp., as well as bacteria and viruses. Likewise, Lake Tahoe is taken here as a study case, while the model is readily applicable to any water body.

4.2.2 Pathogen model

The pathogen model consists of a Release-module, a Transport-module and a Survival-module. The modules run sequentially and independently of each other. The model is driven by external computations that simulate hydrodynamic conditions prevailing in the lake. A Cartesian grid formed the domain for all simulations. A more detailed description of the dispersal model and the links between the different modules and external computations can be found in chapter 2.

The **R**elease-module (or R-module) simulates the process of pathogen release into the water column by direct released from body contact recreation. Pathogens may be released from skin surface during contact with water (shedding) and through accidental fecal release (AFR). The number of oocysts released by recreators at an instant of time t, $N(t)$, is given by

(Anderson *et al.*, 1998)

$$N_B(t) = R(t) \cdot (IM_S C_P + IFM_A C_P) \tag{4.1}$$

Here I is the average infection rate (%) and M_S represents the mass of fecal material shed by a recreator ($grecreator^{-1}$). C_P is the pathogen content of the fecal material (number of pathogens g^{-1}), F is the rate of AFR, and M_A is the mass of AFR ($grecreator^{-1}$). These parameters are taken to be constant over time. The mean recreator density, R ($recreatorsm^{-2}d^{-1}$), is variable in time, being typically higher at weekends than at week days. Beach areas may be defined by substrate (sand) and a critical water column depth H_{cr}. Only those grid cells that are equal or lower then H_{cr} ($H \leq H_{cr}$) are considered to be contributing pathogens released by recreators into the water column. Pathogen release was assumed to occur during the day by recreators and during night time from the sediments through resuspension (Wu *et al.*, 2009; Abdelzaher *et al.*, n.d.). The solution of the module consists of a time series of number of pathogens released into the pelagic over a given time period tl.

The **T**ransport-module (or T-module), simulates the pathways of released pathogens between beach areas and water intakes. Time varying 3D velocity fields and vertical diffusivity profiles from the external hydrodynamic computations are the drivers of these simulations. The simulations of the T-module are carried out using a Lagrangian model. In this model, particles are free to move independently of the model grid. However, the underlying hydrodynamic information (i.e. 3D velocity field, temperature and the vertical eddy diffusivity) is provided as input to the model based on the Cartesian grid and then interpolated to the particle position. For a detailed description of the 3D time-varying particle tracking model see Appendix A-1. Pathogens are treated as free particles in accordance with their strongly negative surface charge (at neutral pH) and their resistance to form aggregates with natural soil particles (Ongerth & Pecoraro, 1996; Dai & Boll, 2003; Dai *et al.*, 2004)) or organic particles (Brookes *et al.*, 2004a). Particles are back-tracked from the intake to their points of origin. This back-dispersion method comprises calculating the particle displacement at each time step from (a) the inverted

3D velocity field and (b) a random component representing the effect of horizontal and vertical diffusion (Han *et al.*, 2005). Transport simulations start every Δt_0 with the release of N_0 particles from the source cell (i_0, j_0) at time t_0 that are tracked during a period of ΔT. Pathogens infectivity is known to be sensitive to solar radiation in the ultraviolet (UV) wavelengths (Häder, 2003; Betancourt & Rose, 2004, and references therein). The most energetic and damaging part of the UV spectrum reaching the earth surface, UV-B radiation (290-315nm), is approximately 1% of the global radiation (Grant *et al.*, 1997). The UV-B radiation reaching a given individual l at time t is calculated from its vertical position $z(l,t)$, below the surface, and from the incident short wave radiation reaching the free surface $I_0(t)$ (Wm^{-2}), as follows,

$$I(l,t) = 0.01 \cdot I_0(t) \cdot exp[-k_{UV}(t) \cdot z(l,t)] \tag{4.2}$$

Here $k_{UV}(t)$ is the constant (in time and space) light attenuation coefficient set to $0.15m^{-1}$ (Rose *et al.*, 2009). The time-dependent light intensity reaching a given particle is then used to calculate the light dose over a given period of time period. The light dose experienced by the individual l, as it travels, $ID(l,t)$ (Jm^{-2}), is calculated as the amount of energy received, as follows

$$ID(l,t) = \sum_{t_0}^{t} I(l,t) \cdot \Delta t_T \tag{4.3}$$

Here Δt_T is the time step of the transport module. Note that the dose is a cumulative variable, and provides a measure of the energy levels that a given individual may have received, from time t_0 when it was released to the time t it reaches a source beach site (i,j), t_s $(t = t_s)$. The solution of each of these model runs consists of time-varying particle positions and the history of environmental conditions (temperature and solar radiation) that acted on each individual during its journey.

The **S**urvival-module (or S-module) accounts for the survival (or inactivation) of pathogens during their transport subject to the environmental conditions recorded in the T-module. Particles withdrawn at the intake are

considered to be pathogens released by recreators if (a) they originate from a swimming beach and (b) if the environmental conditions endured during their journey do not affect their survival (infectivity). Therefore, the probability P_V of a given intake to be contaminated by pathogens released at any beach source B_S at an instant of time t is expressed as the product of the probability of beach origin P_B and the probability of survival P_S

$$P_V(t) = P_B(t) \times P_S(t) \tag{4.4}$$

The probability of beach origin P_B is the fraction of particles withdrawn that originate from a beach source areas, identified by substrate type (sand) and water column depth H. Here H must be lower than or equal to a critical depth H_{cr} ($H \leq H_{cr}$). The probability that a pathogen remains viable or infectious, P_S, in the presence of the water temperatures and solar radiation endured is expressed as

$$P_S = P_T \times P_I \tag{4.5}$$

The probabilities P_T and P_I correspond to temperature and light, respectively. The probability of survival due to water temperature, P_T, is calculated from the temperature inactivation rate proposed by Walker & Stedinger (1999)

$$P_T = 1 - (10^{-2.68} \cdot 10^{0.058\theta}) \tag{4.6}$$

The probability P_T is evaluated for the mean temperature θ over the time it takes for a given particle to travel from the beach area to the intake. Pathogen inactivation due to solar radiation is defined in terms of infectivity. A given pathogen is considered inactivated when it receives a light dose sufficiently high to inhibit cell division and, hence, infectivity - though it may still be viable (Monis *et al.*, 2014). For simplicity, the light dose necessary to reduce pathogen infectivity to 0.01% (4-log inactivation), ID_{99}, is taken as a critical value and all particles that receive this dose are deemed to be inactivated. This approach may overestimate the number of infectious pathogens, compared to a probability density function, and may be considered to repre-

sent the worst case scenario. The solution of the S-module is a time series of the probability of pathogens to be withdrawn at the intake, calculated every Δt_0 seconds. Here, the pulses of withdrawn pathogens at time t represent the fraction of infectious pathogen originating from recreational beaches.

4.2.3 Application to *Cryptosporidium* in Lake Tahoe

The pathogen dispersion model was applied to the intestinal parasite *Cryptosporidium* in Lake Tahoe to simulate the potential dispersion of pathogens during a 2 month summer period, from July 1 (Day 183) to August 27 (Day 240), 2008 (the study period). The location of the water intake and known beach areas that may be potential sources of pathogens to the intake are indicated in Figure 4.1b. Recreator density was assumed to be $0.01 ind.m^{-2}d^{-1}$ during weekends, and 60% of that value on week days. In spite of reports on different infection rates between children and adults (see Gerba 2000 and references therein), daily age-structured observations of bathers are difficult to obtain and an average value was utilized. The infection rate I was assumed to be 3% (Anderson *et al.*, 1998; Gerba, 2000) with a mass of fecal material shed M_S of $0.1 g \text{recreator}^{-1}$ (Gerba, 2000). *Cryptosporidium* mean contents of feces were set at 10^6 oocysts g^{-1} feces (Jakubowski, 1984; Robertson *et al.*, 1995). Accidental fecal releases were assumed to occur for 1 in 1000 bathers, $F = 10^{-3}$ (Anderson *et al.*, 1998) and AFR mass M_A was $125 gAFR^{-1}$ (Feachem *et al.*, 1983; Bitton, 1994).

The intake was assumed to be at a water depth of 15.85m and 1.8m above the lake bed. The intake pumping rate was considered continuous at a value of $18 Ls^{-1}$. Particle releases commenced five days after the beginning of the hydrodynamic simulations, at day 188, to allow the hydrodynamic information to depart from the initial conditions (model spin up). In the T-module, a normal-distributed particle cloud was initialized on an hourly basis ($\Delta t_0 = 1h$), centered at the intake with a standard deviation $\rho_{xy} = 20m$ (one horizontal grid cells) and $\rho_z = 0.2m$ in the horizontal and vertical, respectively. The module was then run backward in time with a time step $\Delta t_T = 10s$, to satisfy the convergence criterion for particle tracking simulations (Ross & Sharples, 2004). The transport simulations were driven using

velocity and diffusivity fields from the hydrodynamic model. The hydrodynamic information and simulated temperature was given to the T-module every 3600s ($\Delta t_{h-output} = 1h$) and interpolated to Δt_T. Solar radiation data at 10 minute intervals was also passed to the T-module backward in time to estimate UV exposure. The number N_0 of particles released in each T-simulation was set to 10^3, to guarantee feasible computational costs. A single settling velocity $w_s = 10^{-7} ms^{-1}$ was defined based on the value for *Cryptosporidium* predicted by Stokes' law and supported by empirical estimates (Medema *et al.*, 1998; Dai & Boll, 2006). For the back-dispersion simulations, the settling velocity was inverted to become a buoyancy velocity. The simulations ended when at least 99% of the particles reached a light dose three-fold the critical value for 99.99% inactivation, ID_{99} (in terms of infectivity). Generally, this criterion was met within a time period $\Delta T \leq 1d$. The inactivation dose ID_{99} was defined based on empirical values found in the literature (Rochelle *et al.*, 2005; Connelly *et al.*, 2007; King *et al.*, 2008). Most studies on *Cryptosporidium* inactivation have focused on the UV-C radiation of 254nm (e.g. Craik *et al.*, 2001; Morita *et al.*, 2002; Hijnen *et al.*, 2006) and found ID_{99} of $\mathcal{O}(10) - \mathcal{O}(10^2) Jm^{-2}$. Given that UV-C radiation is attenuated in the atmosphere before reaching the earth surface and that UV-B radiation is of larger and less energetic wavelength, the critical light dose ID_{99} was taken to be one order of magnitude higher, $ID_{99} = 10^3 Jm^{-2}$.

4.2.4 Hydrodynamic simulations

The hydrodynamic simulations of lake currents and mixing variables were carried out using a parallel version of the semi-implicit 3D hydrodynamic model of Smith (2006) (Acosta *et al.*, 2010), and based on the numerical solution of the 3D form of the shallow water equation. The high-resolution hydrodynamic simulations were carried out in a two step nested procedure: In the first step, the whole lake domain was run with low spatial resolution, on a 100m grid in both the EW and NS directions. This model run produced the boundary conditions for the high resolution simulation. In the second step, these boundary conditions were used to run a reduced domain of the lake (Fig.4.1b) on a 20m horizontal grid. The vertical resolution

was variable, ranging from $\Delta z = 0.5m$ at the surface to $\Delta z = 10m$ near the bottom (i.e. at a depth of 500m) and equal for both horizontal resolutions. The model was forced using surface heat and momentum fluxes derived from local atmospheric variables (short and long wave radiation, air temperature, relative humidity, and wind speed and direction) observed at 10 locations around the lake (Fig.4.1a). Wind records were corrected for height and roughness (*see* Appendix A-2). The interpolation method proposed by Barnes (1964) (*see* Appendix A-2) was applied to construct the spatially variable wind fields used to force the model. The bathymetry was based on Gardner *et al.* (1998). The time step of the hydrodynamic model was 50s and 10s for the 100m and 20m simulations, respectively. The horizontal eddy diffusivity K_h was estimated based on the horizontal grid resolution and the time step, following Castanedo & Medina (2002), and set to $1ms^{-1}$ (100m grid) and $0.01ms^{-1}$ (20m). The initial temperature profile setup a stable stratification with a maximum of 19.75℃ (surface) and a minimum of 5.12℃ (hypolimnion) obtained from thermistor chain records (moored at T1, Fig.4.1a).

4.3 Results and discussion

4.3.1 Sources

A very small percentage (0.02%) of the water withdrawn during the study period was shown to originate from the shallow near-shore beach areas. Withdrawn water originated mainly (99.98%) from a depth below that associated to the shallow beach areas. There were days when 100% of the withdrawal originated from deeper waters, thus, assumed to be free from pathogens. In contrast, in extreme cases, up to 11% of the daily water volume was predicted to come from recreational beaches. Of the pathogens that reached the intake originated 81% from the beaches south of the intake and to 19% from beaches north of the intake (Fig.4.2). These pathogens were transported by the currents in the coastal boundary layer. The near-shore circulation is driven mainly by the local winds acting on the lake surface. Moderate SE and strong SW winds at Timber Cove (Fig.4.3) induce persistent and strong northward currents over the shelf along the southeastern shore. These currents were in

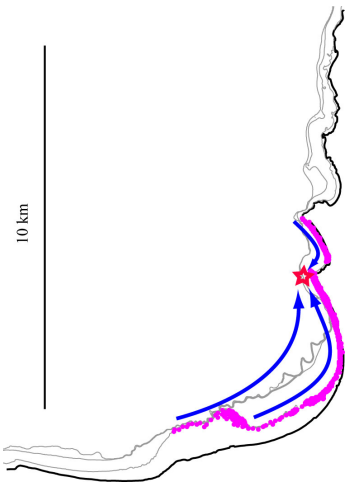

Figure 4.2: Horizontal distribution of pathogen sources over the study period. Star marks intake locations. Depth contours show 2, 9, and 16m isobaths for orientation.

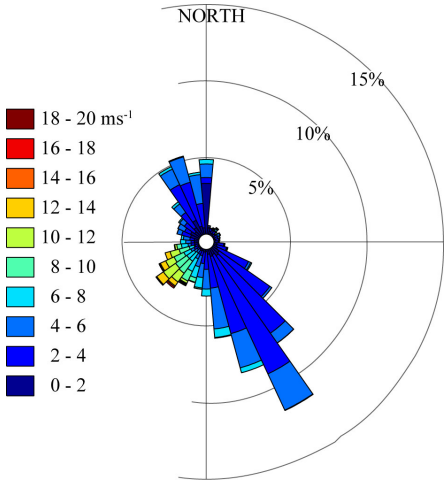

Figure 4.3: Wind speed and direction at Timber Cove (*see* Fig.4.1).

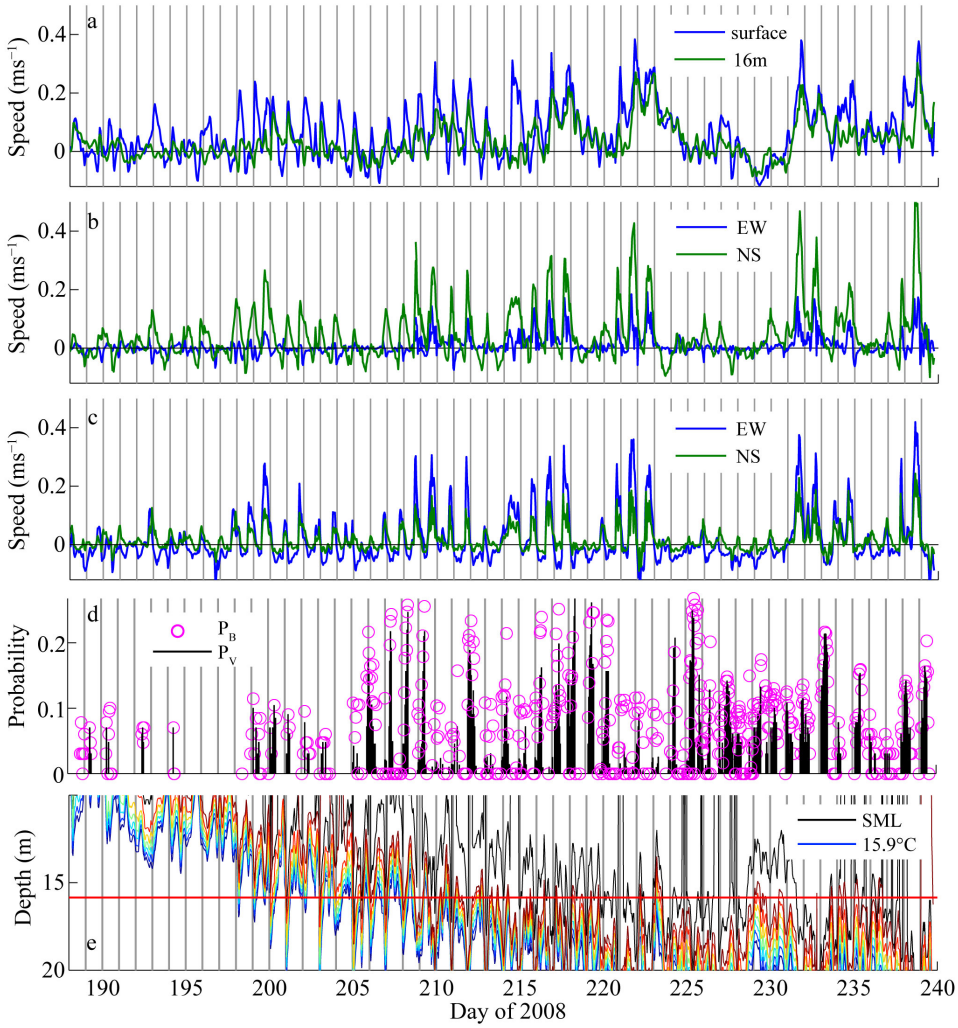

Figure 4.4: Simulated velocity currents at the intake (a) in the NS direction at the surface (blue) and 16m (green) depth, S2 (b) and S1 (c) in the EW (blue) and NS (green) direction at the surface. North and East are shown as positive. Pulses of pathogen withdrawal expressed as fraction of particles released in the T-module. Black lines indicate fraction of active pathogens. Circles mark the sum of active and inactivated pathogens. Depth of diurnal surface mixed layer (black line) (d) calculated from simulated temperature and isotherms (colored lines) at the thermocline between 15 and 16.2°C (0.2°C increments) (e). Horizontal red line marks depth of intake and vertical gray bars mark midnight for reference.

the same direction as the basin-scale currents associated to a large cyclonic gyre (counter-clockwise) at the south of the lake (*see* Chapt.3). High surface currents ($> 0.1 ms^{-1}$) are seen to occur nearly on a daily basis. Cross-shore currents at the intake were weaker than the alongshore currents, typical for flow in coastal boundary layers (Largier, 2003; Rao & Schwab, 2007; Nickols *et al.*, 2012). The contrast between along-shore and cross-shore currents intensity was also seen at S2 (Fig.4.4b) and S1 (Fig.4.4c). Daily alongshore currents exceeded $0.2 ms^{-1}$, while across-shore currents where generally less than $0.05 ms^{-1}$. Pathogens originating north of the intake were most likely to be transported to the south during the morning, when winds came from the NW (onshore winds due to land warming). These winds induced weak to moderate along-shore currents toward the intake (Fig.4.4a).

There were three main transportation pathways from of the source areas to the intake (Fig.4.2): (i) southward along the shoreline of the bay north of the intake, (ii) northward along the south-eastern shore following the 2m contour, and (iii) northward, from the southern shore across the open water toward the intake. Southward transport occurred during weak to intermediate wind forcing from the NW, while northward transport was driven by strong SW and predominantly weak SE winds (Fig.4.3). Time scales of transport from beach areas to the intake varied between 1.7h and 24h depending on the point of origin and the local current velocities. The shortest transport times were observed for pathogens released at the south-eastern beach area (1.7-22.8h) given its proximity to the intake and the elevated currents generated in the late evening (Fig.4.4b). Intermediate transport times were also observed for pathogens originating from beaches north of the intake (6.4-16.9h), mainly due to its proximity as southward currents were weak ($< 0.05 ms^{-1}$, Fig.4.4a). Pathogens released at the southern beach area revealed the highest range of transport times (2.2-24h).

4.3.2 Withdrawal

Withdrawal of pathogens increased overall during the study period and varied on a daily basis, being highest at night and in the morning (3-12h). Pulses of pathogens were predicted to enter the intake on a regular basis.

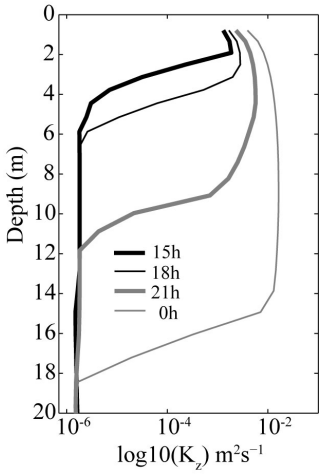

Figure 4.5: Vertical eddy diffusivity profiles at day 209 15h, 18h, 21h, and day 210 0h.

During the study period, three phases were discerned in function of the frequency and amount of pathogens withdrawn at the intake. During phase 1, from day 188 to day 198, the probability of pathogens withdrawn was small ($P_V < 0.1$, Fig.4.4d). From day 199 to day 205 (phase 2), there was an episodic but low withdrawal of pathogens ($P_V \leq 0.1$). After day 205 until day 240 (phase 3), pathogens were withdrawn regularly and at significantly higher amounts compared to phases 1 and 2 ($P_V \leq 0.3$). Loads of pathogens occurred mainly between 3h and 12h, with highest values at 10h. Between 1h and 10h, almost all pathogens that reached the intake were active (or infectious). The highest numbers of inactivated pathogens were withdrawn between 12h and 14h. The temporal variability of withdrawn pathogens during the day suggests that the pattern of pathogen withdrawal is controlled by the temporal dynamics of vertical dispersion associated with lake motions. The differences between active and inactivated pathogens that reach the intake indicates that these pathogens are highly sensitive to environmental conditions (temperature or light) endured during their journey toward the intake.

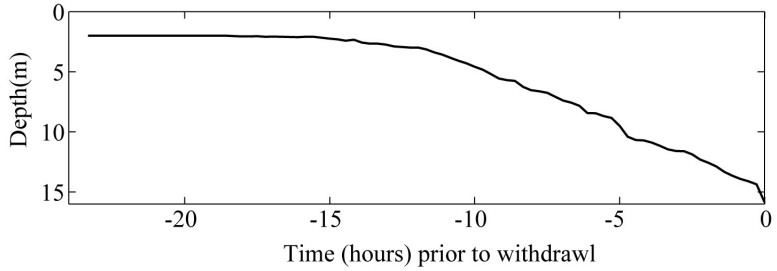

Figure 4.6: Mean pathogen vertical excursion.

4.3.3 Vertical dispersion

The vertical dispersion of pathogens was tightly linked to the temporal dynamics of the depth of the surface mixed layer (SML), over which they are dispersed constantly and uniformly. The depth of the thermocline of Lake Tahoe ranged from 10-20 m during the study period (Fig.4.4e) and the stability of the water column was high. The Wedderburn number, W, and the Lake number, L_N, (Stevens & Imberger, 1996), used to parameterize the balance between stabilizing thermal stability and destabilizing wind forcing, were both well above unity at all times. Assuming a two-layer stratification with an upper mixed layer of thickness H, the displacement of the interface, Δh, driven by wind forcing can be estimated as $\Delta h = 0.5H/W$ (Shintani *et al.*, 2010). Interface displacement was of order 8m, suggesting that the intake at the 16m isobaths was at times within the SML.

The depth of the diurnal SML varied between the near surface and the top of the metalimnion given the diurnal temperature variations (Fig.4.4e). The SML depth was derived from the simulated temperatures time series at the location of the intake, and taken to be the depth where the density difference $d\rho$ between the density ρ_z and the surface density ρ_0 yielded a linear gradient equal to $0.02\,kgm^{-4}$ (Reynolds, 1984). The three phases identified earlier can be related to the maximal depth of the diurnal SML during night time cooling: (i) At the beginning the study period, from day 188 to day 199 (phase 1), the SML was relatively shallow and deepened to a maximal depth of 10m (Fig.4.4e). During phase 2, the maximal depth of the SML during the night increased from 10m to 16m from day 199 to day 205, respectively. After day 205 until day 240 (phase 3), the depth of

the SML exceeded 16m almost on a daily basis. Consequently, the intake ($z = 15.85m$) was located at or below the depth of the SML during 80% of the time during this phase. The deepening of the SML below the depth of the intake exposes the intake to surface (epilimnetic) waters, which are typically of lower water quality and may carry potential contaminants, such as human waterborne pathogens.

The vertical excursions of pathogens from the shallow beach areas to the intake vary in function of vertical mixing intensities. *Cryptosporidium* oocysts with a settling velocity $w_s = 10^{-7}\, ms^{-1}$, typical from *Cryptosporidium* (Dai & Boll, 2006), are practically neutrally buoyant in turbulent environments. With a diurnal SML depth H of O(10)m, as predicted for Lake Tahoe, the vertical eddy velocity $v_z (= K_z/H)$ is $10^{-7}\, ms^{-1}$ and of the same order of magnitude as the settling velocity of *Cryptosporidium* oocysts. Even for a settling velocity of $\mathcal{O}(10^{-6})\, ms^{-1}$, as reported for *Giardia lambia* cysts (Dai & Boll, 2006), turbulence intensities (indicated by K_z) in the SML of Lake Tahoe can keep these pathogens in suspension over extended period of time. Vertical eddy diffusivity K_z at the intake was estimated to be of $\mathcal{O}(10^{-4})\, m^2 s^{-1}$ to $\mathcal{O}(10^{-2})\, m^2 s^{-1}$ in the epilimnion and, thus, 2-4 orders of magnitude larger than the molecular diffusivity (Fig.4.6). The vertical excursion of the pathogen originating from near-shore areas <2m depth and withdrawn at the intake reveal a transport pattern consisting of two phases in function of the vertical particle position (VPP): (i) the VPP changes frequently between the surface and the bottom of the shallow near-shore and (ii) the VPP increases progressively until it reaches the depth of the intake (Fig.4.6). Note that the mean vertical pathogen excursion shown in Fig.4.6 does not reveal the frequent changes in the VPP between the surface and the lake bottom or depth of the SML. In general, variations of the VPP were restricted to the SML layer and spatially separated from the strongly stratified metalimnion where turbulent is greatly reduced. Consequently, the deepening of the SML caused the pathogens to be transported to greater depth and eventually to the depth of the intake initially located below the SML (Fig.4.4e). Deepening of the SML occurred in response to enhanced vertical mixing induced by convective cooling and wind shear on a daily basis, thus, increasing the depth to which pathogens were dispersed. The vertical

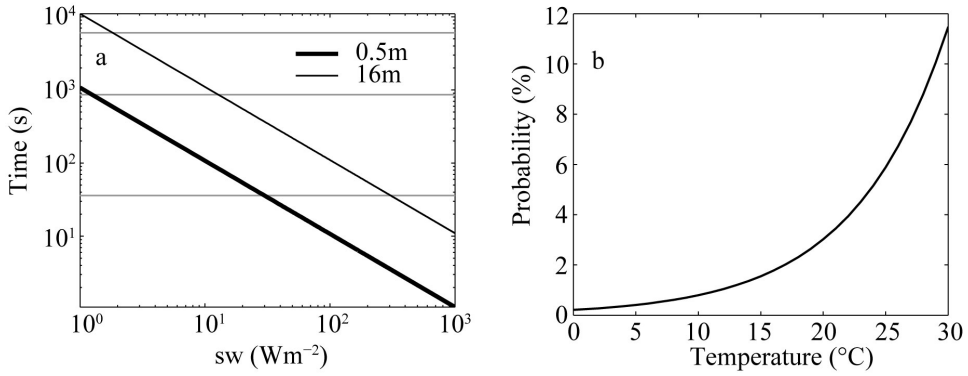

Figure 4.7: Probability of *Cryptosporidium* inactivation: (a) time scale for inactivation due to solar radiation at 0.5m and 16m depth and (b) probability of inactivation due to water temperature following the inactivation rate proposed by Walker & Stedinger (1999). Gray bars in (a) mark 1h, 1d, and 1 week for reference.

position of a given particle within the water column, in turn, determines the pathogen's survival and inactivation due to temperature and light.

4.3.4 Inactivation

The oocysts of *Cryptosporidium* are highly sensitive to solar radiation resulting in a high light inactivation rates in the very clear waters and high UV flux typical at Lake Tahoe. About 61% of those individuals that originated from shallow beach areas were inactivated due to solar radiation, while temperature inactivation occurred for less than 1% of individuals. The damaging effects of light, especially ultraviolet radiation (UVR), on DNA and the consequences for health and survival or organisms are well known (Sinha & Häder, 2002; Häder & Sinha, 2005). Tucker *et al.* (2010) showed, for example, how UVR limits the habitat of the invasive bluegill sunfish (Lepomis macrochirus) in Lake Tahoe, being present only in zone of high turbidity where UV radiation is attenuated rapidly with depth. The effect of radiation on the pathogen infectivity became evident in difference between the number of active (infectious) and inactive pathogens withdrawn during the morning hours (Fig.4.4d). During the night, 95% of the pathogens withdrawn were infectious, as they travelled in absence of solar radiation during large part of their trajectory. However, after sunrise a fraction of pathogens

were inactivated by UVR and the number of infectious pathogens withdrawn was inferior to the total amount of pathogens that reached the intake.

Given incident short wave radiation values between 1 and $10^3 Wm^{-2}$, typical for Lake Tahoe, a light attenuation coefficient k_{UV} of $0.15m^{-1}$ and a 4-log inactivation dose ID_{99} of $10^3 Jm^{-2}$, the time needed to inactivate 99.99% of potential pathogens ranges from $\mathcal{O}(1)$min-$\mathcal{O}(1)$d at 0.5m depth (Fig.4.7a). At 16m depth, in contrast, inactivation time scale are one order of magnitude higher, ranging from $\mathcal{O}(10)$min-$\mathcal{O}(10)$d. The different inactivation time scale between 0.5m and 16m depth explain how pathogens could reach the intake during the early morning hours without being inactivated. Once the pathogens have reached a depth were UVR is significantly attenuated, they may continue travelling in spite of the increasing solar radiation reaching the free surface. The predicted time scales are in accordance with (Connelly *et al.*, 2007) who found that *Cryptosporidium* is inactivated by $>$99.99% during 10h of light exposure during a mid-summer day at temperatures comparable to those found at Lake Tahoe (10-20°C). However, inactivation rates depend on the critical light dose for inactivation ID_{99}. For example, for a critical value of $\mathcal{O}(10^2) Jm^{-2}$, and thus one order of magnitude smaller than the one used in the present study, 79% of the pathogens released would be inactive before reaching deeper waters and, thus, potential water intakes. For a critical value ID_{99} of $10^2 Jm^{-2}$ (short wave radiation of $1 - 10^3 Wm^{-2}$, $k_{UV} = 0.15m^{-1}$), inactivation time scales would range from $\mathcal{O}(10)$s to $\mathcal{O}(1)$h at 0.5m depth.

The predicted scales indicate that pathogens released in shallow water, where they are exposed to high solar radiation intensities, are inactivated within $<$O(1)d. The inactivation of pathogens is likely to occur within short periods of time as the hours of maximal bathing activity coincide with hours of maximal solar radiation (late morning until early evening). Consequently, the light dose received due to exposure to UVR would have to be low in order for pathogens to be infective when being withdrawn at the intake. Low light (UVR) doses can result from (i) short transport time scales due to short transport distance or high current velocities, and (ii) transport at times or depths of low light intensity.

Solar radiation is the dominant abiotic agent for pathogen inactivation.

In Lake Tahoe, almost 40% the pathogens withdrawn were predicted to be inactivated due to solar radiation while losses due to temperature were close to zero. The relatively strong effect solar radiation on pathogen inactivation in this large alpine lake might result from high intensities of solar radiation and high clarity (i.e. low light attenuation with depth), but moderate water temperatures compared to lakes at low altitude and similar latitude. Nonetheless, even for an extreme case of a tropic lake of high turbidity (high light attenuation) and a mean surface temperature of 30°C, the daily pathogen inactivation due to temperature would be 10% (Fig.4.7b), while the time scale for a 99,99% inactivation due to light at 0.5m depth would be 7.5min, assuming a ID_{99} of $10^3 Jm^{-2}$, an attenuation coefficient k_{UV} of $3.0m^{-1}$, and an incident short wave radiation of $10^3 Wm^{-2}$. The high sensitivity of *Cryptosporidium* to radiation is beneficial for the purpose of water disinfection. Low wavelength UVR (typically between 200 and 280 nm) is increasingly applied for disinfection during drinking water treatment (Betancourt & Rose, 2004; USEPA, 2006; Monis *et al.*, 2014). Solar radiation the pathogens are exposed to is the principle factor of pathogen inactivation with rates exceeding those of temperature inactivation or losses due to settling.

The importance of solar radiation for pathogen inactivation found is in contrast to other studies that did not consider the effect of solar radiation on pathogen infectivity (Anderson *et al.*, 1998; Stewart *et al.*, 2002) or those that considered settling to significantly reduce oocyst concentrations in the water column (Medema *et al.*, 1998; Hawkings *et al.*, 2000). The finding that solar radiation reduces the number of viable pathogens entering drinking water intakes through pathogen inactivation is in agreement with Hipsey *et al.* (2004). Both pathogen inactivation rates and time scales depend on the specific light parameters (light attenuation coefficient k_{UV} and critical inactivation dose ID_{99}) used, representing the light conditions of a particular lake or lake region. Light attenuation coefficients are typically determined from off-shore Secchi disk measurements (Swift, 2004; Rose *et al.*, 2009). However, near-shore (littoral) waters are known to be exposed to higher amount of organic matter (imported from rivers and terrestrial ecosystems) and, thus, are of lower clarity (Swift *et al.*, 2006; Rose *et al.*, 2009). Therefore, off-shore light attenuation coefficients may overestimate UVR intensities and,

thus, underestimate the risk of pathogen contamination.

4.3.5 Risk of contamination

The risk of pathogens entering drinking water intakes is low (0.02%), but is not totally absent. The risk of pathogens entering water intakes is tightly linked to the stability of the water column, in particular, to the depth of the surface mixed layer. During early summer, intakes located below the SML are protected by the metalimnion. However, as the summer proceeds, water temperatures decrease and the SML deepens, those intakes, if they are not below the SML depth, are likely to be exposed to surface water potentially containing human water-borne pathogens. Further, daily fluctuation of the thermocline and the diurnal mixed layer, due to convective mixing at night have been shown to affect the risk of pathogen withdrawal. Thus, the vertical position of the intake in relationship to the expected depth of the thermocline, its seasonal and daily variations, influences the risk of viable pathogens being withdrawn. Drinking water intake, hence, should be located at a depth below the maximal oscillation of the seasonal SML to minimize the risk of human water-borne pathogens origination from body contact recreation. Such consideration would also need to take into account likely lake levels in the face of extreme drought events, during which the intake is closer to the water surface. Further a sufficiently large distance between the intake and known recreational beaches located upwind of the intake reduces the risk of pathogen contamination given the higher probability of UVR inactivation.

Knowledge about daily variation of risk of pathogen withdrawal may help to schedule the times of water withdrawal. High risk was observed to occur during the night with peak intensities in the early morning, as pathogens travel in the dark, protected from harmful solar radiation, and remain infectious when reaching the intake. In contrast, during day time, pathogens dispersed within the shallower SML are inactivated rapidly by solar radiation before reaching the intake and water withdrawal appears to be safe. Thus, water companies could alternate between water withdrawal, during times of near-zero risk, and no withdrawal during times of elevated risk. Special care should be taken at the weekends and holidays when beach

visitor density is increased and hours of beach activity may be extended. Also period of strong wind forcing and, thus, strong current velocities may contain a potential risk of pathogens entering water intakes as transport times and exposure times to solar radiation decrease.

Increased light attenuation at the near-shore, where potential pathogens are released, reduces the light intensities to which pathogens are exposed and increases the risk of pathogen contamination at water intakes. If the light attenuation in the shallow near-shore is unknown or cannot be determined with certainty, using a higher critical light dose for pathogen inactivation may help to prevent underestimating the contamination risk, considering worst case conditions. The high sensitivity of pathogens to solar radiation stresses the importance of water clarity. In clear lakes and reservoirs, solar radiation acts as a mechanism of natural water disinfection. Therefore, water clarity helps to improve water quality and, thus, its maintenance should be of high priority in lake and reservoir management, especially in drinking water sources.

Chapter 5

Conclusions

1. The dispersal of Asian clam in the surface water of lakes is largely controlled by the wind regime, the magnitude of wind events and their timing.

2. The likelihood of Asian clam entrainment, transport and dispersal increases during episodic events of strong wind forcing.

3. Larvae dispersal occurs in form of pulses in response to episodic events of strong wind forcing.

4. Dispersal of Asian clam occurs along a discrete number of preferential pathways.

5. Under predominantly weak wind forcing, the impact of UV-radiation during the pelagic stages on Asian clam mortality is low as a result of the short dispersal distances associated with relatively high larval settling velocity.

6. The final distribution of dispersed larvae and the probability of their survival are sensitive to the larval settling velocity.

7. Flow inside bays tends to exhibit recirculating currents, likely as the results of flow separation at the bay boundary.

8. Bays that are characterized by low current velocities and re-circulation act as traps for suspended benthic larvae.

9. For the study case of Lake Tahoe, the risk of drinking water contamination by human water-borne pathogens originating from recreational

beaches is low, but significant.

10. The risk of pathogens contamination is strongly related the depth of the thermocline in relation the depth of the intake.

11. The risk of pathogen contamination increases with the seasonal deepening of the surface mixed layer.

12. The risk of pathogen contamination increases at night when the surface mixed layer deepens through convective mixing and inactivation by UV radiation is eliminated.

Chapter 6

Conclusiones

1. *La dispersión de la almeja asiática en aguas superficiales de lagos es controlada en gran medida por el régimen de viento, la magnitude de los eventos de viento y su ocurrencia temporal.*

2. *La probabilidad de la resuspension de la almeja asiática, su transporte y su dispersión aumenta durante periodos episódicos de vientos fuertes.*

3. *La dispersión de larvas ocurre en forma de pulsos en respuesta a eventos episódicos de vientos fuertes.*

4. *La dispersión de la almeja asiática tiene lugar a través de un número discreto de rutas preferenciales.*

5. *Bajo vientos predominantemente suaves, el impacto sobre la mortalidad de la almeja asiática de la radiación ultravioleta durante el estado pelágico es bajo ya que las distancias que recorren tras cada evento son cortas, debido a la relativamente alta velocidad de sedimentación de las larvas.*

6. *La distribución final de las larvas dispersadas y su probabilidad de supervivencia son sensibles a la magnitud de la velocidad de sedimentación de las mismas.*

7. *La sensibilidad a la velocidad de la sedimentación se ve aumentada en las regiones de bahías, donde la separación del flujo de las paredes laterales del lago crea corrientes de recirculación.*

8. *La recirculación en las bahías unida con la baja magnitud de las velocidades de la corriente, actúan como trampas de sedimentación para las larvas de especies bentónicas en suspensión.´*

9. *El estudio de la dispersión de Cryptosporidium en el Lago Tahoe revela que el riesgo de que patógenos humanos acuáticos, provenientes de playas de uso recreativo, lleguen a una toma de agua potable is bajo pero significante.*

10. *El riesgo de contaminación por patógenos viene determinado por la profundidad de la termoclina con respecto a la profundidad de la toma de agua.*

11. *El riesgo de contaminación por patógenos aumenta a lo largo del verano con el aumento de la profundidad de la capa de mezcla.*

12. *El riesgo de contaminación por patógenos aumenta asimismo a escala diaria, durante la noche, cuando la capa de mezcla aumenta en profundidad debido a la mezcla convectiva y la inactivación debida a la radiación ultravioleta es eliminada.*

Appendix

A-1 Particle tracking

Particle trajectories were simulated using a Random Displacement Model. The model has been successfully validated for purely advective and advective-diffusive water motions, for particle settling as well as for particle resuspension in a closed basin under wind-forcing. In this model, the particle trajectory is calculated as the summation of successive infinitesimal particle displacements dx_i over time. The particle displacement dx_i, in turn, are described as follows

$$dx_i = \underbrace{a_i(\mathbf{x},t)\cdot dt}_{\text{(term 1)}} + \underbrace{\sum_{j=1}^{N} b_{ij}(\mathbf{x},t)\cdot dW_j(t)}_{\text{(term 2)}} \tag{A-1}$$

where the right hand side consists of a deterministic part (term 1) and a stochastic part (term 2). The coefficients a_i and b_{ij} satisfy the following equations (Dunsbergen & Stelling, 1993)

$$a_i = \mathbf{u}_i + \sum_{j=1}^{N} \frac{\partial D_{ij}}{\partial x_j} \tag{A-2}$$

$$\frac{1}{2}\sum_{k=1}^{N} b_{ik}b_{jk} = D_{ij} \tag{A-3}$$

Here N is the number of dimensions, $\mathbf{x}$ and $\mathbf{u}$ are the particle position and velocity, D_{ij} is the isotropic diffusion tensor in the flow field, and ΔW_j is a Wiener or Brownian motion process. The velocity data is derived from the hydrodynamic simulations, through interpolation from grid points in the computational domain to the present position of a given particle. This in-

terpolation is done following the method proposed by Pollock (1988). The eddy diffusivity K_i in the model varies quadratically with vertical direction between three consecutive nodes in a grid column (quadratic interpolation), and it is assumed constant in the horizontal directions (Rueda, 2001). The deterministic part represents the advective transport and also includes the influence of the gradient of turbulent diffusivity, needed for consistency with the advection-diffusion equation (*see* Dimou & Adams, 1993; Kitanidis, 1994). The stochastic displacement mimics the effect of turbulent processes in the particle trajectory. The discretization of Eq.A-1 that represents the transition from the state (or particle position) at $n\Delta t$ to the state at $(n+1)\Delta t$ is given as

$$\begin{aligned} x_i^{(n+1)} = \quad & x_i^{(n)} + a_i(\mathbf{x}^{(n)}, n\Delta t) \cdot \Delta t \\ & + \sum_{j=1}^{N} b_{ij}(\mathbf{x}^{(n)}, n\Delta t) \cdot \Delta W_j(n\Delta t) \end{aligned} \tag{A-4}$$

where the bold variables are vector quantities. The factor $\Delta W_j(t)$ is simulated by a Gaussian number generator, with $E(\Delta W_j) = 0$ and $E(\Delta W_i \Delta W_j) = \delta_{ij}\Delta t$.

A-2 Wind observations

A-2.1 Height and roughness correction

To estimate wind stress, wind speed records had to be adjusted to 10-meter height. In doing this readjustment, atmospheric conditions above the reservoir surface and the surrounding landscape during these observation periods were assumed thermally neutral and stable (Cook, 2000). Under those conditions, the wind speed above the land-water surface follows a logarithmic law. The following expression that relates wind speeds measured at a particular height (U_z) and theoretical wind speeds occurring at a 10-meter height can be derived (see Amorocho & DeVries, 1980)

$$U_{10} = U_z + \frac{u_*}{\kappa} ln(10/z) \tag{A-5}$$

where u_* is the wind shear velocity ($u_* = \sqrt{\tau_w/\rho_{air}}$) ($ms^{-1}$), τ_w is the wind shear stress at the water surface ($pa\,m^{-2}$), ρ_{air} is the density of air (kgm^{-3}), and κ is the von Kármán constant (0.4, dimensionless).

In addition, Amorocho & DeVries (1980) developed theoretical relationships between wind shear velocities u_* and wind speeds measured at a 10-meter height U_{10}, based upon empirical data they gathered themselves and from several other studies. These relationships express shear velocities as functions of wind velocities, as follows

$$u_* = 0.0323 \cdot U_{10} \qquad 0ms^{-1} < U_{10} < 7ms^{-1} \qquad \text{(A-6)}$$

$$u_* = 0.06015 \cdot U_{10} - 0.1949 \qquad 7ms^{-1} < U_{10} < 20ms^{-1} \qquad \text{(A-7)}$$

$$u_* = 0.0504 \cdot U_{10} \qquad 20ms^{-1} < U_{10} \qquad \text{(A-8)}$$

These investigators found that three distinct stress relationships occur during the development of a wind field. Prior to the onset of breaking wind waves, the wind stress coefficient of drag is fairly constant ($C_D \sim 1.4 \times 10^{-3}$). This seemed to occur when $U_{10} < 7ms^{-1}$. After the formation of the first breaking waves a transition region occurred wherein the density of breaking waves trended toward a limit in the velocity range: $7ms^{-1} < U_{10} < 20ms^{-1}$. In this region, the drag coefficient "varies nonlinearly with U_{10}". Once a water body became saturated with breaking waves, i.e. when $U_{10} \sim 20ms^{-1}$, the C_D was again found to be constant ($C_D \sim 2.54 \times 10^{-3}$). Note that the coefficient of drag was assumed to increase linearly with wind speed in the region of $7ms^{-1} < U_{10} < 20ms^{-1}$. Introducing Equations A-5 into Equations A-6 - A-8, and considering the relationship between shear velocity and wind velocity, results in simplified expressions to convert observed wind speeds at other heights to U_{10} values.

The roughness correction procedures was based on the theory of boundary layer flow perpendicular to a sharp transition between two flat surfaces of different roughness (Tayler & Lee, 1984). For any given land based weather station, the wind speed over water was estimated from the observed wind speed over land by multiplying the records by a fixed factor of 1.45 for offshore winds.

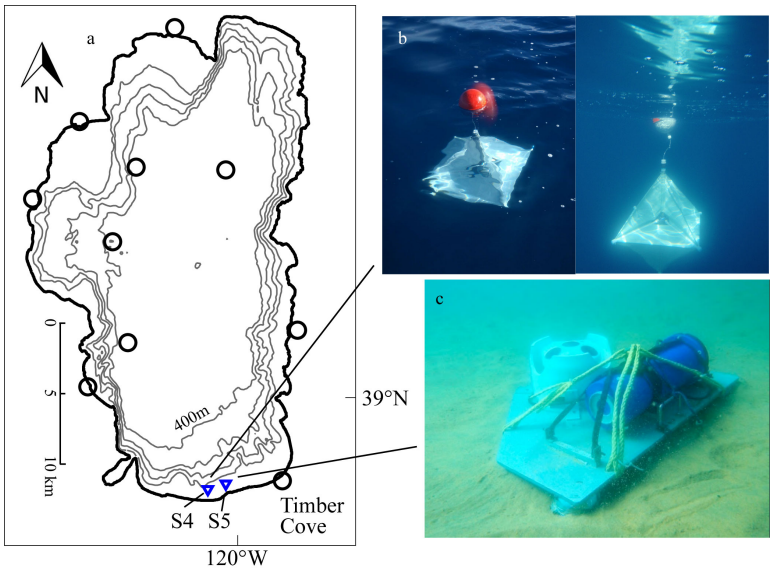

Figure A-1: Lake Tahoe: (a) location of meteorological stations (circles) and instruments deployed for circulation and currents measurements (triangles), (b) Lagrangian drifter (drogue), courtesy of Brant Allen, and (c) Nortek Acoustic Doppler Wave and Current Profile (AWAC), courtesy of Geoff Schladow.

A-2.2 Spatial interpolation

The spatial interpolation method developed by Barnes (1964, 1994a,b) was followed to produce continuous fields of wind over Lake Tahoe, from records collected at discrete locations (meteorological stations, Fig.A-1a). Those continuous fields are sampled, in turn, at the nodes of the computational Cartesian grid constructed for the hydrodynamic model. The method of Barnes is an iterative approach, and requires several iterations to reduce the interpolation error. Here the method is outlined using only two iterations, as presently included in the hydrodynamic model. At any given time n, the wind velocity in the EW direction u_a at any given node (i, j) is estimated as a weighted average of the records available at N meteorological stations.

$$u_a\,(\,i,j,t\,) = \sum_{s=1}^{N} \eta\,(\,i,j,s\,) \cdot u_a\,(s,t\,) \tag{A-9}$$

Equivalently, the weighted average of the wind velocity in the NS direc-

tion v_a is

$$v_a\,(\,i,j,t\,) = \sum_{s=1}^{N} \eta\,(\,i,j,s\,) \cdot v_a\,(s,t\,) \tag{A-10}$$

The weight given at node (i,j) to the observations from a given station s is a function of the distance r between the node (i,j) and the station site (s) as follows

$$\eta\,(\,i,j,s\,) = exp\Big(-\frac{r^2}{4k}\Big) \tag{A-11}$$

The parameter k determines the shape of the weighting factor, and was, in turn, calculated as in Koch *et al.* (1983)

$$k = -\left(\frac{2\Delta n}{\pi}\right)^2 \ln D_0(2\Delta n) \tag{A-12}$$

Where Δn is the average distance between the stations and D_0 is a response function

$$D_0(\lambda) = \Big[D_0(2\Delta n)\Big]^{(2\Delta n/\lambda)^2} \tag{A-13}$$

Where λ is the wave length. During this interpolation method, the first pass interpolation of the meteorological observation V, V_I, is carried out as follows

$$V_I = \sum_{s=1}^{N} V \cdot \frac{\eta(s)}{S_\eta} \tag{A-14}$$

Where S_η is the sum of the weighting parameters η at each grid point and N is the number of meteorological stations. After interpolating at each grid point, the interpolated field is compared to the original observations. The error, or residual value, is calculated as the difference between the original observations and the calculated wind field at that point

$$E = V_I - V \tag{A-15}$$

Based on this error, a second pass interpolation is carried out to correct

Table A-1: Field instruments deployed for circulation and currents measurements.

Instrument	Location	Coordinates	Time period
Drogue 1-3	S4	758110,4314200	219-226,2008
Nortek AWAC	S5	N38,94281°, W120.01964°	204-247,2008

the first pass interpolation. Again each stations is assigned a new weighting factor η' for each grid point and a second interpolation is carried out. The second pass weighting factors are calculated as follows

$$\eta'(i,j,s) = \eta(i,j,s)^{(1/\gamma^{nit})} \tag{A-16}$$

where γ is a numerical convergence parameter and nit is the number of iterations. The second pass interpolation is given by

$$V_{II} = V_I + \sum_{s=1}^{N} E \cdot \frac{\eta'(s)}{S_{\eta'}} \tag{A-17}$$

here $S_{\eta'}$ is the sum of the new weighting parameters η' at each grid point.

A-3 Validation of the lake hydrodynamic model

A-3.1 Data set for lake hydrodynamic model validation

The basin-scale motions and the local current conditions predicted by the hydrodynamic model were validated against data from two types of measurements. Basin-scale lake motion was characterized with Lagrangian drifters (Fig.A-1b). Three Lagrangian drifters (drogues) were deployed during the summer of 2008 and their GPS positions were recorded at 10min intervals. The drogue trajectories depicted circulation patterns and were used to determine the scale of circulation, the general direction of the circulation and to estimate surface current velocity magnitudes in Lake Tahoe. The drogues were released on day 219, 2008, centered at a depth of 1 m below the free surface (default) at site S4 (Fig.A-1a, *see* Tab.A-1 for exact coordinates). They were retrieved 7 days later, on day 226. The drogues were released between 400m and 500m from shore, and at the same time. The model results used

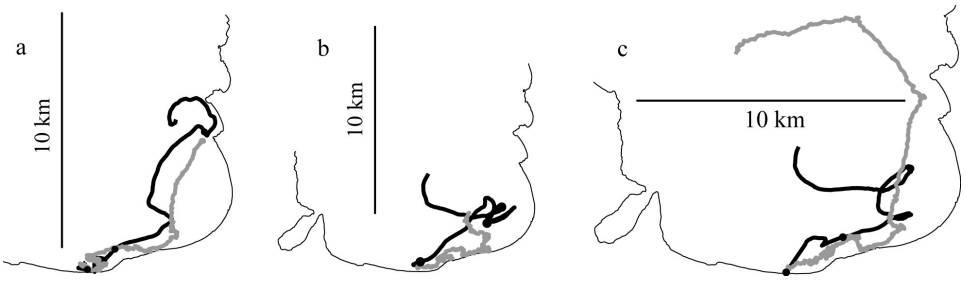

Figure A-2: Observed drogue trajectories (black) and simulated particle trajectories (gray) for (a) Drogue 1, (b) Drogue 2 and (c) Drogue 3.

for the validation of the basin-scale motion consisted of three particle trajectories. The particle tracking model (Appendix A-1) released 10,000 particles at S4 (Fig.A-1a) and tracked their motion with the horizontal velocity field obtained from the hydrodynamic simulations (*see* Wave- and hydrodynamic simulations). As the real drogues are constrained to travel at a constant depth, the depth of the particles was kept constant. Local current measurements in the near-shore environment in Lake Tahoe collected using a Nortek Acoustic Doppler Wave and Current Profile (AWAC) (Fig.A-1c). The profiler was moored at S5 (Fig.A-1a, Tab.A-1 at ∼5m depth directed upward to record current velocity and direction from the lake bottom to the surface (except for a blanking distance of ∼1m) every 10min. The current measurements extended from day 204 to day 247 in 2008. A simulated time series of horizontal velocities was output at the grid cell closest to S5 to validate against the AWAC velocity measurements.

A-3.2 Basin-scale circulation

The known circulation pattern of Lake Tahoe in the pelagic generally comprises three counter-rotating gyres: (i) a cyclonic gyre in the south, (ii) an anticyclonic gyre in the center, and (iii) a cyclonic gyre in the north of the basin (Fig.3.2a). This basin-scale circulation pattern is conform with previous observations from satellite images (Steissberg *et al.*, 2005). These gyres are highly variable in both their size and their position, being highly influenced by the diurnal wind field and the variable wind direction over the lake. Within the littoral zone less is known, and these drogue measurements were

the first to explore connections between littoral motions and the pelagic motions. The results are shown in Figure A-2. The black lines represent the measured drogue trajectories, and the gray lines are the simulated trajectories. At the outset, the drogues were initially very close together (within one or two grid cells) within the littoral zone. Despite this initial proximity, across the duration of the experiment the drogues trajectories took very different paths. Seemingly, small differences in the initial location made very large differences to the trajectories followed. This is in part explainable by the random nature of the forcing, but also by the location of the drogues in the interface region between the littoral and the pelagic. As is evident in Figure 3.2, in this areas there are regions of velocity shear and even flow reversals close to shore, and the notion of the trajectories of two drogues diverging in this region is easily understood.

For the simulated drogue trajectories all the same caveats apply, but with one major additional one. While the real drogues were driven by currents induced by the actual wind field, the simulations used an approximation to the spatial wind field, derived from an interpolation between ten wind stations on and around the lake. Spatial and temporal changes in the wind field would be damped out. Thus the forcing experienced in the simulations is different. Given that the trajectories of the three real drogues displayed great separation despite their initial proximity, it was realized that the expectation of close agreement between real and simulated over a week-long period was unrealistic. While the currents experienced at a point may be close, the integrated effect over a week-long period would likely produce large departures. Therefore, the goal of the validation was not to try and seek a match between the real and the simulated trajectories - that would be an extremely onerous task in a complex wind field of a high mountain lake. Rather it was to ensure that the scale and directionality of the motions were consistent.

The real drogues all tracked to the north-east initially, following the lake bathymetry. However, their paths diverged after the first 24-36 hours. Drogue 1 (Fig.A-2a) moved toward Marla Bay (the area of the highest *C. fluminea* density, Fig.2.1a) and appeared to remain trapped by the secondary recirculation in that vicinity, before moving to the southwest as part of the

cyclonic gyre. Drogue 2 and 3 (Figure A-2b,c) both initially traveled toward the northeast, but then took an unexpected turn across the lake toward the west. Drogue 2 eventually became entrained in a northward jet up the west shore before being entrained into the northern-most cyclonic gyre. Drogue 3 ran aground on the west shore before the end of the experiment.

The particles actually agreed quite well with the drogues for the first 24-36 hours, moving in the same direction and at about the same speed. During this time, they were close to a meteorological station (Timber Cove, Fig.A-1a) so the effect of wind interpolation would have been minimized. Beyond this point the particles and the drogues parted ways. However, there were two important characteristics that were preserved. First, the particles and drogues that arrived in the vicinity of Marla Bay, all appeared to get trapped there by small scale recirculating currents. Second, at some stage the drogues and the particles all moved rapidly across the lake to the west and were caught up in the large scale pelagic circulation of the lake.

This validation exercise demonstrated that for the first 1-2 days, the particles and the drogues actually tracked reasonably well. Beyond that time, and especially as the particles moved further away from meteorological stations, the trajectories departed, although the general characteristics were preserved. As the present purpose of the model is to track the motion of larvae for just 48 hours, the performance of the model is believed to be satisfactory.

A-3.3 Local-scale validation

The hydrodynamic model reproduced the pattern and magnitude of local scale surface current recorded by the AWAC reasonably well. These currents were most intense in EW direction (along-shore) with daily maxima in the evening (Fig.A-3). Currents in the NS direction were of slightly lower magnitude. The current direction was predominantly toward the northeast, consistent with winds blowing from the south-west recorded at Timber Cove (not shown, but *see* interpolated records for Marla Bay, Fig.3.3a). Short-term changes and oscillations were revealed well by the model, for example, between day 208 and 209. The model was also able to reproduce correctly

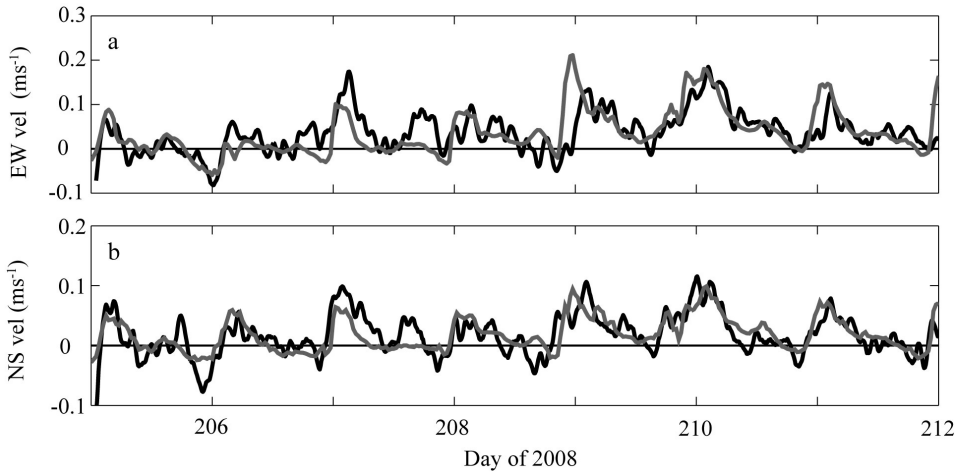

Figure A-3: Observed (black) and simulated (gray) surface current velocities in (a) EW and (b) NS direction at S5 (Fig.A-1a.

the magnitude of the current. The overall RMSE was $4.53 \times 10^{-2} ms^{-1}$ and $2.78 \times 10^{-2} ms^{-1}$ for the EW and NS velocity, respectively. These error values represent a good match and are comparable with other values reported in the literature. For example, Jin *et al.* (2000) reported error from 1.52 to $4.76 \times 10^{-2} ms^{-1}$. Similarly, Rueda & Schladow (2003) found errors between velocity measurements and model results of $2 - 5 \times 10^{-2} ms^{-1}$.

Bibliography

Abdelzaher, A.M, Wright, M.E., Ortega, C., Solo-Gabriele, H.M., Miller, G., Elmir, S., Newman, X., Shih, P., Bonilla, J.A., Bonilla, T.D., Palmer, C.J., Scott, T., Lukasik, J., Harwood, V.J., McQuaig, S., Sinigalliano, C., Gidley, M., Plano, L.R.W., Zhu, X., Wang, J.D., & Fleming, L.E. Presence of pathogens and indicator microbes at a non-point source subtropical recreational marine beach.

Acosta, M.C., Anguita, M., Rueda, F.J., & Fernández-Baldomero, F.J. 2010. Parallel Implementation of a Semi-implicit 3-D Lake Hydrodynamic Model. *Pages 1026–1037 of: Proc. of the 2010 Int. Conf. on Comp. and Math. Methods in Science and Eng. (CMMSE) IV.*

Aldridge, D.W., & McMahon, R.F. 1978. Growth, Fecundity, and Bioenergetics in a natural Population of the Asiatic Freshwater Clam, *Corbicula manilensis philippi*, from North Central Texas. *J. Mollus. Stud.*, **44**(1), 49–70.

Amorocho, J., & DeVries, J. J. 1980. A new evaluation of the wind stress coefficient over water surfaces. *J. Geophys. Res.*, **85**, 433–442.

Andersen, M.C., Adams, H., Hope, B., & Powell, M. 2004. Risk Assessment of Invasive Species. *Risk Anal.*, **24**(4), 787–793.

Anderson, M.A., Stewart, M.H, Yates, M.V., & Gerba, C.P. 1998. Modeling the impact of body-contact recreation on pathogen concentrations in a source drinking water reservoir. *Water Res.*, **32**(11), 3293–3306.

Andow, D.A., Kareiva, P.M., Levin, S.A., & Okubo, Akira. 1990. Spread of invading organisms. *Landscape Ecol.*, **4**(2), 177–188.

Bagnold, R.A. 1966. *An approach to the sediment transport problem from general physics.* U.S. Geol. Surv.

Barnes, S. L. 1964. A Technique for Maximizing Details in Numerical Weather Map Analysis. *J. Appl. Meteorol.*, **3**, 396–409.

Barnes, S. L. 1994a. Applications of the Barnes objective analysis scheme. Part I: Effects of undersampling, wave position, and station randomness. *J. Atmos. Ocean. Technol.*, **11**, 1433–1448.

Barnes, S. L. 1994b. Applications of the Barnes objective analysis scheme. Part III: Tuning for Minimum Error. *J. Atmos. Ocean. Technol.*, **11**, 1459–1479.

Beletsky, D., Mason, D.M., Schwab, D.J., Rutherford, E.S., Janssen, J., Clapp, D.F., & Dettmers, J.M. 2007. Biophysical model of larval yellow perch advection and settlement in Lake Michigan. *J. Great Lakes Res.*, **33**(4), 842–866.

Betancourt, W. Q, & Rose, J.B. 2004. Drinking water treatment processes for removal of *Cryptosporidium* and *Giardia*. *Vet. Parasitol.*, **126**(1), 219–234.

Bitton, G. 1994. *Wastewater Microbiology*. New York: John Wiley & Sons, Inc.

Blumberg, A.F., & Georgas, N. 2008. Quantifying uncertainty in estuarine and coastal ocean circulation modeling. *J. Hydraul. Eng.*, **134**(4), 403–415.

Bossenbroek, J.M., Kraft, C.E., & Nekola, J.C. 2001. Prediction of Long-Distance Dispersal Using Gravity Models: Zebra Mussel Invasion of Inland Lakes. *Ecol. Appl.*, **11**(6), pp. 1778–1788.

Brookes, J.D., Davies, C., Hipsey, M.R., & Antenucci, J.P. 2004a. Association of Cryptosporidium with Bovine Faecel Particles and Implications for Risk Reduction by Settling within Water Supply Reservoirs. *J. Water Health*, **4**, 87–98.

Brookes, J.D., Antenucci, J., Hipsey, M., Burch, M.D., Ashbolt, N.J., & Ferguson, C. 2004b. Fate and transport of pathogens in lakes and reservoirs. *Environ. Int.*, **30**(5), 741–759.

Brooks, D.A., Baca, M.W, & Lo, Y.-T. 1999. Tidal circulation and residence time in a macrotidal estuary: Cobscook Bay, Maine. *Estuar. Coast. Shelf S.*, **49**(5), 647–665.

Buchan, L.A.J., & Padilla, D.K. 1999. Estimating the Probability of Long-Distance Overland Dispersal of Invading Aquatic Species. *Ecol. Appl.*, **9**(1), pp. 254–265.

Carpenter, S.R., Caraco, N.F., Correll, D.L., Howarth, R.W., Sharpley, A.N., & Smith, V.H. 1998. Nonpoint Pollution of Surface Waters with Phosphorus and Nitrogen. *Ecol. Appl.*, **8**(3), 559–568.

Carr, M.L., Rehmann, C.R., Stoeckel, J.A., Padilla, D.K., & Schneider, D.W. 2004. Measurements and consequences of retention in a side embayment in a tidal river. *J. Marine Sys.*, **49**(1), 41–53. Biophysical Factors Affecting the Growth and Survival of Aquatic Organisms.

Carswell, K.J., Symons, J.M., & Robeck, G.G. 1969. Research on recreational use of watersheds and reservoirs. *J. Am. Water Works Ass.*, **61**, 297–304.

Castanedo, S., & Medina, R. 2002. Análisis de los modelos 3D para la simulación de flujo en aguas de transición. *Ingeniería del Agua*, **9**(4), 467–481.

Cataldo, D., Colombo, J.C., Boltovskoy, D., Bilos, C., & Landoni, P. 2001. Environmental toxicity assessment in the Paraná river delta (Argentina): simultaneous evaluation of selected pollutants and mortality rates of *Corbicula fluminea* (Bivalvia) early juveniles. *Environ. Pollut.*, **112**(3), 379–389.

CDC, Center for Disease Control. 2000. Outbreak of grastroenteritis associated with an interactive water fountain at a beachside park - Florida, 1999. *MMWR*, **49**, 565–568.

CDC, Center for Disease Control. 2001. Notice to readers: responding to fecal accidents in disinfected swimming venues. *MMWR*, **50**, 416–417.

CEC, Council of the European Communities. 1976. Council Directive 76/160/EEC of 8 December 1975 concerning the quality of bathing water. *Official Journal of European Communities*, **L031**, 1–7.

Chader, S.A., Mohr, M.C., Morang, A., Ward, D., & Curtis, W.R. 2006. *Sheldon Marsh-Section 227 Demonstration Project-Physical Model Study.* Tech. rept. DTIC Document.

Chung, E.G., Bombardelli, F.A., & Schladow, S.G. 2009. Sediment resuspension in a shallow lake. *Water Resour. Res.*, **45**(5), W05422.

Coe, W.R. 1953. Resurgent populations of littoral marine invertebrates and their dependence on ocean currents and tidal currents. *Ecology*, **34**(1), 225–229.

Connelly, S.J., Wolyniak, E.A., Williamson, C.E., & Jellison, K.L. 2007. Artificial UV-B and solar radiation reduce in vitro infectivity of the human pathogen *Cryptosporidium parvum*. *Environ. Sci. Technol.*, **41**(20), 7101–7106.

Cook, C.B. 2000. *Internal dynamics of a terminal basin lake: a numerical model for management of the Salton Sea.* Ph.D. thesis, University of California, Davis.

Coupe, S., Delabre, K., Pouillot, R., Houdart, S., Santillana-Hayat, M., & Derouin, F. 2006. Detection of *Cryptosporidium*, *Giardia* and *Enterocytozoon bieneusi* in surface water, including recreational areas: a one-year prospective study. *FEMS Immunol. Med. Mic.*, **47**(3), 351–359.

Cox, G.W. 1999. *Alien Species in North America and Hawaii. Impacts on Natural Ecosystems.* Inland Press.

Craik, S.A., Weldon, D., Finch, G.R., Bolton, J.R., & Belosevic, M. 2001. Inactivation of *Cryptosporidium Parvum* oocysts using medium-and low-pressure ultraviolet radiation. *Water Res.*, **35**(6), 1387–1398.

Craun, G.F., Calderon, R.L., & Craun, M.F. 2005. Outbreaks associated with recreational water in the United States. *Int. J. Environ. Heal. R.*, **15**(4), 243–262.

Dai, X., & Boll, J. 2003. Evaluation of attachment of *Cryptosporidium parvum* and *Giardia lamblia* to soil particles. *J. Environ. Qual.*, **32**, 296–304.

Dai, X., & Boll, J. 2006. Settling velocity of *Cryptosporidium parvum* and *Giardia lamblia*. *Water Res.*, **40**(6), 1321 – 1325.

Dai, X., Boll, J., Hayes, M.A, & Aston, D.E. 2004. Adhesion of *Cryptosporidium parvum* and *Giardia lamblia* to solid surface: the role of surface charge and hydrophobicity. *Colloid. Surface. B.*, **34**, 259–263.

Denton, M.E., Chandra, S., Wittmann, M.E., Reuter, J., & Baguley, J.G. 2012. Reproduction and Population Structure of *Corbicula fluminea* in an Oligotrophic Subalpine Lake. *J. Shellfish Res.*, **31**(1), 145–152.

Dimou, K. N., & Adams, E. E. 1993. A random-walk, particle tracking model for well-mixed estuarines and coastal water. *Estuar. Coast. Shelf S.*, **37**, 99–100.

Dunsbergen, D.W., & Stelling, G.S. 1993. *A 3-D particle model for transport problems in transformed coordinates.* Tech. rept. Publication number 93-7. Delft University of Technology. Department of Civil Engineering, Hydraulic and Geotechnical Engineering Division, Hydromechanics Group, Delft, The Netherlands.

Farthing, M.J.G. 2006. Treatment options for the eradication of intestinal protozoa. *Nat. Clin. Pract. Gastr.*, **3**(8), 436–445.

Fayer, R. 2004. *Cryptosporidium*: a water-borne zoonotic parasite. *Vet. Parasitol.*, **126**, 37–56.

Feachem, R.G., Bradley, D.J., Garelick, H., & Mara, D.D. 1983. *Sanitation and Disease.* New York: John Wiley & Sons, Inc.

Figuerola, J., & Green, A.J. 2002. Dispersal of aquatic organisms by waterbirds: a review of past research and priorities for future studies. *Freshwater Biol.*, **47**(3), 483–494.

Forrest, A.L., Wittmann, M.E., Schmidt, V., Raineault, N.A., Hamilton, A., Pike, W., Schladow, S.G., Reuter, J.E., Laval, B.E., & Trembanis, A.C. 2012. Quantitative assessment of invasive species in lacustrine environments through benthic imagery analysis. *Limnol. Oceanogr.-Meth.*, **10**, 65–74.

Gallaher, M.M., Herndon, J.L., Nims, L.J., Sterling, C.R., Grabowski, D.J., & Hull, H.F. 1989. Cryptosporidiosis and surface water. *Am. J. Public Health*, **79**(1), 39–42.

Gardner, J.V., Mayer, L.A., & Hudges Clark, J.E. 1998. *Cruise Report, RV Inland Surveyor Cruise IS-98: The bathymetry of Lake Tahoe, California-Nevada: U.S. Geological Survey Open File-Report 98-509, 28 p.* Tech. rept. USGS.

Gaylord, B., & Gaines, S.D. 2000. Temperature or Transport? Range Limits in Marine Species Mediated Solely by Flow. *Am. Nat.*, **155**(6), pp. 769–789.

Gerba, C.P. 2000. Assessment of enteric pathogen shedding by bathers during recreational activity and its impact on water quality. *Quantitative Microbiology*, **2**(1), 55–68.

Gillis, P.L. 2012. Cumulative impacts of urban runoff and municipal wastewater effluents on wild freshwater mussels (*Lasmigona costata*). *Sci. Total Environ.*, **431**, 348–356.

Gosselin, L.A., & Qian, P.-Y. 1997. Juvenile mortality in benthic marine invertebrates. *Mar. Ecol.-Prog. Ser.*, **146**(1), 265–282.

Graczyk, T.K., Sunderland, D., Tamang, L., Lucy, F.E., & Breysse, P.N. 2007. Bather density and levels of *Cryptosporidium*, *Giardia*, and pathogenic microsporidian spores in recreational bathing water. *Parasitol. Res.*, **101**(6), 1729–1731.

Grant, R. H., Heisler, G. M., & Gao, W. 1997. Ultraviolet sky radiance distributions of translucent overcast skies. *Theor. Appl. Climatol.*, **58**, 129–139. 10.1007/BF00865013.

Green, A.J., & Figuerola, J. 2005. Recent advances in the study of long-distance dispersal of aquatic invertebrates via birds. *Divers. Distrib.*, **11**(2), 149–156.

Griffiths, R.W., Schloesser, D.W., Leach, J.H., & Kovalak, W.P. 1991. Distribution and Dispersal of the Zebra Mussel (*Dreissena polymorpha*) in the Great Lakes Region. *Can. J. Fish. Aquat. Sci.*, **48**(8), 1381–1388.

Grifoll, M., Del Campo, A., Espino, M., Mader, J., González, M., & Borja, Á. 2013. Water renewal and risk assessment of water pollution in semi-enclosed domains: Application to Bilbao Harbour (Bay of Biscay). *J. Marine Syst.*, **109-110**, S241–S251.

Guizien, K., Brochier, T., Duchêne, J.-C., Koh, B.-S., & Marsaleix, P. 2006. Dispersal of *Owenia fusiformis* larvae by wind-driven currents: turbulence, swimming behaviour and mortality in a three-dimensional stochastic model. *Mar. Ecol.-Prog. Ser.*, **311**, 47–66.

Hackley, S., Allen, B., Schladow, G., Reuter, J., Chandra, S., & Wittmann, M. 2008. *Lake Tahoe aquatic invasive species incident report: notes on visual observations of clams in Lake Tahoe and on the beaches along the southeast shore - Zephyr Cove to Timber Cove Marina: April 25, 2008.* Tech. rept. University of California at Davis, Tahoe Environmental Research Center.

Häder, D.-P. 2003. UV-B Impact on the Life of Aquatic Plants. *Chap. 7, pages 149–172 of:* Ambasht, R.S., & Ambasht, N.K. (eds), *Modern Trends in Applied Aquatic Ecology.* New York: Kluwer Acadameic/Plenum Publishers.

Häder, D.-P., & Sinha, R.P. 2005. Solar ultraviolet radiation-induced DNA damage in aquatic organisms: potential environmental impact. *Mutat. Res.-Fund. Mol. M.*, **571**(1-2), 221–233.

Hakenkamp, C.C., Ribblett, S.G., Palmer, M.A., Swan, C.M., Reid, J.W., & Goodison, M.R. 2001. The impact of an introduced bivalve (*Corbicula fluminea*) on the benthos of a sandy stream. *Freshwater Biol.*, **46**(4), 491–501.

Hamilton, D.P., & Mitchell, S.F. 1996. An empirical model for sediment resuspension in shallow lakes. *Hydrobiologia*, **317**, 209–220.

Han, Y.-J., Holsen, T.M., Hopke, P.K., & Yi, S.-M. 2005. Comparison between Back-Trajectory Based Modeling and Lagrangian Backward Dispersion Modeling for Locating Sources of Reactive Gaseous Mercury. *Environ. Sci. Technol.*, **39**, 1715–1723.

Harwood, V.J., Levine, A.D., Scott, T.M., Chivukula, V., Lukasik, J., Farrah, S.R., & Rose, J.B. 2005. Validity of the Indicator Organisms Paradigm for Pathogen Reduction in Reclaimed Water and Public Health Protection. *Appl. Environ. Microb.*, **71**(6), 3163–3170.

Hawkings, P.R., Swanson, P., Warnecke, M., Shanker, S.R., & Nicholson, C. 2000. Understanding the Fate of *Cryptosporidium* and *Giarda* in Storage reservoirs: A Legacy of Sydney's Water Contamination Incident. *Aqua*, **49**(6), 289–306.

Heberer, T. 2002. Occurrence, fate, and removal of pharmaceutical residues in the aquatic environment: a review of recent research data. *Toxicol. Lett.*, **131**(1), 5–17.

Herold, M., Metz, J., & Romsos, J.S. 2007. Inferring littoral substrates, fish habitats, and fish dynamics of Lake Tahoe using IKONOS data. *Can. J. Remote Sens.*, **33**(5), 445–456.

Hessen, D.O., Alstad, N.E.W., & Skardal, L. 2000. Calcium limitation in Daphnia magna. *J. Plankton Res.*, **22**(3), 553–568.

Hijnen, W.A.M., Beerendonk, E.F., & Medema, G.J. 2006. Inactivation credit of UV-radiation for viruses, bacteria and protozoan (oo)cysts in water: A review. *Water Res.*, **40**(1), 3–22.

Hipsey, M.R., Antenucci, J.P., Brookes, J.D., Burch, M.D., Regel, R.H., & Linden, L. 2004. A three dimensional model of *Cryptosporidium* dynamics in lakes and reservoirs: A new tool for risk management. *Intl. J. River Basin Management*, **2**(3), 181–197.

Hofmann, H., Lorke, A., & Peeters, F. 2011. Wind and ship wave-induced resuspension in the littoral zone of a large lake. *Water Resour. Res.*, **47**(9), W09505.

Hortal, J., Borges, P.A.V., Jiménez-Valverde, A., de Azevedo, E.B., & Silva, L. 2010. Assessing the areas under risk of invasion within islands through potential distribution modelling: The case of *Pittosporum undulatum* in São Miguel, Azores. *Journal for Nature Conservation*, **18**(4), 247–257.

Hoxie, N.J., Davis, J.P., Vergeront, J.M., Nashold, R.D., & Blair, K.A. 1997. Cryptosporidiosis-associated mortality following a massive waterborne outbreak in Milwaukee, Wisconsin. *Am. J. Public Health*, **87**(12), 2032–2035.

Hrycik, J.M., Chassé, J., Ruddick, B.R., & Taggart, C.T. 2013. Dispersal kernel estimation: A comparison of empirical and modelled particle dispersion in a coastal marine system. *Estuar. Coast. Shelf S.*, **133**, 11–22.

Jakubowski, W. 1984. Detection of *Giardia* cysts in drinking water: State of the art. *Pages 263–285 of: Giardia and Giardiasis, Biology, Pathogenesis and Epidemology.* New York: Plenum Press.

Jellison, K.L., Hemond, H.F., & Schauer, D.B. 2002. Sources and species of *Cryptosporidium* oocysts in the Wachusett Reservoir watershed. *Appl. Environ. Microb.*, **68**(2), 569–575.

Jerde, C.L., & Lewis, M.A. 2007. Waiting for invasions: a frame work for the arrival of nonindigenous species. *Am. Nat.*, **170**, 1–9.

Jin, K.-R., Hamrick, J.H., & Tisdale, T. 2000. Application of Three-Dimensional Hydrodynamic Model for Lake Okeechobee. *J. Hydraul. Eng.*, **126**(10), 758–771.

Jin, K.R., & Sun, D. 2007. Sediment resuspension and hydrodynamics in Lake Okeechobee during the late summer. *J. Engi. Mech.*, **133**(8), 899–910.

Johnson, L.E., Ricciardi, A., & Carlton, J.T. 2001. Overland dispersal of aquatic invasive species: a risk assessment of transient recreational boating. *Ecol. Appl.*, **11**(6), 1789–1799.

Jørgensen, C.B. 1981. Mortality, growth, and grazing impact of a cohort of bivalve larvae, *Mytilus edulis* L. *Mortality*, **20**(2).

Karatayev, A.Y., Burlakova, L.E., Kesterson, T., & Padilla, D.K. 2003. Dominance of the Asiatic clam, *Corbicula fluminea* (Müller), in the benthic community of a reservoir. *J. Shellfish Res.*, **22**(2), 487–493.

Keller, R.P., Lodge, D.M., Lewis, M., & Shogren, S.F. 2009. *Bioeconomics of invasive species: integrating ecology, economics, policy and management.* Oxford University Press.

King, B.J., Hoefel, D., Daminato, D.P., Fanok, S., & Monis, P.T. 2008. Solar UV reduces *Cryptosporidium parvum* oocyst infectivity in environmental waters. *J. Appl. Microbiol.*, **104**(5), 1311–1323.

Kitanidis, P.K. 1994. Particle-tracking equations for the solution of the advection-dispersion equation with variable coefficients. *Water Resour. Res.*, **30**, 3225–3227.

Koch, S.E., desJardins, M., & Kocin, P.J. 1983. An Interactive Barnes Objective Map Analysis Scheme for Use with Satellie and Conventional Data. *J. Climate Appl. Meteorol.*, **22**(9), 1487–1503.

Koelmans, A.A, der Heijde, A Van, Knijff, L.M, & Aalderink, R.H. 2001. Integrated Modelling of Eutrophication and Organic Contaminant Fate & Effects in Aquatic Ecosystems. A Review. *Water Res.*, **35**(15), 3517–3536.

Kolar, C.S., & Lodge, D.M. 2001. Progress in invasion biology: predicting invaders. *Trends Ecol. Evol.*, **16**(4), 199–204.

Kraemer, L.R., & Galloway, M.L. 1986. Larvae development of *Corbicula fluminea* (Mueller) (Bivalvia, Corbiculacea): An appraisal of its heterochrony. *Am. Malacol. Bull.*, **4**, 61–79.

Kryshev, I.I. 1995. Radioactive contamination of aquatic ecosystems following the Chernobyl accident. *J. Environ. Radioactiv.*, **27**(3), 207–219.

Largier, J.L. 2003. Considerations in estimating larval dispersal distances from oceanographic data. *Ecol. Appl.*, **13**(sp1), 71–89.

Lawrence, G.A., Ashley, K.I., Yonemitsu, N., & Ellis, J.R. 1995. Natural dispersion in a small lake. *Limnol. Oceanogr.*, 1519–1526.

LeChevallier, M.W., Norton, W.D., & Lee, R.G. 1991. *Giardia* and *Cryptosporidium* spp. in filtered drinking water supplies. *Appl. Environ. Microb.*, **57**(9), 2617–2621.

Leung, B., Lodge, D.M., Finnoff, D., Shogren, J.F., Lewis, M.A., & Lamberti, G. 2002. An ounce of preventation or a pound of cure: bioeconomic risk analysis of invasive species. *Proc. R. Soc. Lond. B.*, **269**, 2407–2413.

Leung, B., Drake, J.M., & Lodge, D.M. 2004. Predicting Invasions: Propagule Pressure and the Gravity of Allee Effects. *Ecology*, **85**(6), 1651–1660.

Leung, B., Bossenbroek, J.M., & Lodge, D.M. 2006. Boats, pathways, and aquatic biological invasions: estimating dispersal potential with gravity models. *Biol. Invasions*, **8**(2), 241–254.

Lewis, D., & Whitby, G.E. 1997. *Methods and apparatus for controlling zebra and related mussel using ultraviolet radiation.*

Liebhold, A.M., Sharov, A.A., & Tobin, P.C. 2007. *Population Biology of Gypsy Moth Spread.* General Technical Report NRS-6. USDA Forest Service Nothern Research Station.

Liu, L., Phanikumar, M.S., Molloy, S.L., Whitman, R.L., Shively, D.A., Nevers, M.B., Schwab, D.J., & Rose, J.B. 2006. Modeling the Transport and Inactivation of *E. coli* and Enterococci in the Near-shore Region of Lake Michigan. *Environ. Sci. Technol.*, **40**(16), 5022–5028.

Lockwood, J.L., Cassey, P., & Blackburn, T. 2005. The role of propagule pressure in explaining species invasions. *Trends in Ecology & Evolution*, **20**(5), 223–228.

Luettich, R.A., Harlemann, D.R.F., & Somlyody, L. 1990. Dynamic behavior of suspended sediment concentrations in a shallow lake perturbed by episodic wind events. *Limnol. Oceanogr.*, **35**(5), 1050–1067.

MacIntyre, S., Sickman, J.O., Goldthwait, S.A., & Kling, G.W. 2006. Physical pathways of nutrient supply in a small, ultraoligotrophic arctic lake during summer stratification. *Limnol. Oceanogr.*, **51**(2), 1107–1124.

MacIsaac, H., Grigorovich, I., & Ricciardi, A. 2001. Reassessment of Species Invasions Concepts: The Great Lakes Basin as a Model. *Biol. Invasions*, **3**, 405–416.

MacIsaac, H.J., Robbins, T.C., & Lewis, M.A. 2002. Modeling ships' ballast water as invasion threats to the Great Lakes. *Can. J. Fish. Aquat. Sci.*, **59**, 1245–1256.

MacKenzie, W.R., Hoxie, N.J., Proctor, M.E., Gradus, M.S., Blair, K.A., Peterson, D.E., Kazmierczak, J.J., Addiss, D.G., Fox, K.R., Rose, J.B., & Davis, J.P. 1994. A massive outbreak in Milwaukee of *Cryptosporidium* infection transmitted through the public water supply. *N. Engl. J. Med.*, **331**(3), 161–167.

Masur, H., Kaplan, J.E., & Holmes, K.K. 2002. Guidelines for Preventing Opportunistic Infections among HIV-Infected Persons-2002. *Ann. Intern. Med.*, **137**, 435–478.

McMahon, R.F. 1999. Invasive characteristics of the freshwater bivalve *Corbicula fluminea*. *Pages 315–345 of: Nonindigenous Freshwater Organisms: Vector, Biology, and Impacts.* CRC Press LLC.

McMahon, R.F. 2002. Evolutionary and physiological adaptations of aquatic invasive animals: *r* selection versus resistance. *Can. J. Fish. Aquat. Sci.*, **59**(7), 1235–1244.

McMahon, R.F., & Bogan, A.E. 2001. Mollusca: Bivalvia. *Chap. 11, pages 331–429 of:* Thorp, James H., & Covich, Alan P. (eds), *Ecology and Classification of North American Freshwater Invertebrates.* Academic Press.

Medema, G.J., Schets, F.M., Teunis, P.F.M., & Havelaar, A.H. 1998. Sedimentation of Free and Attached *Cryptosporidium* Oocysts and *Giardia* Cysts in Water. *Appl. Environ. Microb.*, **64**(11), 4460–4466.

Moles, A.T., Gruber, M.A.M., & Bonser, S.P. 2008. A new framework for predicting invasive plant species. *J. Ecol.*, **96**(1), 13–17.

Monis, P., King, B., & Keegan, A. 2014. Removal and Inactivation of *Cryptosporidium* from Water. *Pages 515–552 of:* Cacciò, Simone M., & Widmer, Giovanni (eds), *Cryptosporidium: parasite and disease.* Springer Vienna.

Morita, S., Namikoshi, A., Hirata, T., Oguma, K., Katayama, H., Ohgaki, S., Motoyama, N., & Fujiwara, M. 2002. Efficacy of UV irradiation in inactivating *Cryptosporidium parvum* oocysts. *Appl. Environ. Microb.*, **68**(11), 5387–5393.

Nickols, K.J., Gaylord, B., & Largier, J.L. 2012. The coastal boundary layer: predictable current structure decreases alongshore transport and alters scales of dispersal. *Mar. Ecol.-Prog. Ser.*, **464**, 17–35.

Nishimoto, M.M., & Washburn, L. 2002. Pattterns of coastal eddy circulation and abundance of pelagic juvenile fish in the Santa Barbara Channel, California, USA. *Mar. Ecol.-Prog. Ser.*, **241**, 183–199.

Okely, P., Imberger, J., & Antenucci, J.P. 2010. Processes affecting horizontal mixing and dispersion in Winam Gulf, Lake Victoria. *Limnol. Oceanogr.*, **55**(5), 1865–1880.

Ongerth, J.E., & Pecoraro, J.P. 1996. Electrophoretic mobility of *Cryptosporidium parvum* and *Giardia lamblia* cysts. *J. Environ. Eng.*, **122**, 228–231.

Peeters, F., Wüest, A., Piepke, G., & Imboden, D. M. 1996. Horizontal mixing in lakes. *J. Geophys. Res.*, **101**, 18361–18375.

Pimentel, D., Zuniga, R., & Morrison, D. 2005. Update on the environmental and economic costs associated with alien-invasive species in the United States. *Ecol. Econ.*, **52**(3), 273–288.

Pollock, D.W. 1988. Semianalytical computation of path lines for finite difference models. *Groundwater*, **26**(6), 743–750.

Poulos, H.M., Chernoff, B., Fuller, P.L., & Butman, D. 2012. Ensemble forecasting of potential habitat for three invasive fishes. *Aquatic Invasions*, **7**(1), 59–72.

Prezant, R.S., & Chalermwat, K. 1984. Flotation of the Bivalve *Corbicula fluminea* as a Means of Dispersal. *Science*, **225**(4669), 1491–1493.

Rao, Y.R., & Schwab, D.J. 2007. Transport and Mixing Between the Coastal and Offshore Waters in the Great Lakes: a Review. *J. Great Lakes Res.*, **33**(1), 202–218.

Reardon, K.E., Moreno, P.A., Bombardelli, F., Rueda, F.J., & Schladow, S.G. 2014. Wind-driven nearshore sediment resuspension in a deep lake during winter. *In review.*

Reynolds, C.S. 1984. *The ecology of freshwater phytoplankton.* Cambridge Academic Press.

Ricciardi, A., & MacIsaac, H.J. 2008. Evaluating the effectiveness of ballast water exchange plolicy in the Great Lakes. *Ecol. Appl.*, **18**, 1321–1323.

Robertson, L.J., Smith, H.V., & Paton, C.A. 1995. Occurrence of *Giardia* and *Cryptosporidium* oocysts in sewage effluent in six sewage treatment plants in Scotland and the prevalence of cryptosporidiosis and giardiasis diagnosed in the communities served by those plants. *Pages 47–49 of:* Betts, W.B., Casemore, D., Fricker, C., Smith, H., & Watkins, J. (eds),

Protozoan Parasites and Water. Cambridge: The Royal Society of Chemistry.

Rochelle, P.A., Upton, S.J., Montelone, B.A., & Woods, K. 2005. The response of *Cryptosporidium parvum* to UV light. *Trends in Parasitology*, **21**(2), 81–87.

Rose, J.B., Gerba, C.P., & Jakubowski, W. 1991. Survey of potable water supplies for Cryptosporidium and Giardia. *Environ. Sci. Technol.*, **25**(8), 1393–1400.

Rose, J.B., Huffman, D.E., & Gennaccaro, A. 2002. Risk and control of waterborne cryptosporidiosis. *FEMS Microbiol. Rev.*, **26**(2), 113–123.

Rose, K.C., Williamson, C.E., Schladow, S.G., Winder, M., & Oris, J.T. 2009. Patterns of spatial and temporal variability of UV transparency in Lake Tahoe, California-Nevada. *J. Geophys. Res.*, **114**, G00D03.

Ross, O.N., & Sharples, J. 2004. Recipe for 1-D Lagrangian particle tracking models in space-varying diffusivity. *Limnol. Oceanogr.-Meth.*, **2**, 289–302.

Rossignol, J.F., Kabil, S.M., El-Gohary, Y., & Younis, A.M. 2006. Effect of nitazoxanide in diarrhea and enteritis caused by *Cryptosporidium* species. *Clin. Gastroenterol. H.*, **4**, 320–324.

Rothlisberger, J.D., Chadderton, W.L., McNulty, J., & Lodge, D.M. 2010. Aquatic invasive species transport via trailered boats: what is being moved, who is moving it, and what can be done. *Fisheries*, **35**(3), 121–132.

Rouse, H. 1937. Modern Conceptions of the Mechanics of Fluid Turbulence. *Trans. Am. Soc. Civil Engng.*, **102**(1), 463–505.

Rueda, F.J. 2001. *A three-dimensional hydrodynamic and transport model for lake environments.* Ph.D. thesis, University of California, Davis, California.

Rueda, F.J., & Cowen, E.A. 2005. Residence Time of a Freshwater Embayment Connected to a Large Lake. *Limnol. Oceanogr.*, **50**(5), 1638–1653.

Rueda, F.J., & Schladow, S.G. 2002. Quantitative comparison of models for barotropic response of homogeneous basins. *J. Hydraul Eng.*, **128**(2), 201–213.

Rueda, F.J., & Schladow, S.G. 2003. Dynamics of Large Polymictic Lake. II: Numerical Simulations. *J. Hydraul. Eng.*, **129**(2), 92–101.

Rueda, F.J., & Vidal, J. 2009. Currents in the Upper Mixed Layer and in Unstratified Water Bodies. *Pages 568–2057 of:* Likens, G. E. (ed), *Encyclopedia of Inland Waters.* Elsevier Inc.

Rueda, F.J., Schladow, S.G., & Pálmarsson, S.Ó. 2003. Basin-scale interanl wave dynamics during a winter cooling period in a large lake. *J. Geophys. Res.*, **108**(C3), 3097.

Rueda, F.J., Schladow, S.G., & Clark, J.F. 2008. Mechanisms of contaminant transport in a multi-basin lake. *Ecol. Appl.*, **18**, A27–A87.

Schleier III, J.J., Sing, S.E., & Peterson, R.K.D. 2008. Regional ecological risk assessment for the introduction of *Gambusia affinis* (western mosquitofish) into Montana watersheds. *Biol. Invasions*, **10**(8), 1277–1287.

Shen, L., Peterson, S., Sedaghat, A.R., McMahon, M.A., Callender, M., Zhang, H., Zhou, Y., Pitt, E., Anderson, K.S., Acosta, E.P., & Siliciano, R.F. 2008. Dose-response curve slope sets class-specific limits on inhibitory potential of anti-HIV drugs. *Nat. Med.*, **7**, 762–766.

Sherchand, J.B. 2012. Future Emerging Issues in waterborne diseases and microbial agents. *J. Inst. Med.*, **34**(3), 1–3.

Sherry, J.P. 1986. Temporal distribution of faecel pollution indicators and opportunistic pathogens at a Lake Ontario bathing beach. *J. Great Lakes Res.*, **12**, 154–160.

Shigesada, N., & Kawasaki, K. 1997. *Biological invasions: theory and practice*. Oxford University Press.

Shintani, T., de la Fuente, A., Niño, Y., & Imberger, J. 2010. Generalization of the Wedderburn number: parameterizing upwelling in stratified lakes. *Limnol. Oceanogr.*, **55**, 1377–1389.

Siegel, D.A., Kinlan, B.P., Gaylord, B., & Gaines, S.D. 2003. Lagrangian descriptions of marine larval dispersion. *Mar. Ecol.-Prog. Ser.*, **260**, 83–96.

Signor, R.S., Roser, D.J., Ashbolt, N.J., & Ball, J.E. 2005. Quantifying the impact of runoff events on microbiological contaminant concentration entering surface drinking source waters. *J. Water Health*, **3**, 453–468.

Simberloff, D. 2005. Non-native Species DO Threaten the Natural Environment! *J. Agr. Environ. Ethic.*, **18**(6), 595–607.

Sinha, R.P., & Häder, D.-P. 2002. UV-induced DNA damage and repair: a review. *Photochem. Photobiol. Sci.*, **1**, 225–236.

Skellam, J.G. 1951. Random Dispersal in Theoretical Populations. *Biometrika*, **38**(1/2), pp. 196–218.

Smith, H.V., & Corcoran, G.D. 2004. New drugs and treatment for cryptosporidiosis. *Curr. Opin. Infect. Dis.*, **17**, 557–564.

Smith, J.M. 2007. *Modeling nearshore waves for Hurricane Katrina.* Tech. rept. DTIC Document.

Smith, J.M., & Sherlock, A.R. 2007. Full-plane STWAVE with bottom friction: II. Model overview. *System-Wide Water Resources Program Technical Note, Vicksburg, MS: US Army Engineer Research and Development Center.*

Smith, J.M., Sherlock, A.R., & Resio, D.T. 2001. *STWAVE: Steady-State Spectral Wave Model User's manual for STWAVE, Version 3.0.* Tech. rept. ERDC/CHL SR-01-1. US Army Corps of Engineers, Engineering Research and Development Center.

Smith, P.E. 2006. *A Semi-implicit, Three-dimensional Model for Estuarine Circulation.* Open-File Report 2006-1004. U.S. Department of the Interior, U.S. Geological Survey.

Sousa, R., Antunes, C., & Guilhermino, L. 2008. Ecology of the invasive Asian clam *Corbicula fluminea* (Müller, 1774) in aquatic ecosystems: an overview. *Ann. Limnol.-Int. J. Lim.*, **44**(02), 85–94.

Standish-Lee, P., & Loboschefsky, E. 2006. Protecting public health from the impact of body-contact recreation. *Water Sci. Technol.*, **53**(10), 201–207.

Steissberg, T.E., Hook, S.J., & Schladow, S.G. 2005. Measuring surface currents in lakes with high spatial resolution thermal infrared imagery. *Geophys. Res. Lett.*, **32**, L11402.

Stevens, C., & Imberger, J. 1996. The initial response of a stratified lake to a surface shear stress. *J. Fluid Mech.*, **312**, 39–66.

Stewart, M.H., Yates, M.V., Anderson, M.A., Gerba, C.P., Rose, J.B., De Leon, R., & Wolfe, R.L. 2002. Predicted public health consequences of body-contact recreation on a potable water reservoir. *J. Am. Water Works Ass.*, **94**(5), 84–97.

Stuart, D.G., Bissonnette, T.D., Goodrich, W.G., & Walter, W.G. 1971. Effect of multiple use on water quality of high-mountain watersheds: bacteriological investigations of mountain streams. *Appl. Environ. Microb.*, **22**, 1048–1054.

Sun, Y., Wells, M.G., Bailey, S.A., & Anderson, E.J. 2013. Physical dispersion and dilution of ballast water discharge in the St. Clair River: Implications for biological invasions. *Water Resour. Res.*, **49**, 2395–2407.

Sunderland, D., Graczyk, T.K., Tamang, L., & Breysse, P.N. 2007. Impact of bathers on levels of *Cryptosporidium parvum* oocysts and *Giardia lamblia* cysts in recreational beach waters. *Water Res.*, **41**(15), 3483–3489.

Swift, T.J. 2004. *The aquatic optics of Lake Tahoe CA-NV.* Ph.D. thesis, University of California, Davis.

Swift, T.J., Perez-Losada, J., Schladow, S.G., Reuter, J.E., Jassby, A.D., & Goldman, C.R. 2006. Water clarity modeling in Lake Tahoe: Linking suspended matter characteristics to Secchi depth. *Aquat. Sci.*, **68**, 1–15.

Tang, L., Sheng, J., Hatcher, B.G., & Sale, P.F. 2006. Numerical study of circulation, dispersion, and hydrodynamic connectivity of surface waters on the Belize shelf. *J. Geophys. Res.*, **111**(C1), C01003.

Tapia, F.J., Pineda, J., Ocampo-Torres, F.J., Fuchs, Heidi L, Parnell, P.Edward, Montero, Paulina, & Ramos, Sergio. 2004. High-frequency observations of wind-forced onshore transport at a coastal site in Baja California. *Cont. Shelf Res.*, **24**, 1573–1585.

Tatem, A.J., Hay, S.I., & Rogers, D.J. 2006. Global traffic and disease vector dispersal. *P. Natl. Acad. Sci.*, **103**(16), 6242–6247.

Tayler, P.A., & Lee, R.J. 1984. Simple guidelines for estimating wind speed variations due to small-sclae topographic features. *Climatol. Bull.*, **18**, 3–32.

Teixeira, T.P., Neves, L.M., & F.G.Araújo. 2009. Effects of a nuclear power plant thermal discharge on habitat complexity and fish community structure in Ilha Grande Bay, Brazil. *Mar. Environ. Res.*, **68**(4), 188–195.

Trefethen, L.N., & Bau III, D. 1997. *Numerical linear algebra.* Society for Industrial Mathematics.

Tucker, A.J., Williamson, C.E., Rose, K.C., Oris, J.T., Connelly, S.J., Olson, M.H., & Mitchell, D.L. 2010. Ultraviolet radiation affects invasibility of lake ecosystems by warm-water fish. *Ecology*, **91**(3), 882–890.

USEPA, U.S. Enrionmental Protection Agency. 1989. *National primary drinking water regulations; infiltration and disinfection; turbidity; Giardia lamblia; viruses; Legionella, and heterotrophic bacteria.* Fed. Reg. 54, 27486-27541. Office of Research and Development, Office of Water, Washington, DC, USA.

USEPA, U.S. Enrionmental Protection Agency. 2006. *Ultraviolet disinfection guidance manual.* Tech. rept. EPA-815-R-06-007. USEPA, Washington, DC, USA.

USEPA, U.S. Environmental Protection Agency. 2002. *Implementation criteria for ambient water quality criteria for bacteria.* EPA-823-B-02-003. Office of Research and Development, Office of Water, Washington, DC, USA.

Vander Zanden, M.J., & Olden, J.D. 2008. A management framework for preventing the secondary spread of aquatic invasive species. *Can. J. Fish. Aquat. Sci.*, **65**(7), 1512–1522.

Vander Zanden, M.J., Hansen, G.J.A., Higgis, S.N., & Kornis, M.S. 2010. A pound of preventaion, plus a pound of cure: Early detection and eradication of invasive species in the Laurentian Great Lakes. *J. Great Lakes Res.*, **36**, 199–205.

Vaughn, C.C., & Hakenkamp, C.C. 2001. The functional role of burrowing bivalves in freshwater ecosystems. *Freshwater Biol.*, **46**(11), 1431–1446.

Wade, T.J., Calderon, R.L., Sams, E., Beach, M., Brenner, K.P., Williams, A.H., & Dufour, A.P. 2006. Rapidly measured indicators of recreational water quality are predictive of swimming-associated gastrointestinal illness. *Environ. Health Persp.*, **114**(1), 24.

Walker, F.R., & Stedinger, J. 1999. Fate and Transport Model of CRYPTOSPORIDIUM. *J. Environ. Eng.*, **125**(4), 325–333.

Wang, W., Liu, S., Zhang, S., & Chen, J. 2011. Assessment of a model of pollution disaster in near-shore coastal waters based on catastrophice theory. *Ecol. Modell.*, **222**, 307–312.

Wells, M.G., Bailey, S.A., & Ruddick, B. 2011. The dilution and dispersion of ballast water discharged into Goderich Harbor. *Mar. Poll. Bull.*, **62**, 1288–1296.

Werner, S., & Rothhaupt, K.-O. 2008. Mass mortality of the invasive bivalve Corbicula fluminea induced by a severe low-water event and associated low water temperatures. *Pages 143–150 of: Ecological Effects of Water-Level Fluctuations in Lakes.* Springer.

WHO, World Health Organisation. 2008. *Guidelines for Drinking Water Quality.* Tech. rept. 1. WHO, Geneva, Switzerland.

Wilcove, D.S., Rothstein, D., Dubow, J., Phillips, A., & Losos, E. 1998. Quantifying threats to imperiled species in the United States. *BioScience*, **48**(8), 607–615.

Williams, C.J., & McMahon, R.F. 1989. Annual variation of tissue biomass and carbon and nitrogen content in the freshwater bivalve Corbicula fluminea relative to downstream dispersal. *Can. J. Zoolog.*, **67**(1), 82–90.

Wittmann, M., Reuter, J., Schladow, G., Hackley, S., Allen, B., Chandra, S., & Caires, A. 2009 (December). *Asian clam (Corbicula fluminea) of Lake Tahoe: Preliminary scientific findings in support of a management plan.* Tech. rept. UC Davis - Tahoe Environmental Research Center.

Wittmann, M.E., Chandra, S., Reuter, J.E., Schladow, S.G., Allen, B.C., & Webb, K.J. 2012. The Control of an Invasive Bivalve, *Corbicula fluminea*, Using Gas Impermeable Benthic Barries in a Large Natural Lake. *Environ. Manage.*, **49**(6), 1163–1173.

Wu, J., Rees, P., Storrer, S., Alderisio, K., & Dorner, S. 2009. Fate and Transport Modeling of Potential Pathogens: The Contribution From Sediments. *J. Am. Water Resources Ass.*, **45**(1), 35–44.

Yoder, J.S., Blackburn, B.G., Craun, G.F., Hill, V., Levy, D.A., Chen, N., Lee, S.H .and Calderon, R.L., & Beach, M.J. 2004. Surveillance for Waterborne-Disease Outbreaks associated with Recreational Water - United States, 2001-2002. *MMWR Surveill. Summ.*, **53**(8), 1–22.

Zeng, E.Y., & Venkatesan, M.I. 1999. Dispersion of sediment DDTs in the coastal ocean off southern California. *Sci. Total Environ.*, **229**(3), 195–208.